

# Chemistry–A European Journal

Supporting Information

## **Towards Luminescent Vanadium(II) Complexes with Slow Magnetic Relaxation and Quantum Coherence**

Matthias Dorn, David Hunger, Christoph Förster, Robert Naumann, Joris van Slageren,\* and  
Katja Heinze\*

**General Procedures.** Glassware used for storage of dry solvents and in the synthesis of vanadium(II) precursors and title complexes was treated according to standard Schlenk procedures prior to use. Syntheses involving vanadium complexes were generally carried out in dry solvents. Diethyl ether and acetonitrile were distilled under an argon atmosphere over sodium and calcium hydride, respectively. Sodium tetraphenylborate (99.5 %; abcr) was dried under reduced pressure at 180°C for 18 h prior to use. Vanadium(III) chloride (anhydrous, 95 %; abcr) for the preparation of hexa(acetonitrile)vanadium(II) tetraphenylborate<sup>[1]</sup> was used as received. The ligand ddpd<sup>[2]</sup> and hexa(acetonitrile)vanadium(II) tetraphenylborate<sup>[1]</sup> were prepared according to reported procedures. NMR spectroscopic and mass spectrometric data matched the literature values. A glovebox (UniLab/MBraun, Ar 4.8, O<sub>2</sub> < 1 ppm, H<sub>2</sub>O < 0.1 ppm) was used for storage and weighing of sensitive compounds and degassed solvents.

**IR spectra** were recorded with a *Bruker Alpha II FT-IR* spectrometer with a Platinum Di-ATR module inside an Ar filled glove box.

**ESI<sup>+</sup> mass spectra** were recorded on a *Micromass Q-TOF-Ultima* spectrometer by the central analytical facility of the Department of Chemistry of the University of Mainz.

**Electrochemical experiments** were carried out on a *BioLogic SP-200* voltammetric analyzer using platinum wires as counter and working electrodes and a 0.01 M Ag/Ag[NO<sub>3</sub>] electrode as reference electrode. Cyclic voltammetry measurements were carried out at scan rates of 50–200 mV s<sup>-1</sup> using 0.1 M [<sup>n</sup>Bu<sub>4</sub>N][PF<sub>6</sub>] in CH<sub>3</sub>CN as supporting electrolyte. Potentials are referenced against the ferrocene/ferrocenium couple.

**UV/Vis/NIR spectra** were recorded on a *JASCO V-770* spectrophotometer using 1.0 cm inert gas cells.

**Luminescence experiments** were carried out on an *Edinburgh FLS 1000* photoluminescence spectrometer. Photomultiplier detectors PMT-980 and N-G09 PMT-1700 were used for luminescence measurements in the visible and NIR spectral region. A xenon arc lamp Xe2 (450 W) was used for excitation in steady-state measurements. Measurements at low temperature were conducted using a liquid nitrogen cooled cryostat *Optistat DN 0.8* from Edinburgh Instruments. For luminescence measurements in deoxygenated solvents, the respective solvent was degassed by freezing it with liquid nitrogen, evacuating the vessel for 30 minutes and warming to room temperature. The procedure was repeated until no more gas evolution occurred upon thawing, but at least three times.

**High-frequency electron paramagnetic resonance (HF-EPR) spectra** were recorded on pressed powder pellets by means of a home-built spectrometer that has been described in the literature.<sup>[3]</sup> Simulations were carried out by using the Easyspin tool.<sup>[4]</sup>

**Magnetic circular dichroism (MCD) spectra** were recorded on frozen solution samples by means of a home-built spectrometer based on an *Aviv 41CD* spectrometer and an Oxford Instruments 10T Spectromag optical cryomagnet.<sup>[5]</sup>

**Pulsed Q-band EPR measurements** were performed on a home-built spectrometer that has been described in the literature.<sup>[6,7]</sup> Samples were freeze-pump-thaw degassed three times prior to measurement. The echo-detected spectra, as well as  $T_M$  decay curves were recorded by a Hahn echo sequence  $\pi/2-\tau-\pi-\tau$ -echo with constant  $\tau = \tau_{\text{fix}}$  for the former and variable  $\tau$  for the latter. The spin-lattice relaxation time  $T_1$  was determined by means of the inversion recovery sequence  $\pi-T-\pi/2-\tau_{\text{fix}}-\pi-\tau_{\text{fix}}$ -echo. Simulations were carried out by using the Easyspin tool.<sup>[4]</sup>

**DC and AC magnetic studies** were carried out on a Quantum Design MPMS3 SQUID magnetometer. Measurements were carried out at a constant magnetic field of 1000 Oe in a temperature range from 1.8 K to 50 K and at 10 000 Oe in a temperature range from 40 K to 300 K. The measured data in the intersection of the temperature ranges served to compensate for possible ferromagnetic impurities. Samples were

pressed into a pellet with a diameter of 5 mm and fixed in a plastic tube. Data were corrected for the diamagnetic contribution to the susceptibility by means of Pascal's constants. All sample handling was done under a nitrogen atmosphere due to the air sensitivity of the samples.

**Elemental analyses** were carried out by the *Mikroanalytisches Labor Kolbe*, Oberhausen, Germany.

**Crystal structure determination.** Intensity data were collected with a *STOE IPDS-2T* diffractometer and an Oxford cooling system and corrected for absorption and other effects using Mo-K $\alpha$  radiation ( $\lambda = 0.71073 \text{ \AA}$ ). The diffraction frames were integrated using the *STOE X-Area* software package<sup>[8]</sup>, and most were corrected for absorption with *MULABS*<sup>[9]</sup> of the *PLATON* package<sup>[10]</sup>. The structure was solved by direct methods and refined by the full-matrix method based on  $F^2$  using the *SHELXTL* software package.<sup>[11,12]</sup> All non-hydrogen atoms were refined anisotropically, while the positions of all hydrogen atoms were generated with appropriate geometric constraints and allowed to ride on their respective parent carbon atoms with fixed isotropic thermal parameters. CCDC 2177572 (*mer*-[V(ddpd)<sub>2</sub>][BPh<sub>4</sub>]<sub>2</sub>) and 2177573 (*cis-fac*-[V(ddpd)<sub>2</sub>][PF<sub>6</sub>]<sub>2</sub>) contain the supplementary crystallographic data for this paper. These data are provided free of charge by The Cambridge Crystallographic Data Centre.

## Computational Details

**Static unrestricted Kohn-Sham orbitals DFT (UKS):** All calculations were performed with the quantum computing suite ORCA 5.0.1.<sup>[13]</sup> Unrestricted Kohn-Sham orbitals DFT (UKS) and the B3LYP functional<sup>[14]</sup> in combination with Ahlrichs' split-valence triple- $\zeta$  basis set def2-TZVPP for all atoms were employed in the geometry optimizations (Tables S3, S4, S11, S12).<sup>[15]</sup> Tight convergence criteria were chosen for geometry and frequency calculations (keywords `tightscf` and `tightopt`). All DFT-UKS calculations make use of the resolution of identity (Split-RI-J) approach for the Coulomb term in combination with the chain-of-spheres approximation for the exchange term (COSX).<sup>[16]</sup> The zero order relativistic approximation was used to describe relativistic effects in all calculations (keyword ZORA).<sup>[17,18]</sup> Grimme's empirical dispersion correction D3(BJ) was employed (keyword D3BJ).<sup>[19,20]</sup> A conductor-like screening model (keyword CPCM) modeling acetonitrile was used in all calculations to incorporate solvent effects.<sup>[21]</sup> Explicit solvent molecules and/or counter ions were neglected. TD-DFT calculations were conducted at the same level of theory using unrestricted Kohn-Sham orbitals (UKS). Seventy vertical spin-allowed transitions were calculated. The charge transfer number analyses of the time-dependent DFT (TD-DFT) calculated transitions were done using TheoDRE 2.2.<sup>[22,23]</sup>

**CASSCF(12,7)-SC-NEVPT2:** Calculations of ground- and excited-state properties of pure metal-centered (MC) states were performed using the complete-active-space self-consistent field method including spin-orbit coupling (SOC-CASSCF)<sup>[24,25]</sup> in conjunction with the strongly contracted N-electron valence perturbation theory to second order (SC-NEVPT2)<sup>[26,27]</sup> to recover missing dynamic electron correlation. SOC was treated through the mean-field (SOMF) approximation<sup>[28,29]</sup> and the effective Hamiltonian approach<sup>[30-32]</sup> was used to compute the spin-Hamiltonian parameters. An active space of (7,12) along with 10 quartet roots and 10 doublet roots was chosen (Tables S5 and S6). In addition to the minimal active space of (3,5), two occupied V–N  $\sigma$  bonding orbitals and a second d shell were included.

**MCD Spectrum:** The MCD spectrum of *mer*-[V(ddpd)<sub>2</sub>][BPh<sub>4</sub>]<sub>2</sub> was modelled using CASSCF methods with NEVPT2. As an active space a CAS(7,7) was chosen, after identifying orbitals with significant d orbital character. 10 quartet and 9 doublet roots were calculated. The best overlap with the experiment was obtained with the smallest basis set (def2-SVP). Additional larger basis sets (def2-TZVP and def2-TZVPP) resulted in a red shift of the calculated spectra.

**ZFS splitting:** From the CASSCF(12,7) (TZVPP basis) calculation of *cis-fac*-[V(ddpd)<sub>2</sub>]<sup>2+</sup>, the second-order spin-orbit coupling contribution and the effective Hamiltonian spin-orbital coupling as implemented in ORCA 5.0.1 yield  $D = -0.31 \text{ cm}^{-1}$ ,  $E = 0.10 \text{ cm}^{-1}$  and  $D = -0.32 \text{ cm}^{-1}$ ,  $E = -0.10 \text{ cm}^{-1}$ , respectively. These values change negligibly to  $D = -0.32 \text{ cm}^{-1}$ ,  $E = 0.10 \text{ cm}^{-1}$  and  $D = -0.33 \text{ cm}^{-1}$ ,  $E = 0.11 \text{ cm}^{-1}$ , respectively, after the NEVPT2 treatment. The corresponding calculated values for *mer*-[V(ddpd)<sub>2</sub>]<sup>2+</sup> are  $D = -0.28 \text{ cm}^{-1}$ ,  $E = -0.04 \text{ cm}^{-1}$ ,  $D = -0.27 \text{ cm}^{-1}$ ,  $E = -0.04 \text{ cm}^{-1}$  and  $D = -0.27 \text{ cm}^{-1}$ ,  $E = -0.04 \text{ cm}^{-1}$ ,  $D = -0.29 \text{ cm}^{-1}$ ,  $E = -0.05 \text{ cm}^{-1}$  after NEVPT2. Irrespective of the method employed and inclusion of the NEVPT2 treatment, the sign of  $D$  differs from the experimental values. This discrepancy might be a signature of the missing  $\pi$  accepting ligand orbitals and hence missing charge transfer contributions in the CASSCF calculations of the vanadium(II) complexes.

With a smaller basis set (def2-SVP) and a smaller active space CAS(7,7), as used for the MCD spectrum of *mer*-[V(ddpd)<sub>2</sub>][BPh<sub>4</sub>]<sub>2</sub>, a positive value  $D = 0.076 \text{ cm}^{-1}$  is obtained.

## Experimental details

**Synthesis of *cis-fac*-[V(ddpd)<sub>2</sub>][BPh<sub>4</sub>]<sub>2</sub>:** [V(NCCH<sub>3</sub>)<sub>6</sub>][BPh<sub>4</sub>]<sub>2</sub> (170 mg, 0.17 mmol, 1.0 eq) was suspended in acetonitrile (15 mL) under an argon atmosphere under vigorous stirring to yield a turquoise suspension. A pale yellow solution of ddpd (101.4 mg, 0.35 mmol, 2.0 eq.) in acetonitrile (2 mL) was added. Within two hours, a dark red solution formed, which was stirred for another 15 h. The solvent was removed under reduced pressure. A reddish-brown powder (143.5 mg) was isolated and washed with diethyl ether (2x15 mL). The product was recrystallized from an acetonitrile solution (3.5 mg mL<sup>-1</sup> CH<sub>3</sub>CN) via diethyl ether diffusion to yield small, dark red crystals in the course of several days. Yield: 143.5 mg (0.11 mmol, 66 %). C<sub>82</sub>H<sub>74</sub>B<sub>2</sub>N<sub>10</sub>V: Calcd. C 77.42; H 5.86; N 11.01 %; found: C 77.20; H 5.91; N 10.98 %. IR (ATR):  $\tilde{\nu}$  = 3052 (w), 3034 (w), 3006 (w), 2997 (w), 2980 (w), 2915 (w), 1592 (m), 1579 (m), 1332 (m), 1332 (m), 1484 (s), 1445 (s), 1432 (s), 1274 (w), 1193 (w), 1163 (m), 1133 (m), 1120 (m), 1084 (w), 1098 (w), 1012 (w), 946 (w), 864 (w), 844 (w), 794 (m), 779 (m), 774 (m), 732 (s), 704 (s), 675 (w), 623 (w), 612 (s), 584 (w), 560 (w), 495 (w), 467 (w), 438 (w), 421 (w), 412 (w) cm<sup>-1</sup>. MS (ESI<sup>+</sup>, CH<sub>3</sub>CN):  $m/z$  (%) = 292.1 (25) [ddpd+H]<sup>+</sup>, 316.6 (100) [M-2BPh<sub>4</sub>]<sup>2+</sup>, 952.4 (80) [M-BPh<sub>4</sub>]<sup>+</sup>. UV/Vis/NIR (CH<sub>3</sub>CN):  $\lambda$  ( $\epsilon$ ) = 303 (26400), 486 (4400 M<sup>-1</sup>cm<sup>-1</sup>) nm. CV ([<sup>n</sup>Bu<sub>4</sub>N][PF<sub>6</sub>]/CH<sub>3</sub>CN, vs. ferrocene):  $E_{1/2}$  = -0.20 (qrev.), -2.30 (qrev.) V.

**Synthesis of *cis-fac*-[V(ddpd)<sub>2</sub>][PF<sub>6</sub>]<sub>2</sub> for XRD analysis:** *cis-fac*-[V(ddpd)<sub>2</sub>][BPh<sub>4</sub>]<sub>2</sub> (20 mg, 0.016 mmol, 1.0 eq) was dissolved in acetonitrile (8 mL) under an argon atmosphere at room temperature while stirring to yield a dark red solution. [<sup>n</sup>Bu<sub>4</sub>N][PF<sub>6</sub>] (31 mg, 0.03 mmol, 5.0 eq.) was added to the solution. The solution was stirred for a few minutes before filtering through a syringe filter (0.3  $\mu$ m pore size). Slow diffusion of diethyl ether into the solution yielded small, dark crystal platelets after one week. The crystals were re-dissolved in acetonitrile (6 mL) and the process was repeated with another batch of [<sup>n</sup>Bu<sub>4</sub>N][PF<sub>6</sub>] (30 mg, 0.03 mmol, 5. eq.), stirring, filtration and crystallization by ether diffusion. Crystals of *cis-fac*-[V(ddpd)<sub>2</sub>][PF<sub>6</sub>]<sub>2</sub> were obtained suitable for XRD analysis.

**Synthesis of *mer*-[V(ddpd)<sub>2</sub>][BPh<sub>4</sub>]<sub>2</sub>:** [V(NCCH<sub>3</sub>)<sub>6</sub>][BPh<sub>4</sub>]<sub>2</sub> (380 mg, 0.41 mmol, 1.0 eq) was suspended in acetonitrile (30 mL) under an argon atmosphere while stirring to yield a turquoise suspension. A pale yellow solution of ddpd (243 mg, 0.83 mmol, 2.0 eq.) in acetonitrile (10 mL) was added after a few minutes. The reaction mixture was heated to reflux for 17 h before cooling to ambient temperature. The solvent volume was reduced to approximately 10 mL under reduced pressure. Diethyl ether (50 mL) was added and a dark solid precipitated. The solid was collected on a glass frit under an argon atmosphere and washed with diethyl ether (2x15 mL). Yield: 330 mg (0.26 mmol, 63 %). The product was recrystallized as dark red crystals from acetonitrile via diethyl ether diffusion. C<sub>82</sub>H<sub>74</sub>B<sub>2</sub>N<sub>10</sub>V: Calcd. C 77.42; H 5.86; N 11.01 %; found: C 77.06; H 5.83; N 10.95 %. IR (ATR):  $\tilde{\nu}$  = 3052 (w), 3034 (w), 3006 (w) 2998 (w), 2981 (w), 2902 (w), 1599 (m), 1589 (m), 1577 (m), 1564 (m), 1480 (m), 1445 (m), 1428 (s), 1360 (m), 1331 (m), 1308 (w), 1266 (w), 1251 (w), 1231 (m), 1190 (vw), 1167 (m), 1129 (m), 1094 (m), 1082 (w), 1061 (w), 1033 (w), 1013 (w), 944 (w), 859 (w), 845 (w), 801 (m), 775 (m), 745 (m), 732 (s), 704 (s), 645 (w), 623 (w), 611 (s), 581 (m), 522 (vw), 509 (w), 468 (w), 457 (w), 432 (w), 427 (w) cm<sup>-1</sup>. MS (ESI<sup>+</sup>, CH<sub>3</sub>CN):  $m/z$  (%) = 316.6 (100) [M-2BPh<sub>4</sub>]<sup>2+</sup>, 952.4 (16) [M-BPh<sub>4</sub>]<sup>+</sup>. UV/Vis/NIR (CH<sub>3</sub>CN):  $\lambda$  ( $\epsilon$ ) = 308 (27200), 490 (4400 M<sup>-1</sup>cm<sup>-1</sup>) nm. CV ([<sup>n</sup>Bu<sub>4</sub>N][PF<sub>6</sub>]/CH<sub>3</sub>CN, vs. ferrocene):  $E_{1/2}$  = -0.28 (qrev.), -2.31 (qrev.) V.

**Chemical oxidation and back-reduction of *cis-fac*-[V(ddpd)<sub>2</sub>][BPh<sub>4</sub>]<sub>2</sub>:** A solution of *cis-fac*-[V(ddpd)<sub>2</sub>][BPh<sub>4</sub>]<sub>2</sub> (4.3 mg, 3.4 mmol, 2 eq.) in acetonitrile (2 mL) was prepared under an argon atmosphere (0.0017 M). The solution was split in two parts A and B of 1 mL volume each. A sample of A (100 μL) was diluted with acetonitrile (2.9 mL), filled into an inert gas cell and an absorption spectrum was recorded. To oxidize the complex, a silver tetrafluoroborate solution in acetonitrile (30 μL, 0.17 M, 3 eq.) was added to solution B while stirring. The color changed immediately from dark red to green and a solid precipitated. The mixture was stirred for 20 min. A sample of B/Ag[BF<sub>4</sub>] (100 μL) was diluted with acetonitrile (2.9 mL), filtered through a syringe filter (0.3 μm pore size) into an inert gas cell and an absorption spectrum was recorded. A cobaltocene solution in acetonitrile (43 μL, 0.11 M, 3.1 eq.) was added to B/Ag[BF<sub>4</sub>]. The solution assumed a brownish red color. A sample of this solution B (100 μL) was diluted with acetonitrile (2.9 mL), filtered through a syringe filter (0.3 μm pore size) into an inert gas cell and an absorption spectrum was recorded. An analogous oxidation procedure with Ag[BF<sub>4</sub>] was performed in butyronitrile to record an emission spectrum at 78 K.

**Chemical oxidation and back-reduction of *mer*-[V(ddpd)<sub>2</sub>][BPh<sub>4</sub>]<sub>2</sub>:** A solution of *mer*-[V(ddpd)<sub>2</sub>][BPh<sub>4</sub>]<sub>2</sub> (4.1 mg, 3.1 mmol, 2 eq.) in acetonitrile (2 mL) was prepared under an argon atmosphere (0.0016 M). The solution was split in two parts A and B of 1 mL volume each. A sample of A (100 μL) was diluted with acetonitrile (2.9 mL), filled into an inert gas cell and an absorption spectrum was recorded. To oxidize the complex, a silver tetrafluoroborate solution in acetonitrile (28 μL, 0.17 M, 3 eq.) was added to solution B while stirring. The color changed immediately from dark red to bluish green and a solid precipitated. The mixture was stirred for 20 min. A sample of B/Ag[BF<sub>4</sub>] (100 μL) was diluted with acetonitrile (2.9 mL), filtered through a syringe filter (0.3 μm pore size) into an inert gas cell and an absorption spectrum was recorded. A cobaltocene solution in acetonitrile (41 μL, 0.11 M, 3.1 eq.) was added to B/Ag[BF<sub>4</sub>]. The solution assumed a dark red color. The mixture was stirred for 20 min. A sample of this solution B (100 μL) was diluted with acetonitrile (2.9 mL), filtered through a syringe filter (0.3 μm pore size) into an inert gas cell and an absorption spectrum was recorded. An analogous oxidation procedure with Ag[BF<sub>4</sub>] was performed in butyronitrile to record an emission spectrum at 78 K.

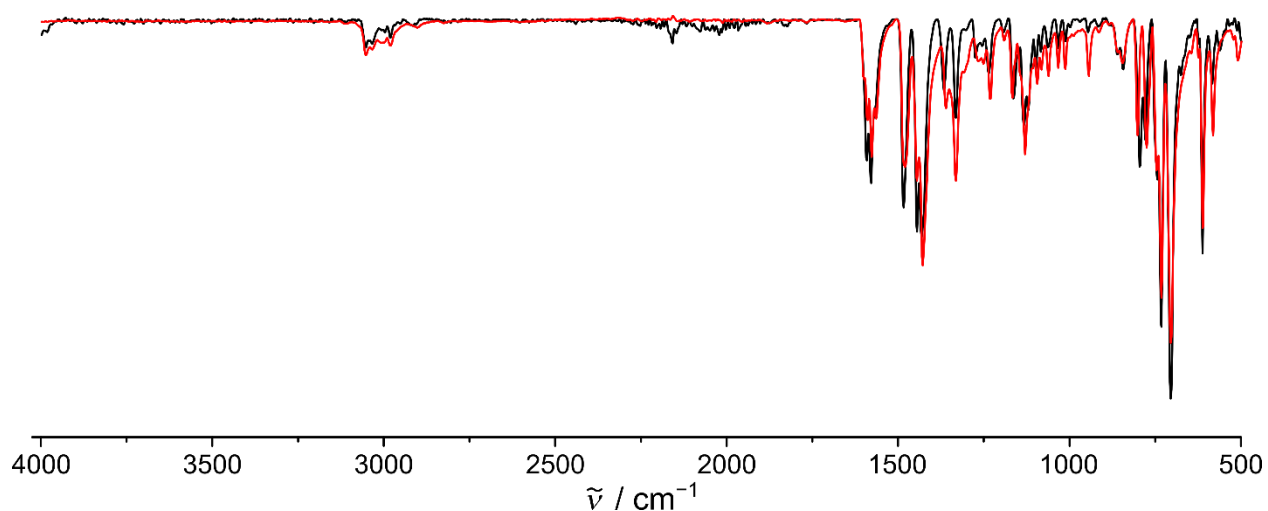


**Figure S1.** ATR-IR spectra of *cis-fac*-[V(ddpd)<sub>2</sub>][BPh<sub>4</sub>]<sub>2</sub> (black) and *mer*-[V(ddpd)<sub>2</sub>][BPh<sub>4</sub>]<sub>2</sub> (red).

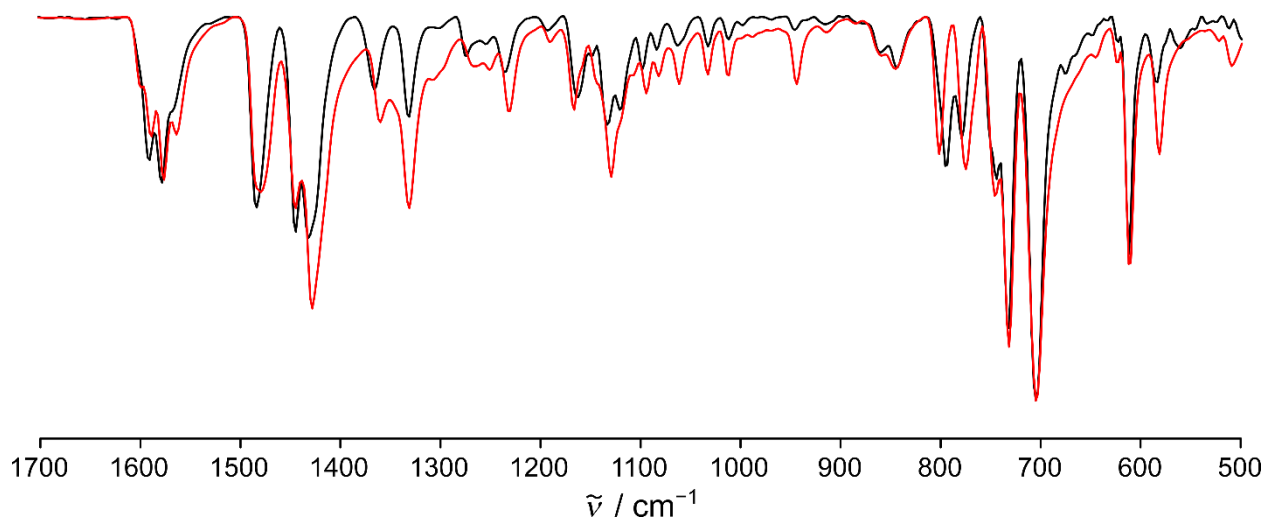


**Figure S2.** ATR-IR spectra of *cis-fac*-[V(ddpd)<sub>2</sub>][BPh<sub>4</sub>]<sub>2</sub> (black) and *mer*-[V(ddpd)<sub>2</sub>][BPh<sub>4</sub>]<sub>2</sub> (red) between 1700 and 500  $\text{cm}^{-1}$ .

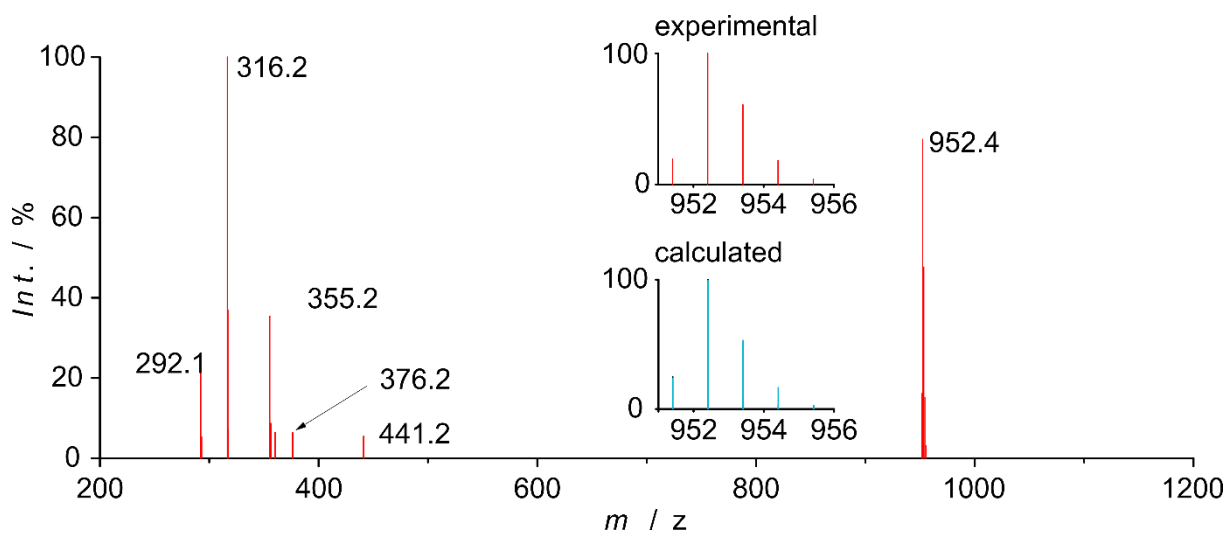


**Figure S3.** ESI<sup>+</sup> mass spectrum of *cis-fac*-[V(ddpd)<sub>2</sub>][BPh<sub>4</sub>]<sub>2</sub> in acetonitrile.

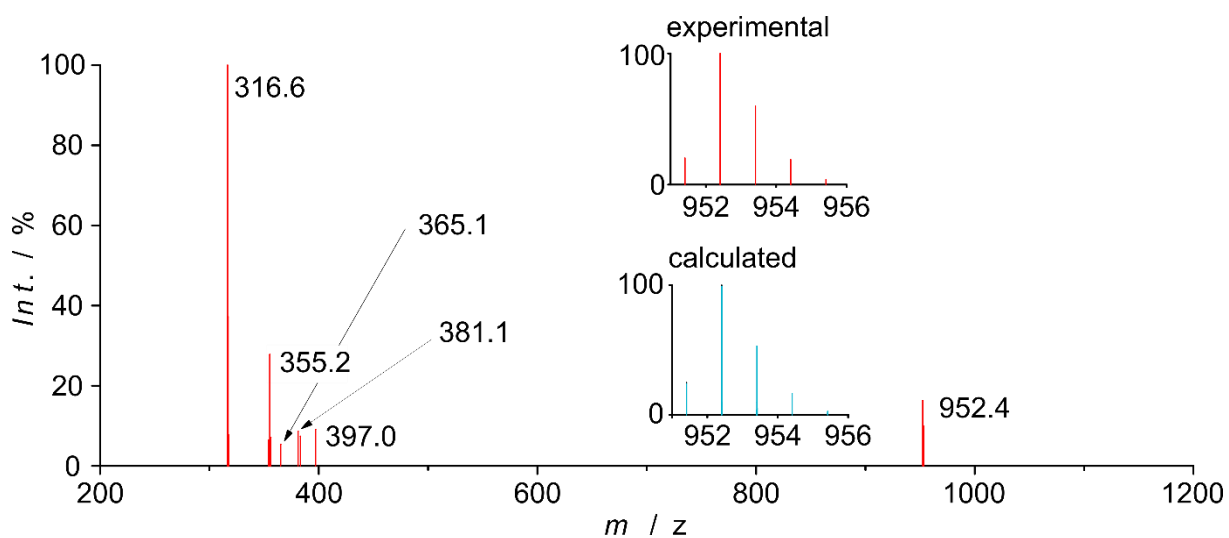


**Figure S4.** ESI<sup>+</sup> mass spectrum of *mer*-[V(ddpd)<sub>2</sub>][BPh<sub>4</sub>]<sub>2</sub> in acetonitrile.



**Table S1.** Selected bond distances / Å and bond angles / ° of *cis-fac*-[V(ddpd)<sub>2</sub>]<sup>2+</sup> (XRD analysis of *cis-fac*-[V(ddpd)<sub>2</sub>][PF<sub>6</sub>]<sub>2</sub> and DFT-UKS calculation of *cis-fac*-[V(ddpd)<sub>2</sub>]<sup>2+</sup>).

	V-N1/ V-N2/ V-N3	N1-V-N3/ N1-V-N8/ N3-V-N5	V-N4/ V-N5/ V-N6	N6-V-N8/ N6-V-N5/ N8-V-N10/	Shape parameter S(OC-6) of the [VN <sub>6</sub> ] polyhedron <sup>[33]</sup>
	2.165(3)	81.67(9)	2.172(3)	79.88(9)	
XRD	2.126(2)	176.15(9)	2.141(3)	165.63(9)	0.88
	2.154(2)	81.63(9)	2.139(2)	83.13(9)	
	2.159	81.65	2.160	81.49	
DFT-UKS	2.151	174.11	2.155	169.65	0.79
	2.160	81.32	2.158	81.44	

**Table S2.** Selected bond distances / Å and angles / ° of *mer*-[V(ddpd)<sub>2</sub>]<sup>2+</sup> (XRD analysis of *mer*-[V(ddpd)<sub>2</sub>][BPh<sub>4</sub>]<sub>2</sub> and DFT-UKS calculation of *mer*-[V(ddpd)<sub>2</sub>]<sup>2+</sup>).

	V-N1/ V-N3/ V-N5	N1-V-N3/ N1-V-N5/ N3-V-N5	V-N6/ V-N8/ V-N10	N6-V-N8/ N6-V-N10/ N8-V-N10/	Shape parameter S(OC-6) of the [VN <sub>6</sub> ] polyhedron <sup>[33]</sup>
	2.120(2)	86.24(7)	2.120(2)	85.52(7)	
XRD	2.094(2)	171.47(7)	2.084(2)	171.08(7)	0.40
	2.117(2)	85.35(7)	2.120(2)	85.62(7)	
	2.137	84.80	2.146	84.56	
DFT-UKS	2.124	169.22	2.117	168.90	0.61
	2.145	84.46	2.147	84.34	

**Table S3.** Cartesian Coordinates of the DFT-UKS calculated ground state geometry of *cis-fac*-[V(ddpd)<sub>2</sub>]<sup>2+</sup>.

Atomic number	x	y	z
23	3.82062	9.31453	15.05076
7	4.7576	7.41266	15.46071
7	6.64681	8.12095	14.21054
7	4.7476	9.00359	13.13523
7	2.74792	9.68181	12.08862
7	2.14037	8.43761	14.01402
7	5.52624	10.42397	15.77568
7	5.22269	11.95039	13.98412
7	3.07569	11.30685	14.70494
7	1.00366	10.68695	15.6385
7	2.68667	9.55399	16.87123
6	4.15858	6.47512	16.22098
1	3.16472	6.70717	16.56771
6	4.75706	5.28941	16.58628
1	4.22657	4.58748	17.21163
6	6.04753	5.03998	16.13076
1	6.55737	4.12066	16.38247
6	6.66938	5.97856	15.32995
1	7.65666	5.79268	14.93941
6	5.99875	7.16056	15.00245
6	8.10552	8.19891	14.32459
1	8.62432	7.48923	13.67802
1	8.3809	8.00619	15.35659
1	8.42014	9.20715	14.06821
6	6.05745	8.6902	13.08241
6	6.82616	8.95865	11.95014
1	7.87443	8.71777	11.91846
6	6.19637	9.50496	10.8462
1	6.76612	9.71037	9.95068
6	4.83263	9.74088	10.86125
1	4.3337	10.10858	9.98183
6	4.12503	9.45574	12.02834
6	2.16714	10.55891	11.06824
1	2.80604	11.42914	10.95391
1	1.195	10.8945	11.41503
1	2.0535	10.06944	10.0994
6	1.86235	8.81933	12.75548
6	0.68557	8.4115	12.11735
1	0.48535	8.71471	11.10307
6	-0.20584	7.59633	12.7879
1	-1.11555	7.27559	12.30006
6	0.09223	7.18787	14.08375
1	-0.57307	6.55384	14.6499
6	1.27081	7.62731	14.64485
1	1.52314	7.3577	15.65756
6	6.25526	9.9962	16.82308
1	5.89342	9.11348	17.32529
6	7.4269	10.59398	17.23241
1	7.97496	10.19109	18.07059

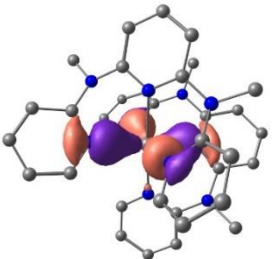
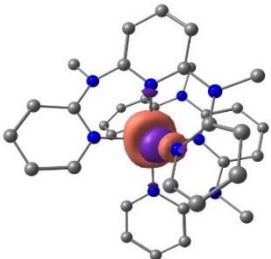
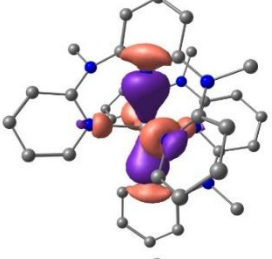
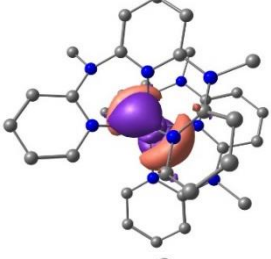
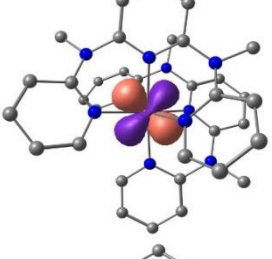
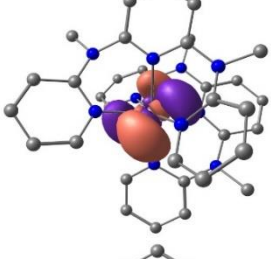
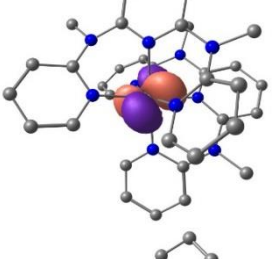
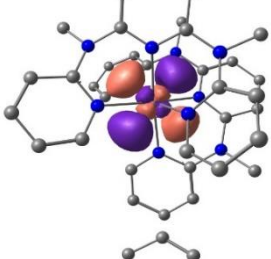
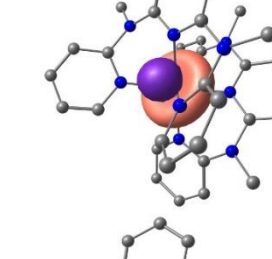
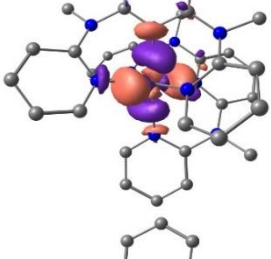
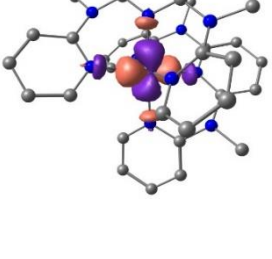
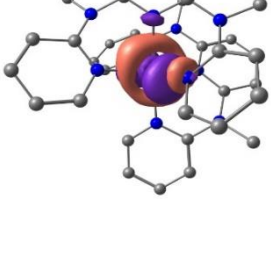
6	7.87139	11.70967	16.5307
1	8.77998	12.22044	16.81703
6	7.12733	12.1716	15.46218
1	7.44046	13.04969	14.92191
6	5.95062	11.50691	15.10194
6	5.98692	12.62267	12.92971
1	5.45043	12.52013	11.99133
1	6.94569	12.12422	12.82894
1	6.15305	13.68229	13.13191
6	3.84605	12.17739	14.0219
6	3.2909	13.25236	13.3287
1	3.90728	13.93991	12.77651
6	1.92115	13.43828	13.39601
1	1.46662	14.26903	12.87435
6	1.1359	12.60032	14.16737
1	0.08028	12.78215	14.26847
6	1.75619	11.54662	14.83918
6	-0.44709	10.66722	15.43165
1	-0.64544	10.64883	14.36339
1	-0.9535	11.52678	15.874
1	-0.845	9.7568	15.8682
6	1.47918	10.15029	16.8444
6	0.67244	10.2095	17.98498
1	-0.28391	10.70496	17.94449
6	1.12181	9.6558	19.16846
1	0.50457	9.70041	20.05476
6	2.38014	9.06348	19.20341
1	2.77928	8.62231	20.10418
6	3.12006	9.04627	18.04168
1	4.09349	8.58357	18.02706

**Table S4.** Cartesian Coordinates of the DFT-UKS calculated ground state geometry of *mer*-[V(ddpd)<sub>2</sub>]<sup>2+</sup>.

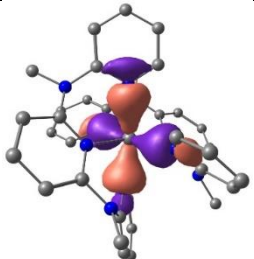
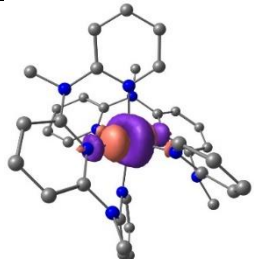
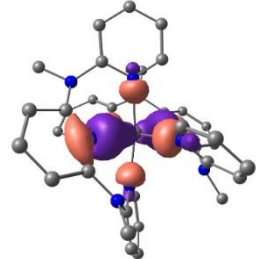
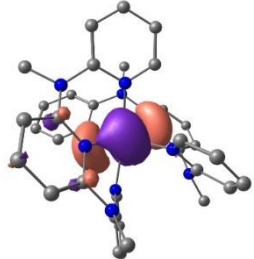
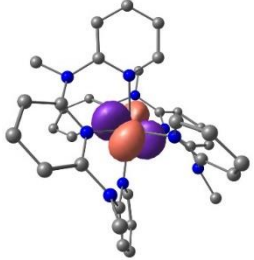
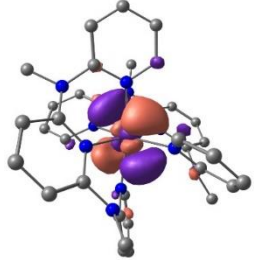
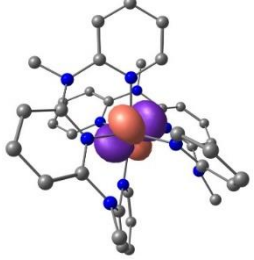
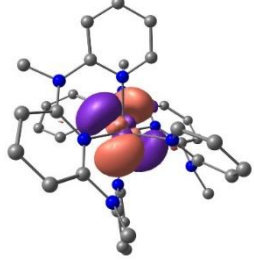
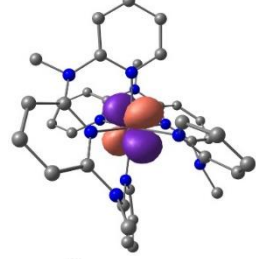
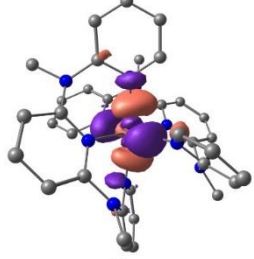
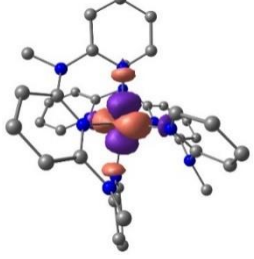
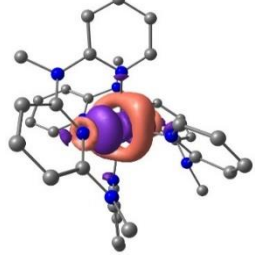
Atomic number	x	y	z
23	-0.456657	4.889414	1.501596
7	0.002849	4.363064	3.520798
7	0.579771	2.20372	2.770289
7	1.205219	3.662114	1.007041
7	1.774298	5.179912	-0.727343
7	-0.580795	5.215553	-0.614454
7	-1.914519	3.3183	1.393928
7	-3.03067	4.29052	3.231535
7	-2.106649	6.111055	2.017284
7	-1.128961	7.889116	0.781278
7	0.677804	6.700074	1.711039
6	-0.18162	5.248191	4.518065
1	-0.419586	6.25608	4.212581
6	-0.108396	4.903625	5.849081
1	-0.280011	5.647244	6.612408
6	0.181414	3.579764	6.167635
1	0.250665	3.262032	7.198754
6	0.407998	2.669189	5.15302
1	0.67458	1.651648	5.386263
6	0.332973	3.09674	3.822299
6	0.389044	0.778073	3.046087
1	-0.531625	0.656157	3.610789
1	1.211872	0.332657	3.607898
1	0.282329	0.257062	2.099107
6	1.442841	2.531668	1.707084
6	2.500786	1.685662	1.390125
1	2.682826	0.795538	1.968956
6	3.341279	2.032926	0.345779
1	4.173144	1.394093	0.084095
6	3.113965	3.200514	-0.362986
1	3.745404	3.473547	-1.192414
6	2.026788	3.993653	-0.011811
6	2.938799	5.878704	-1.279513
1	2.671387	6.920044	-1.437124
1	3.292525	5.456417	-2.221666
1	3.740441	5.835385	-0.548526
6	0.536529	5.429059	-1.33003
6	0.471854	5.912003	-2.642369
1	1.373187	6.085345	-3.20664
6	-0.763325	6.135065	-3.219733
1	-0.821574	6.498724	-4.236047
6	-1.91929	5.873206	-2.489019
1	-2.902283	6.031024	-2.906123
6	-1.777402	5.413811	-1.198759
1	-2.638793	5.214646	-0.578779
6	-1.771112	2.308952	0.514674
1	-1.029992	2.461715	-0.256462
6	-2.479641	1.131217	0.598473

1	-2.310135	0.343619	-0.12029
6	-3.391145	0.9904	1.642219
1	-3.960784	0.079147	1.759916
6	-3.580004	2.034638	2.526336
1	-4.307656	1.951042	3.31643
6	-2.839566	3.212283	2.363309
6	-3.63378	4.007764	4.538652
1	-3.163692	3.118763	4.950739
1	-4.713282	3.851889	4.49463
1	-3.424752	4.844854	5.197094
6	-3.104771	5.622353	2.783754
6	-4.187905	6.409405	3.162476
1	-4.988368	5.99186	3.750045
6	-4.230034	7.729316	2.749197
1	-5.058316	8.36156	3.036328
6	-3.205925	8.236539	1.967697
1	-3.2115	9.267466	1.654612
6	-2.157084	7.397038	1.609928
6	-1.520622	8.890705	-0.213993
1	-0.802523	8.868329	-1.02998
1	-1.565623	9.902435	0.193293
1	-2.495357	8.620758	-0.608911
6	0.220145	7.824241	1.134393
6	1.083431	8.894836	0.866941
1	0.718821	9.787759	0.387671
6	1.957327	6.647974	2.122946
6	2.406925	8.808105	1.254718
6	2.857105	7.668741	1.917629
1	2.257271	5.728128	2.602878
1	3.877891	7.569736	2.254018
1	3.07735	9.6324	1.054878

**Table S5.** Active orbitals of the CASSCF(7,12)-SC-NEVPT2 calculation on *cis-fac*-[V(ddpd)<sub>2</sub>]<sup>2+</sup>, depicted at a contour value of 0.05 a.u. (hydrogen atoms omitted for clarity).

#	<i>E</i> / Ha	orbital	#	<i>E</i> / Ha	orbital
161	-0.53303		167	0.26023	
162	-0.53288		168	0.72996	
163	0.05837		169	0.87278	
164	0.05975		170	0.91617	
165	0.08981		171	1.33304	
166	0.25441		172	1.44659	

**Table S6.** Active orbitals of the CASSCF(7,12)-SC-NEVPT2 calculation on *mer*-[V(ddpd)<sub>2</sub>]<sup>2+</sup>, depicted at a contour value of 0.05 a.u. (hydrogen atoms omitted for clarity).

#	$E / \text{Ha}$	orbital	#	$E / \text{Ha}$	orbital
161	-0.53329		167	0.28845	
162	-0.60713		168	0.77731	
163	0.05634		169	0.76222	
164	0.08107		170	0.90960	
165	0.08650		171	1.19279	
166	0.24438		172	1.51408	

**Figure S5:** Energy diagram of the electronic states of *cis-fac*-[V(ddpd)<sub>2</sub>]<sup>2+</sup> constructed from CASSCF(7,12)-SC-NEVPT2 energies with spin densities in orange (0.01 a.u. isosurface value, hydrogen atoms omitted for clarity, quartet states in blue, doublet states in red; a coordinate system referring to the displayed structures and d orbital labels are shown in the bottom right corner).

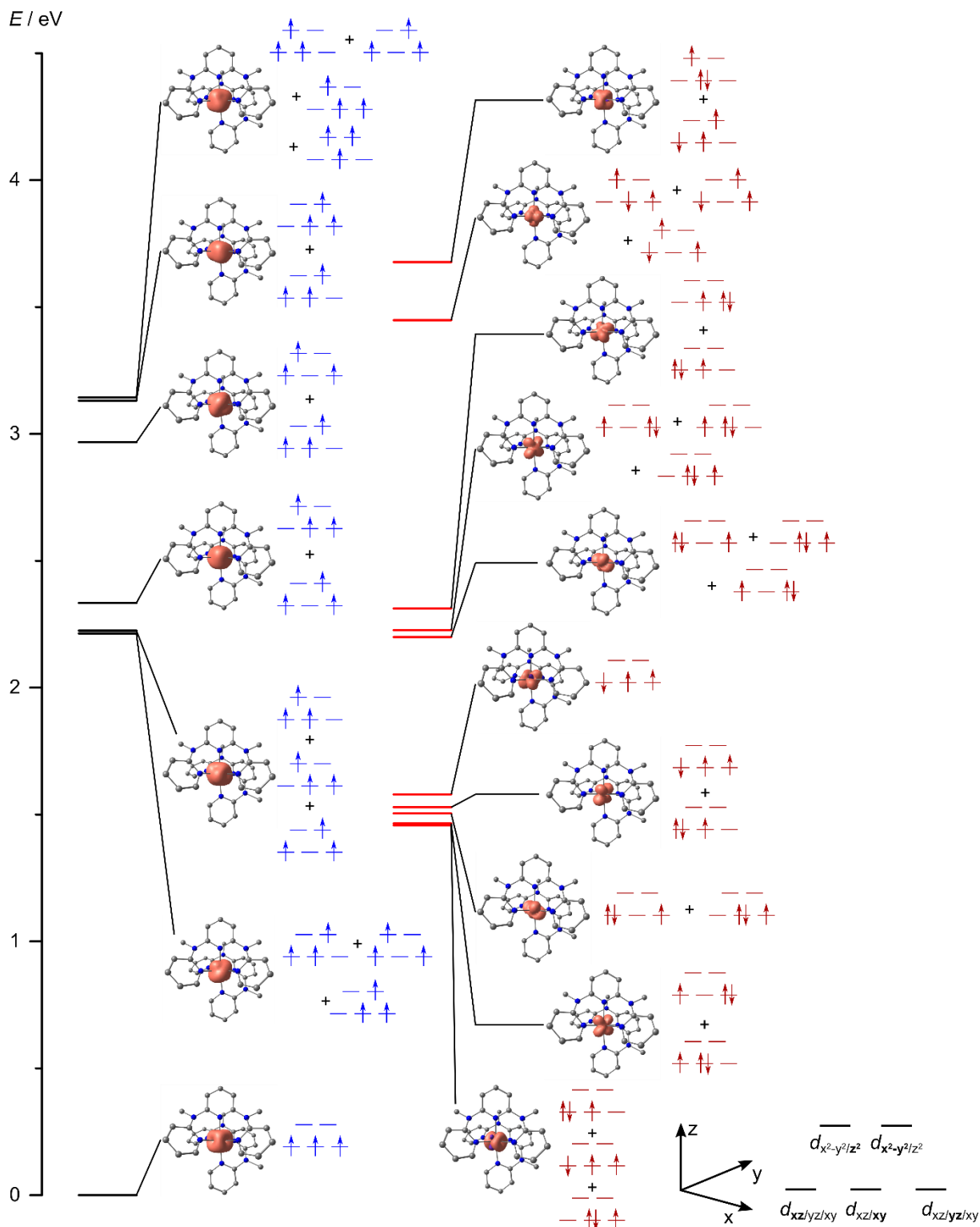




**Figure S6:** Energy diagram of the electronic states of  $mer-[V(ddpd)_2]^{2+}$  constructed from CASSCF(7,12)-SC-NEVPT2 energies with spin densities in orange (0.01 a.u. isosurface value, hydrogen atoms omitted for clarity, quartet states in blue, doublet states in red; a coordinate system referring to the displayed structures and d orbital labels are shown in the bottom right corner).

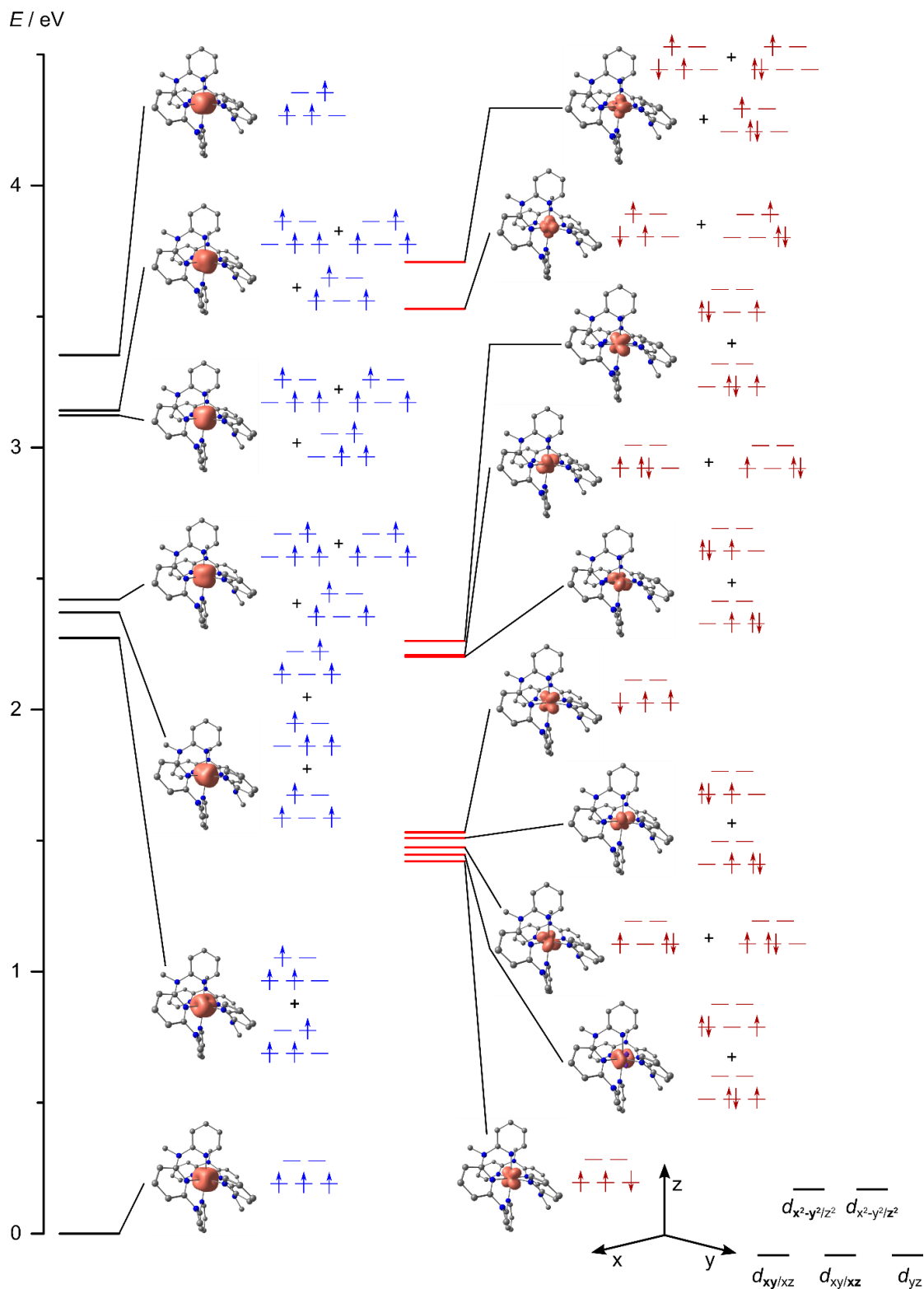


**Figure S7.** Proposed energy level diagram of *cis-fac*-[V(ddpd)<sub>2</sub>]<sup>2+</sup> with the pure metal centred states (black and red) obtained from the CASSCF-NEVPT2 calculation, the <sup>4</sup>MLCT states (blue) estimated from the experimental absorption spectrum and the TD-DFT calculation and the <sup>2</sup>MLCT states (pale blue) set to the <sup>4</sup>MLCT energies. The mixing between <sup>2</sup>E and <sup>2</sup>MLCT states (purple) is set to an arbitrary value. (i) Spin density of the <sup>4</sup>A<sub>2</sub> ground state from the CASSCF-NEVPT2 calculation. (ii) Difference electron density of the lowest <sup>4</sup>MLCT state obtained from the TD-DFT calculation (isosurface value of 0.003 a.u.; purple = electron depletion; orange = electron density gain). (iii) Spin density of the lowest <sup>4</sup>T<sub>2</sub> derived state from the CASSCF-NEVPT2 calculation. (iv) Spin density of the lowest <sup>2</sup>E derived state from the CASSCF-NEVPT2 calculation. (v) Spin density of the optimized lowest doublet state (<sup>2</sup>MC/<sup>2</sup>MLCT) from a DFT geometry optimization calculation with the ligand contributions highlighted by arrows. All spin densities at an isosurface value of 0.006 a.u., except (iv) at an isosurface value of 0.0035 a.u.

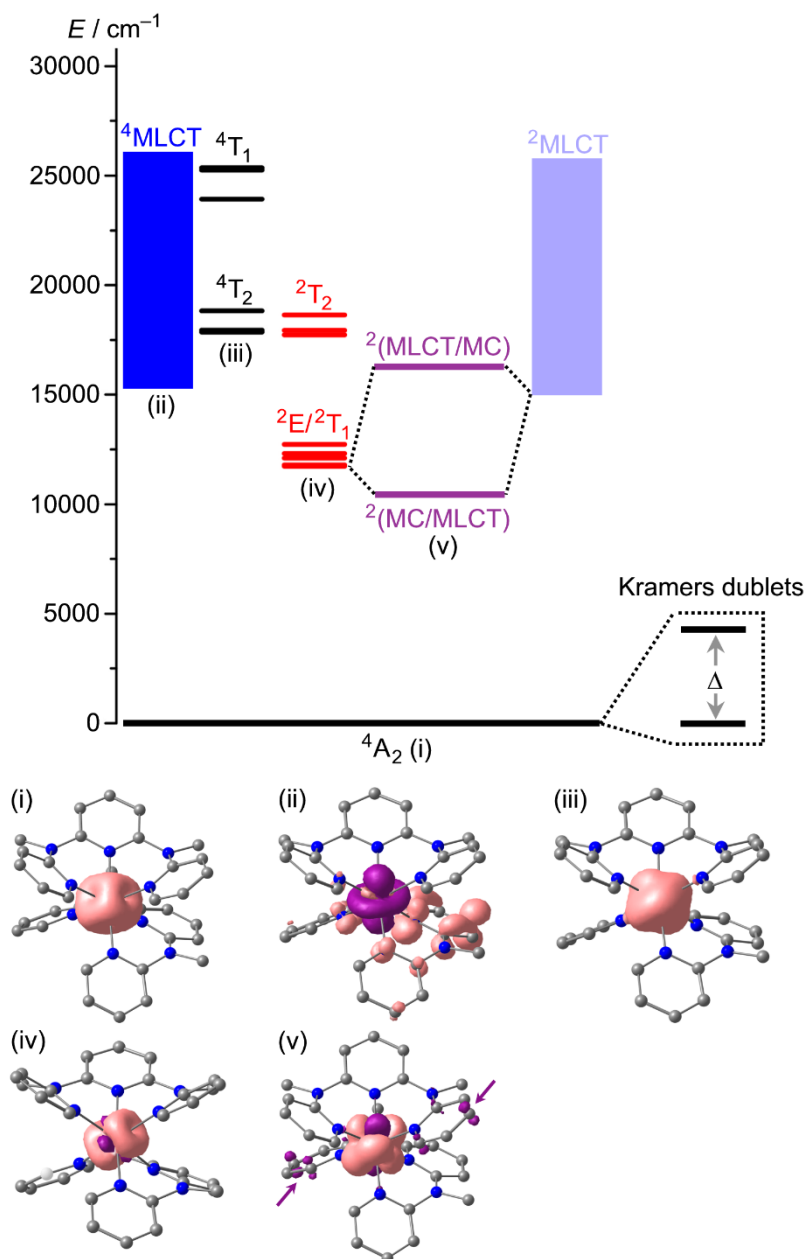


**Figure S8.** Emission spectra of a) *cis-fac*-[V(ddpd)<sub>2</sub>][BPh<sub>4</sub>]<sub>2</sub> and b) *mer*-[V(ddpd)<sub>2</sub>][BPh<sub>4</sub>]<sub>2</sub> in acetonitrile at room temperature during irradiation with a xenon lamp at 300±5 nm excitation wavelength for 300 min. The insets show the emission intensity at the maximum wavelength (395 nm).

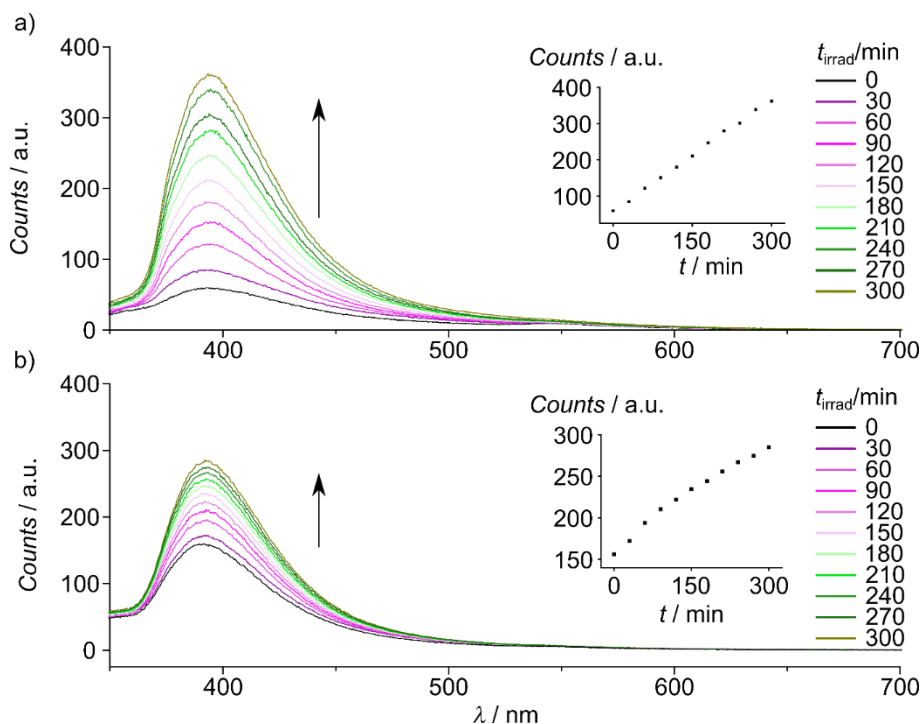


**Figure S9.** Excitation and emission spectra (solid and dotted lines) of *cis-fac*-[V(ddpd)<sub>2</sub>][BPh<sub>4</sub>]<sub>2</sub> (red) and *mer*-[V(ddpd)<sub>2</sub>][BPh<sub>4</sub>]<sub>2</sub> (blue) and excitation spectrum of ddpd (green) in acetonitrile at room temperature with 300 nm excitation.

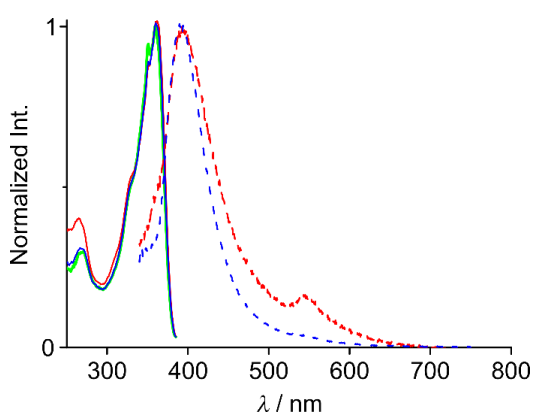


**Figure S10.** Absorption spectra of a) *cis-fac*-[V(ddpd)<sub>2</sub>][BPh<sub>4</sub>]<sub>2</sub> and b) *mer*-[V(ddpd)<sub>2</sub>][BPh<sub>4</sub>]<sub>2</sub> in acetonitrile at room temperature before and after irradiating for 300 min with a xenon lamp at 300±5 nm excitation wavelength.

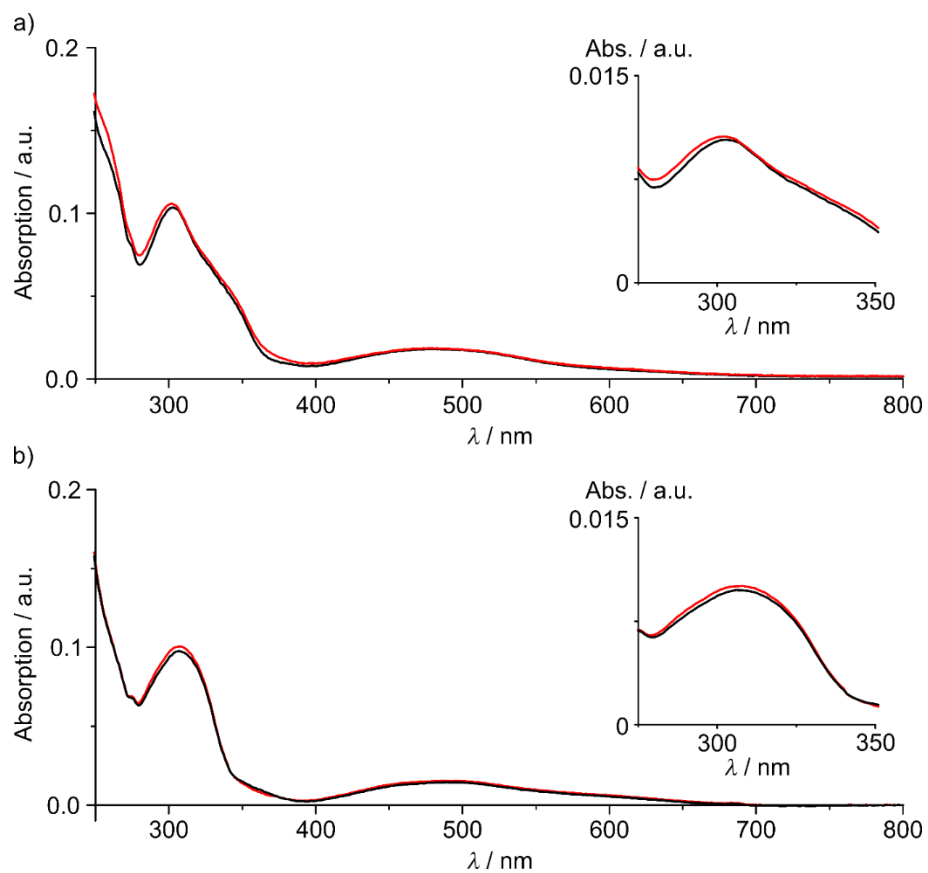


**Table S7.** TD-DFT calculated spin-allowed quartet-quartet transitions of *cis-fac*-[V(ddpd)<sub>2</sub>]<sup>2+</sup>. The assignment was accomplished by evaluation of the transition difference densities with the TheoDRE software package (v2.4).<sup>[22,23]</sup>

State	$E / \text{cm}^{-1}$	$\lambda / \text{nm}$	$E / \text{eV}$	$f_{\text{osc.}}$	Assignment
1	16119	620	1.998	1.00E-2	<sup>4</sup> MLCT
2	16215	617	2.010	1.15E-2	<sup>4</sup> MLCT
3	17743	564	2.200	2.73E-2	<sup>4</sup> MLCT
4	18228	549	2.260	8.47E-4	<sup>4</sup> MLCT
5	18440	542	2.286	6.16E-3	<sup>4</sup> MLCT
6	18636	537	2.311	1.21E-2	<sup>4</sup> MLCT
7	18737	534	2.323	5.27E-2	<sup>4</sup> MLCT
8	19157	522	2.375	5.80E-3	<sup>4</sup> MLCT
9	19425	515	2.408	2.52E-3	<sup>4</sup> MLCT
10	19489	513	2.416	7.54E-4	<sup>4</sup> MLCT
11	19566	511	2.426	1.94E-4	<sup>4</sup> MLCT
12	19869	503	2.463	3.21E-3	<sup>4</sup> MLCT
13	20479	488	2.539	3.16E-3	<sup>4</sup> MLCT
14	20678	484	2.564	1.36E-2	<sup>4</sup> MLCT
15	20725	483	2.570	4.81E-3	<sup>4</sup> MLCT
16	21000	476	2.604	7.71E-3	<sup>4</sup> MLCT
17	21259	470	2.636	6.54E-3	<sup>4</sup> MLCT
18	21863	457	2.711	1.90E-3	<sup>4</sup> MLCT
19	21901	457	2.715	1.38E-4	<sup>4</sup> MLCT
20	21954	456	2.722	3.69E-3	<sup>4</sup> MLCT
21	22978	435	2.849	1.96E-3	<sup>4</sup> MLCT
22	23277	430	2.886	4.75E-3	<sup>4</sup> MLCT
23	24284	412	3.011	8.81E-3	<sup>4</sup> MLCT
24	24426	409	3.028	2.25E-4	<sup>4</sup> MLCT
25	25025	400	3.103	4.46E-4	<sup>4</sup> MLCT
26	25259	396	3.132	9.68E-4	<sup>4</sup> MLCT
27	25329	395	3.140	5.12E-3	<sup>4</sup> MLCT
28	25439	393	3.154	3.49E-4	<sup>4</sup> MLCT
29	25853	387	3.205	3.48E-5	<sup>4</sup> MLCT
30	26420	379	3.276	2.14E-3	<sup>4</sup> LC
31	26610	376	3.299	8.98E-4	<sup>4</sup> LC
32	26631	376	3.302	8.90E-4	<sup>4</sup> MLCT
33	27027	370	3.351	3.61E-3	<sup>4</sup> MLCT
34	27579	363	3.419	6.41E-5	<sup>4</sup> LC
35	27724	361	3.437	4.35E-5	<sup>4</sup> LC
36	27840	359	3.452	4.17E-3	<sup>4</sup> MLCT
37	27886	359	3.457	2.55E-4	<sup>4</sup> MLCT
38	27925	358	3.462	9.53E-5	<sup>4</sup> MLCT
39	28305	353	3.509	1.90E-4	<sup>4</sup> MLCT
40	28361	353	3.516	8.42E-4	<sup>4</sup> LC
41	28466	351	3.529	8.85E-4	<sup>4</sup> LC
42	28744	348	3.564	3.62E-4	<sup>4</sup> MLCT
43	28802	347	3.571	2.37E-4	<sup>4</sup> MLCT

44	28843	347	3.576	1.96E-3	<sup>4</sup> MLCT
45	30157	332	3.739	3.35E-3	<sup>4</sup> LC
46	30257	331	3.751	1.29E-3	<sup>4</sup> LC
47	30266	330	3.753	1.07E-4	<sup>4</sup> MLCT
48	30395	329	3.769	2.36E-4	<sup>4</sup> MLCT
49	30479	328	3.779	8.11E-3	<sup>4</sup> LC
50	30684	326	3.804	1.52E-2	<sup>4</sup> LC
51	30694	326	3.806	3.54E-4	<sup>4</sup> MLCT
52	30722	326	3.809	1.55E-3	<sup>4</sup> LC
53	30902	324	3.831	5.82E-2	<sup>4</sup> LC
54	31368	319	3.889	7.06E-3	<sup>4</sup> MLCT
55	31447	318	3.899	6.30E-3	<sup>4</sup> MLCT
56	31626	316	3.921	1.32E-3	<sup>4</sup> LC
57	31756	315	3.937	6.46E-2	<sup>4</sup> LC
58	31776	315	3.940	1.99E-3	<sup>4</sup> LC
59	31786	315	3.941	4.50E-2	<sup>4</sup> LLCT
60	31837	314	3.947	6.20E-4	<sup>4</sup> LLCT
61	32144	311	3.985	5.00E-2	<sup>4</sup> LLCT
62	32227	310	3.996	1.42E-2	<sup>4</sup> LC
63	32279	310	4.002	3.99E-2	<sup>4</sup> LLCT
64	32446	308	4.023	4.09E-2	<sup>4</sup> LC
65	32595	307	4.041	2.16E-2	<sup>4</sup> LC
66	32723	306	4.057	5.44E-3	<sup>4</sup> LLCT
67	32744	305	4.060	2.25E-2	<sup>4</sup> LC
68	33212	301	4.118	4.52E-3	<sup>4</sup> LC
69	33223	301	4.119	5.40E-2	<sup>4</sup> LC
70	33333	300	4.133	4.71E-2	<sup>4</sup> LC

**Table S8.** TD-DFT calculated spin-allowed quartet-quartet transitions of *mer*-[V(ddpd)<sub>2</sub>]<sup>2+</sup>. The assignment was accomplished by evaluation of the transition difference densities with the TheoDRE software package (v2.4).<sup>[22,23]</sup>

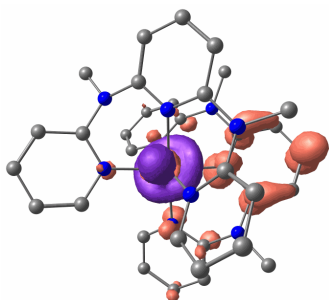
State	$E / \text{cm}^{-1}$	$\lambda / \text{nm}$	$E / \text{eV}$	$f_{\text{osc.}}$	Assignment
1	16083	622	1.994	7.41E-3	<sup>4</sup> MLCT
2	16591	603	2.057	1.16E-2	<sup>4</sup> MLCT
3	16986	589	2.106	2.29E-2	<sup>4</sup> MLCT
4	17478	572	2.167	1.13E-2	<sup>4</sup> MLCT
5	17769	563	2.203	1.02E-2	<sup>4</sup> MLCT
6	18131	552	2.248	4.28E-4	<sup>4</sup> MLCT
7	18252	548	2.263	7.30E-4	<sup>4</sup> MLCT
8	18527	540	2.297	9.64E-3	<sup>4</sup> MLCT
9	18648	536	2.312	6.66E-3	<sup>4</sup> MLCT
10	19454	514	2.412	3.76E-2	<sup>4</sup> MLCT
11	19632	509	2.434	1.22E-2	<sup>4</sup> MLCT
12	19648	509	2.436	7.13E-4	<sup>4</sup> MLCT
13	19817	505	2.457	5.90E-3	<sup>4</sup> MLCT
14	19841	504	2.460	3.94E-3	<sup>4</sup> MLCT
15	20414	490	2.531	4.40E-2	<sup>4</sup> MLCT
16	21003	476	2.604	9.03E-4	<sup>4</sup> MLCT
17	21019	476	2.606	9.49E-3	<sup>4</sup> MLCT
18	21325	469	2.644	3.02E-4	<sup>4</sup> MLCT
19	22205	450	2.753	1.22E-3	<sup>4</sup> MC
20	22584	443	2.800	8.78E-4	<sup>4</sup> MC
21	22745	440	2.820	3.68E-3	<sup>4</sup> MLCT
22	22818	438	2.829	2.29E-3	<sup>4</sup> MLCT
23	23592	424	2.925	8.36E-5	<sup>4</sup> MLCT
24	23995	417	2.975	4.38E-4	<sup>4</sup> MLCT
25	24511	408	3.039	1.14E-3	<sup>4</sup> MLCT
26	24810	403	3.076	2.96E-3	<sup>4</sup> MLCT
27	25358	394	3.144	1.03E-2	<sup>4</sup> MLCT
28	25632	390	3.178	1.48E-3	<sup>4</sup> MLCT
29	25947	385	3.217	9.93E-4	<sup>4</sup> MLCT
30	26092	383	3.235	4.04E-3	<sup>4</sup> MLCT
31	26100	383	3.236	8.03E-4	<sup>4</sup> MLCT
32	26439	378	3.278	2.85E-5	<sup>4</sup> MLCT
33	26850	372	3.329	2.17E-5	<sup>4</sup> MLCT
34	27020	370	3.350	9.21E-5	<sup>4</sup> MLCT
35	27108	369	3.361	8.14E-5	<sup>4</sup> MLCT
36	27641	362	3.427	2.20E-4	<sup>4</sup> MLCT
37	27810	360	3.448	1.07E-2	<sup>4</sup> LC
38	27818	359	3.449	4.52E-5	<sup>4</sup> MC
39	27915	358	3.461	4.14E-4	<sup>4</sup> MLCT
40	27988	357	3.470	2.38E-3	<sup>4</sup> LC
41	28044	357	3.477	2.96E-3	<sup>4</sup> LC
42	28165	355	3.492	1.72E-3	<sup>4</sup> LC
43	28584	350	3.544	2.53E-4	<sup>4</sup> MLCT

44	28722	348	3.561	4.21E-4	<sup>4</sup> LC
45	28738	348	3.563	2.51E-4	<sup>4</sup> MLCT
46	28802	347	3.571	1.78E-3	<sup>4</sup> MLCT
47	28891	346	3.582	4.07E-4	<sup>4</sup> LC
48	30238	331	3.749	2.70E-4	<sup>4</sup> MLCT
49	30367	329	3.765	3.55E-3	<sup>4</sup> LC
50	30665	326	3.802	4.14E-4	<sup>4</sup> LC
51	31093	322	3.855	4.82E-5	<sup>4</sup> LC
52	31569	317	3.914	1.94E-2	<sup>4</sup> LC
53	31843	314	3.948	2.68E-2	<sup>4</sup> LC
54	31924	313	3.958	5.41E-2	<sup>4</sup> LC
55	32287	310	4.003	4.43E-4	<sup>4</sup> LC
56	32633	306	4.046	6.00E-4	<sup>4</sup> LC
57	32650	306	4.048	6.44E-2	<sup>4</sup> LLCT
58	32746	305	4.060	1.29E-2	<sup>4</sup> LC
59	32762	305	4.062	1.63E-1	<sup>4</sup> LC
60	32779	305	4.064	1.39E-2	<sup>4</sup> LC
61	32827	305	4.070	4.91E-3	<sup>4</sup> LC
62	32964	303	4.087	1.65E-2	<sup>4</sup> LLCT
63	33101	302	4.104	4.34E-3	<sup>4</sup> LC
64	33133	302	4.108	8.96E-3	<sup>4</sup> LLCT
65	33351	300	4.135	2.04E-2	<sup>4</sup> LLCT
66	33408	299	4.142	3.71E-3	<sup>4</sup> LC
67	33521	298	4.156	2.81E-3	<sup>4</sup> LC
68	33577	298	4.163	1.67E-2	<sup>4</sup> LLCT
69	33593	298	4.165	1.79E-2	<sup>4</sup> LLCT
70	33593	298	4.165	3.72E-2	<sup>4</sup> LLCT

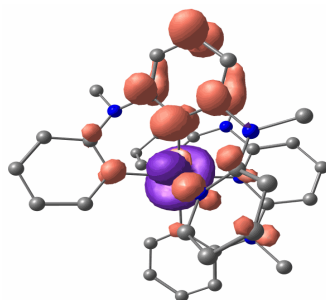


**Table S9:** Difference electron densities of the 70 lowest-lying TD-DFT-UKS calculated quartet states of *cis-fac*-[V(ddpd)<sub>2</sub>]<sup>2+</sup> (isosurface value at 0.003 a.u.; purple = electron depletion; orange = electron density gain; hydrogen atoms omitted).

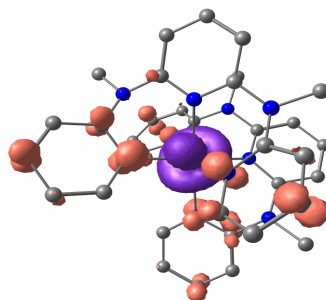
# 1 (620 nm)



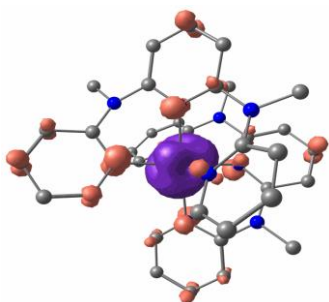
# 2 (617 nm)



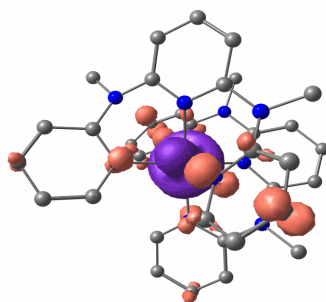
# 3 (564 nm)



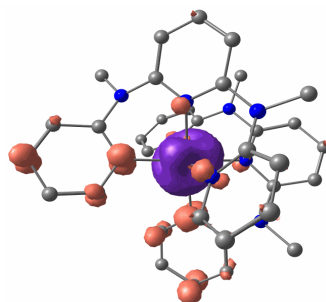
# 4 (549 nm)



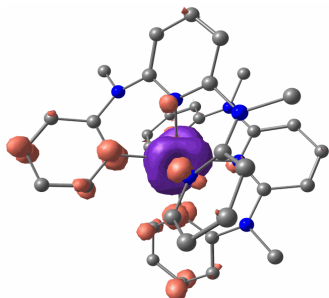
# 5 (542 nm)



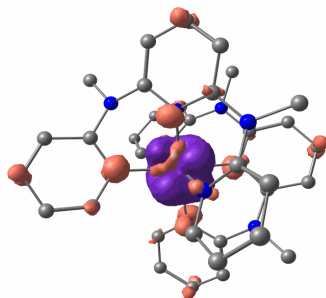
# 6 (537 nm)



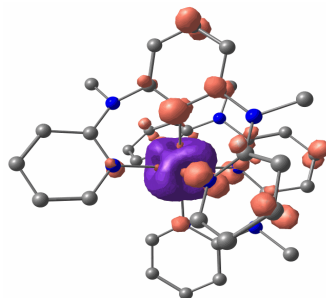
# 7 (534 nm)



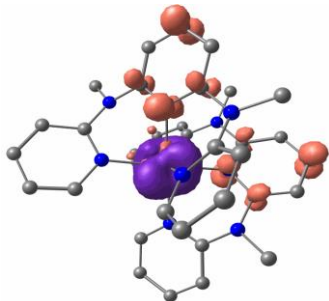
# 8 (522 nm)



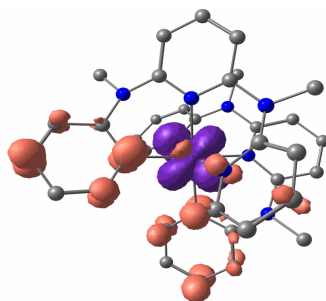
# 9 (515 nm)



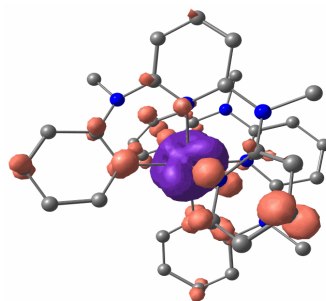
# 10 (513 nm)



# 11 (511 nm)



# 12 (503 nm)



# 13 (488 nm)

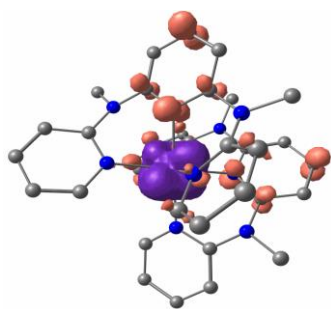


# 14 (484 nm)

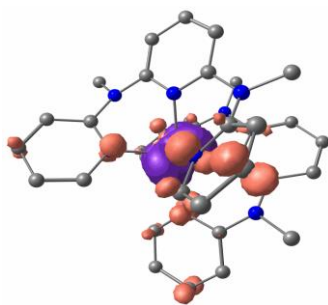


# 15 (483 nm)

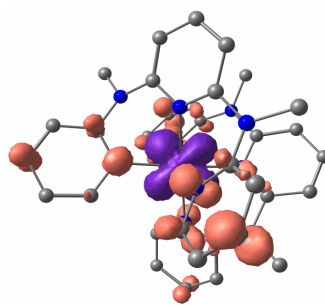




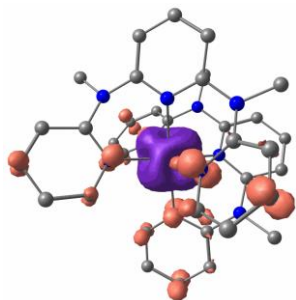
# 16 (476 nm)



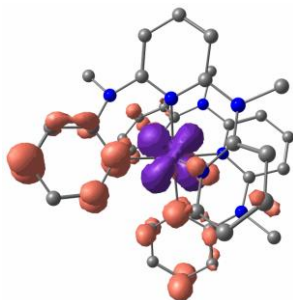
# 17 (470 nm)



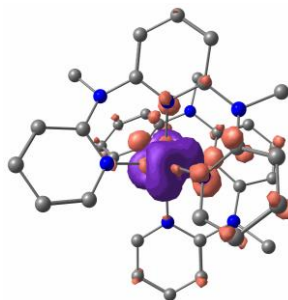
# 18 (457 nm)



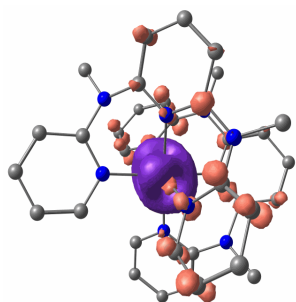
# 19 (457 nm)



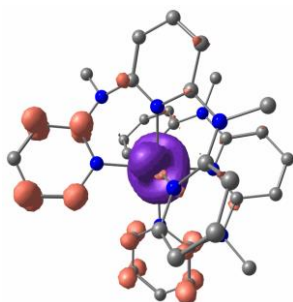
# 20 (456 nm)



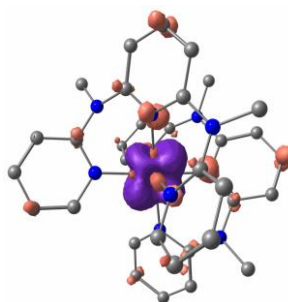
# 21 (435 nm)



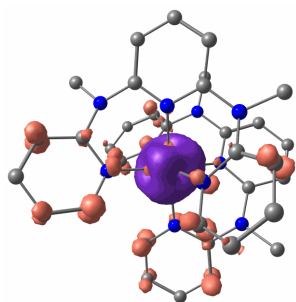
# 22 (430 nm)



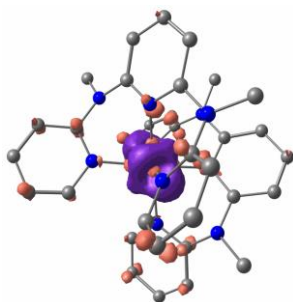
# 23 (412 nm)



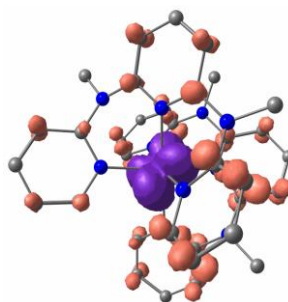
# 24 (409 nm)



# 25 (400 nm)

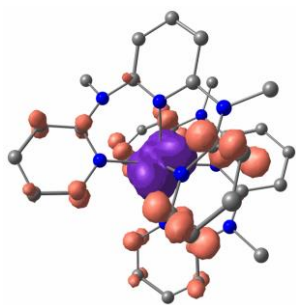


# 26 (396 nm)

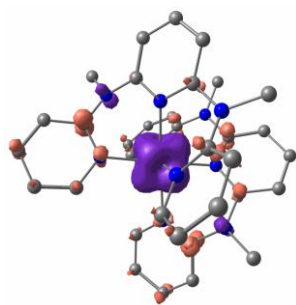


# 27 (395 nm)

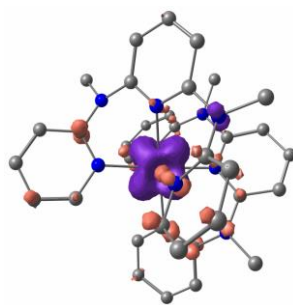




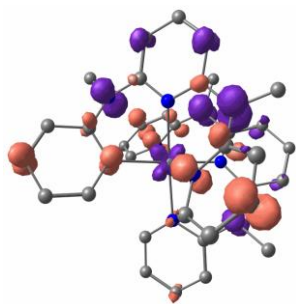
# 40 (353 nm)



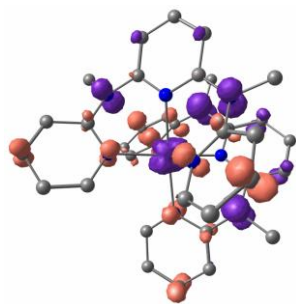
# 41 (351 nm)



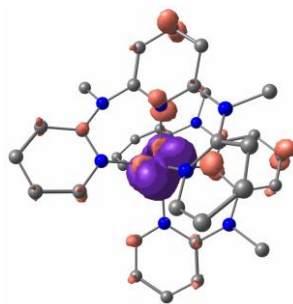
# 42 (348 nm)



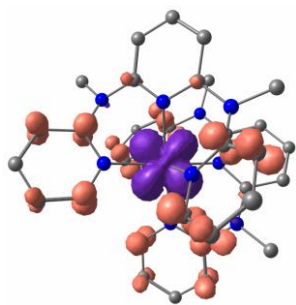
# 43 (347 nm)



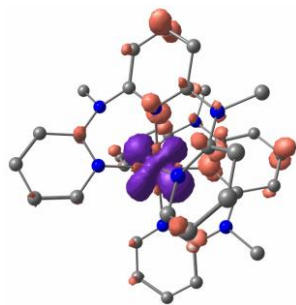
# 44 (347 nm)



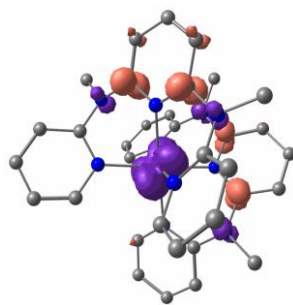
# 45 (332 nm)



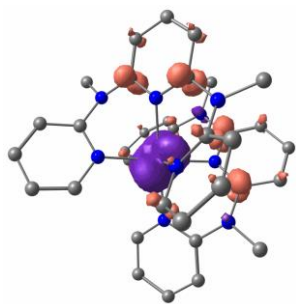
# 46 (331 nm)



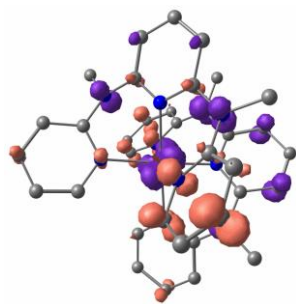
# 47 (330 nm)



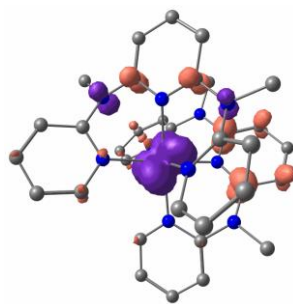
# 48 (329 nm)



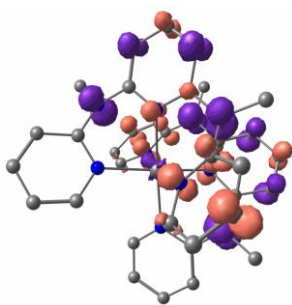
# 49 (328 nm)



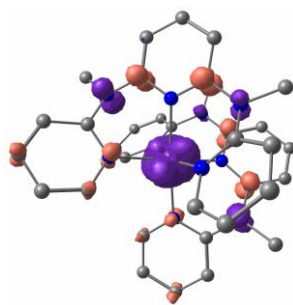
# 50 (326 nm)



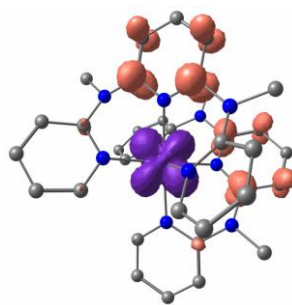
# 51 (326 nm)



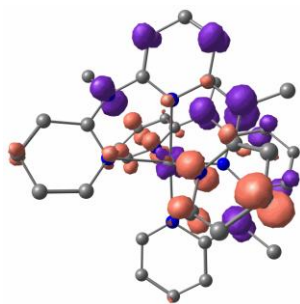
#52 (326 nm)



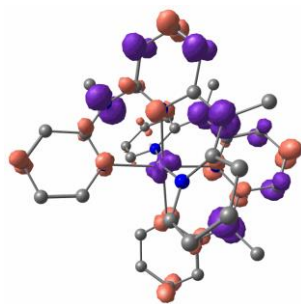
#53 (324 nm)



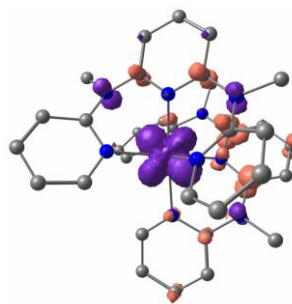
#54 (319 nm)



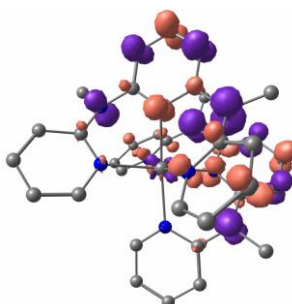
#55 (318 nm)



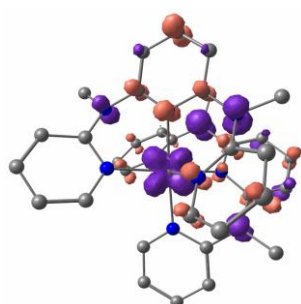
#56 (316 nm)



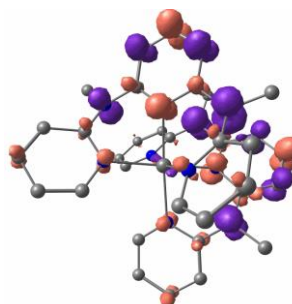
#57 (315 nm)



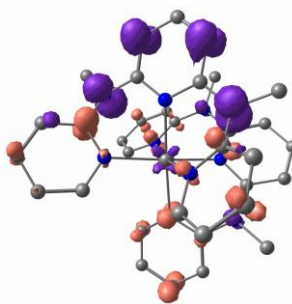
#58 (315 nm)



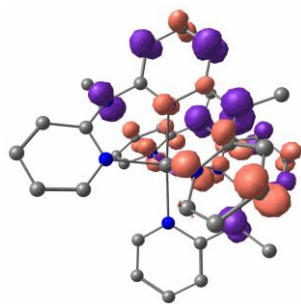
#59 (315 nm)



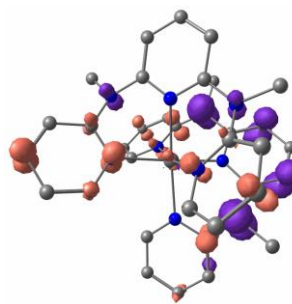
#60 (314 nm)



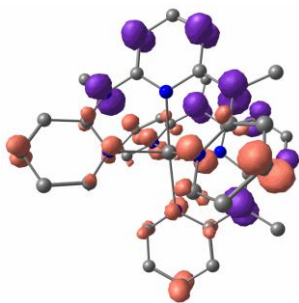
#61 (311 nm)



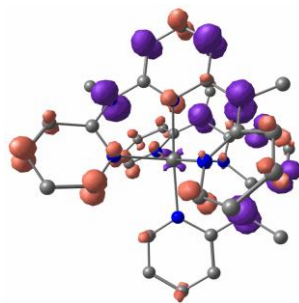
#62 (310 nm)



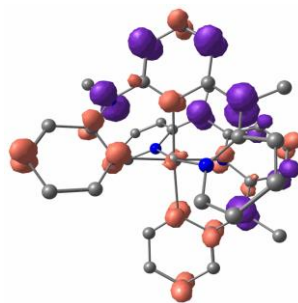
#63 (310 nm)



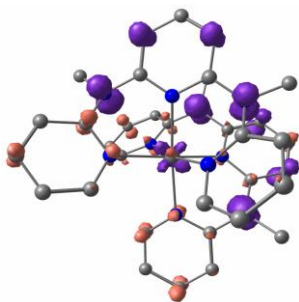
# 64 (308 nm)



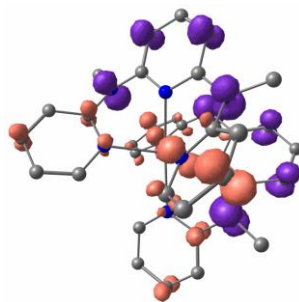
# 65 (307 nm)



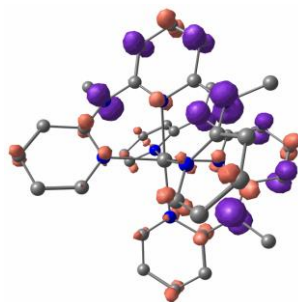
# 66 (306 nm)



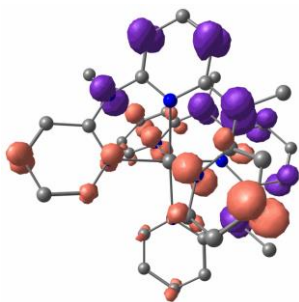
# 67 (305 nm)



# 68 (301 nm)



# 69 (301 nm)



# 70 (300 nm)

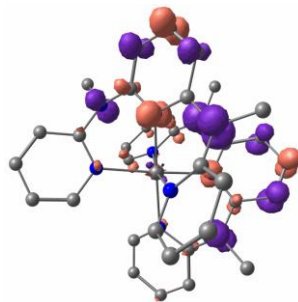
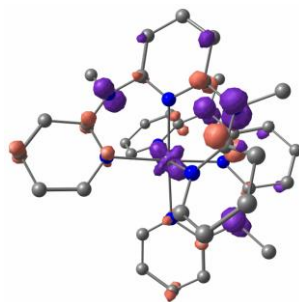
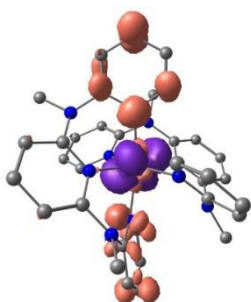
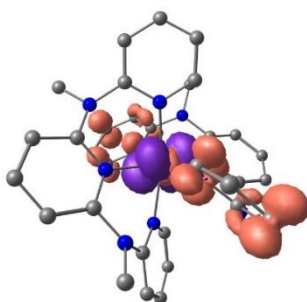


**Table S10:** Difference electron densities of the 70 lowest-lying TD-DFT-UKS calculated quartet states of *mer*-[V(ddpd)<sub>2</sub>]<sup>2+</sup> (isosurface value at 0.007 a.u.; purple = electron depletion; orange = electron density gain; hydrogen atoms omitted).

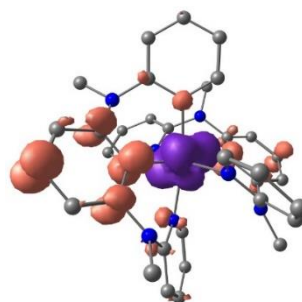
# 1 (622 nm)



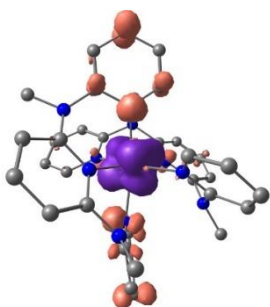
# 2 (603 nm)



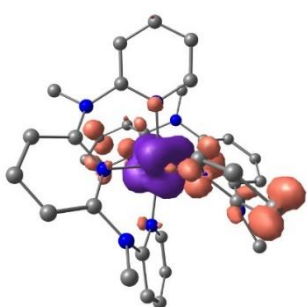
# 3 (589 nm)



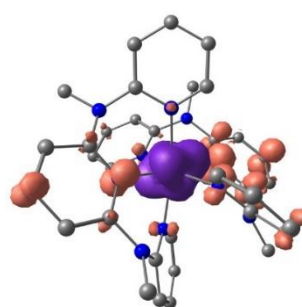
# 4 (572 nm)



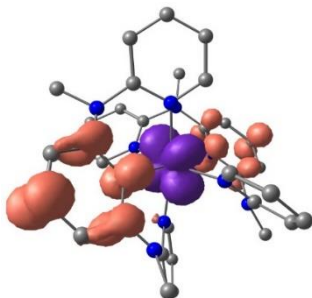
# 5 (563 nm)



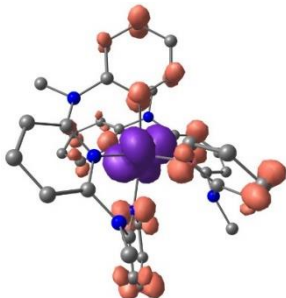
# 6 (552 nm)



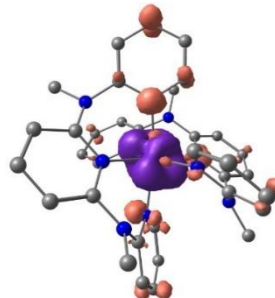
# 7 (548 nm)



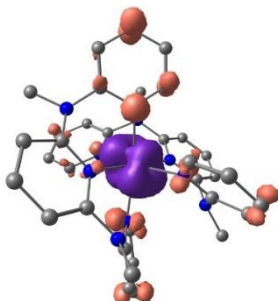
# 8 (540 nm)



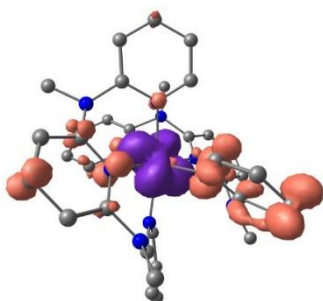
# 9 (536 nm)



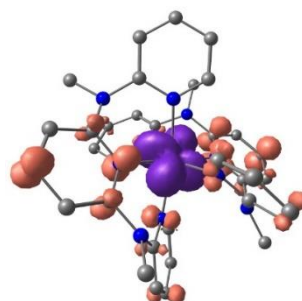
# 10 (514 nm)



# 11 (509 nm)



# 12 (509 nm)



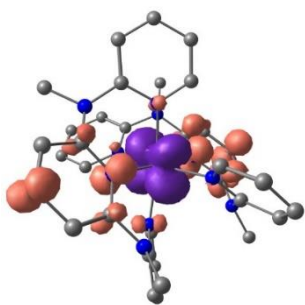
# 13 (505 nm)



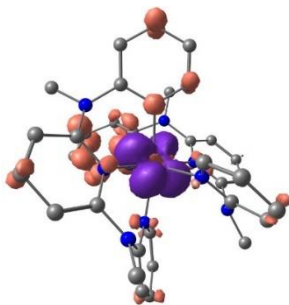
# 14 (504 nm)



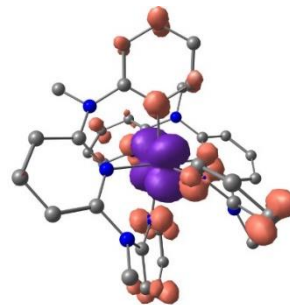
# 15 (490 nm)



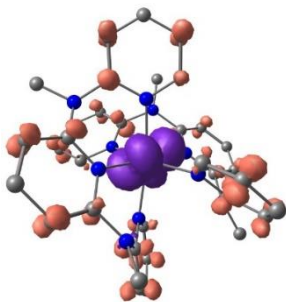
# 16 (476 nm)



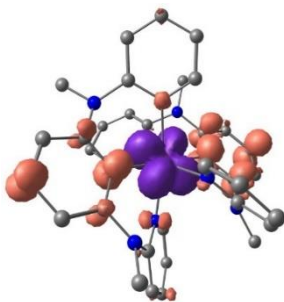
# 17 (476 nm)



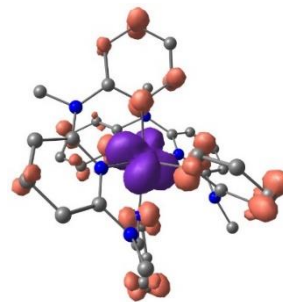
# 18 (469 nm)



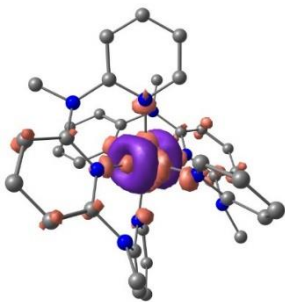
# 19 (450 nm)



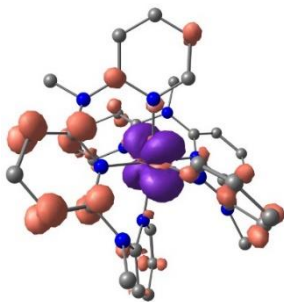
# 20 (443 nm)



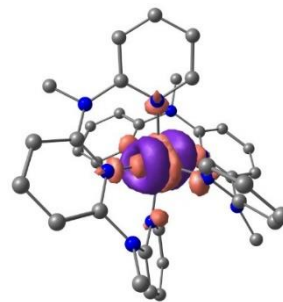
# 21 (440 nm)



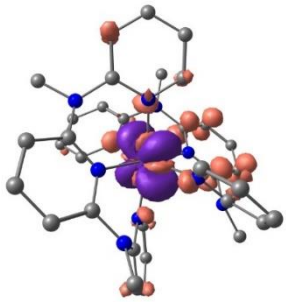
# 22 (438 nm)



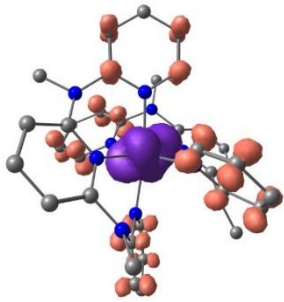
# 23 (424 nm)



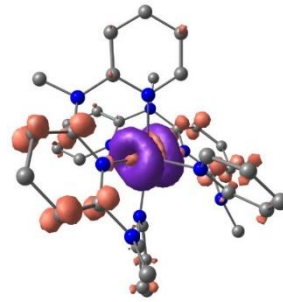
# 24 (417 nm)



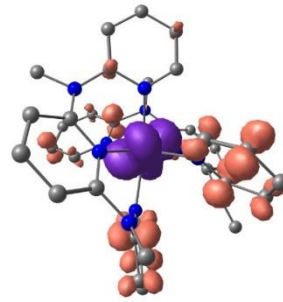
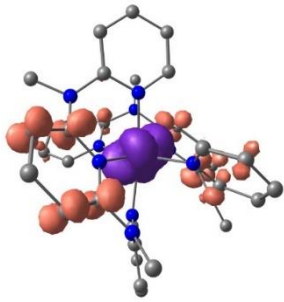
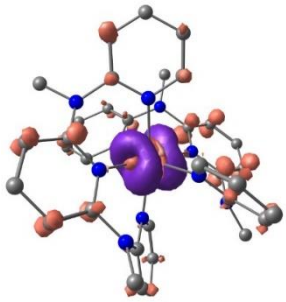
# 25 (408 nm)



# 26 (403 nm)

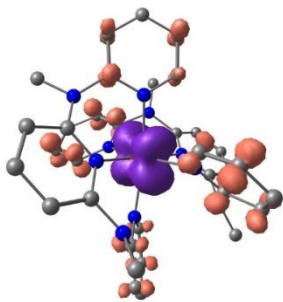


# 27 (394 nm)

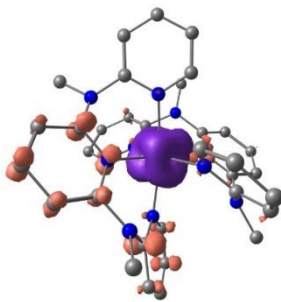




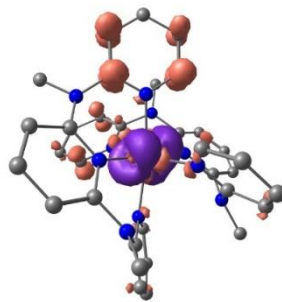
# 28 (390 nm)



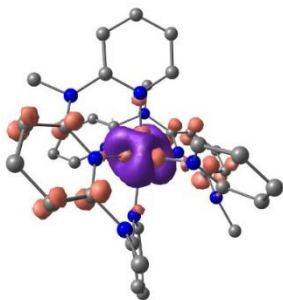
# 29 (385 nm)



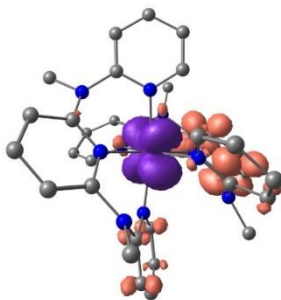
# 30 (383 nm)



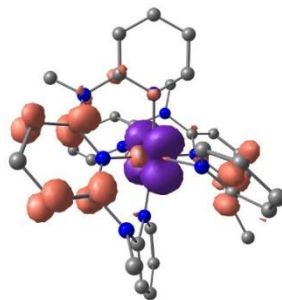
# 31 (383 nm)



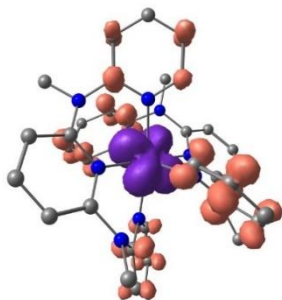
# 32 (378 nm)



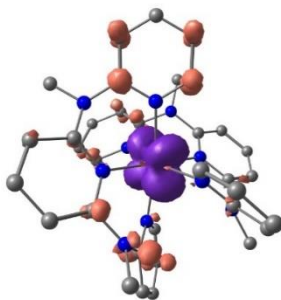
# 33 (372 nm)



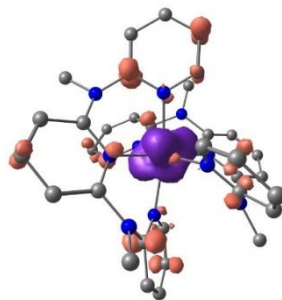
# 34 (370 nm)



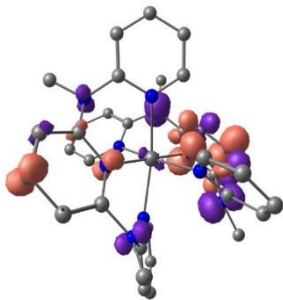
# 35 (369 nm)



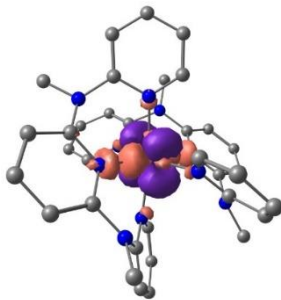
# 36 (362 nm)



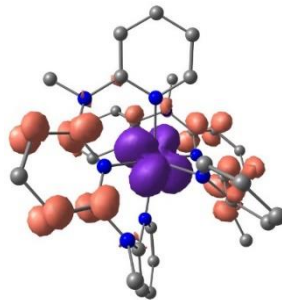
# 37 (360 nm)



# 38 (359 nm)



# 39 (358 nm)



# 40 (357 nm)

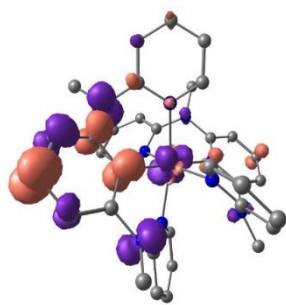


# 41 (357 nm)

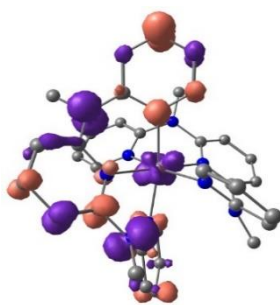


# 42 (355 nm)

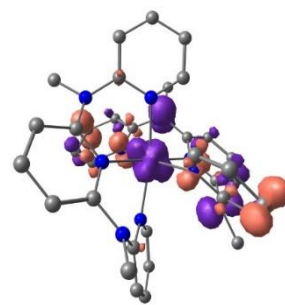




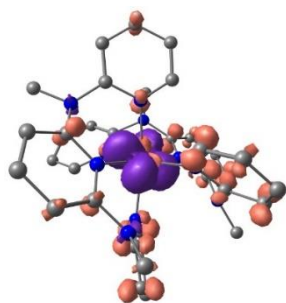
# 43 (350 nm)



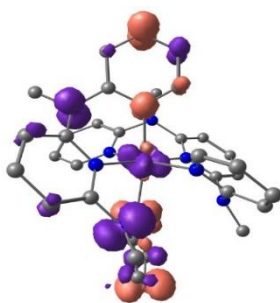
# 44 (348 nm)



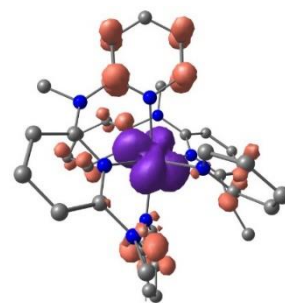
# 45 (348 nm)



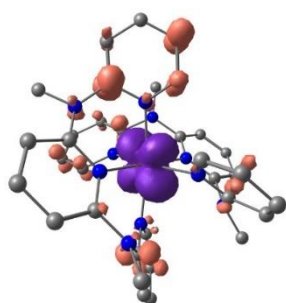
# 46 (347 nm)



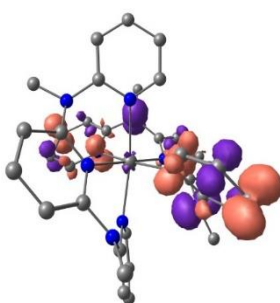
# 47 (346 nm)



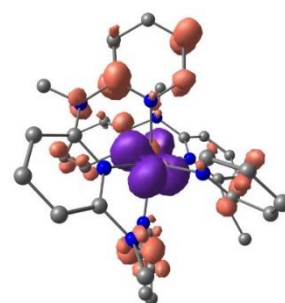
# 48 (331 nm)



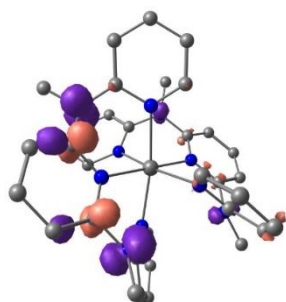
# 49 (329 nm)



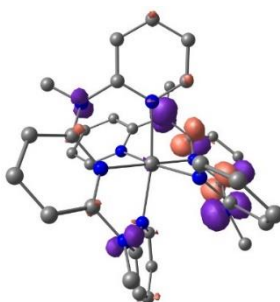
# 50 (326 nm)



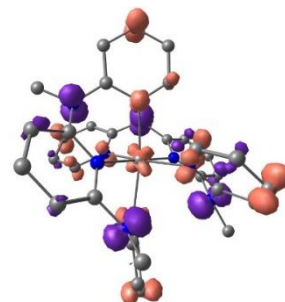
# 51 (322 nm)



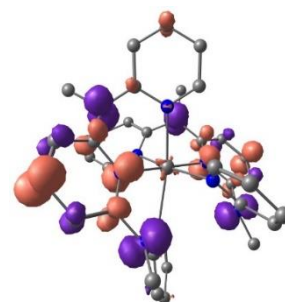
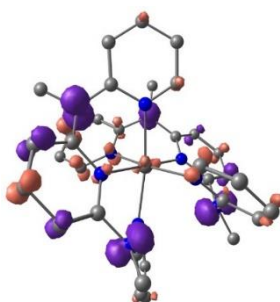
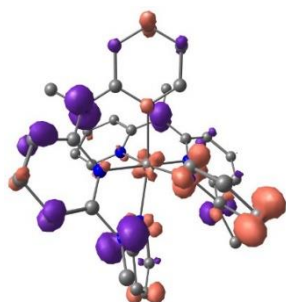
# 52 (317 nm)



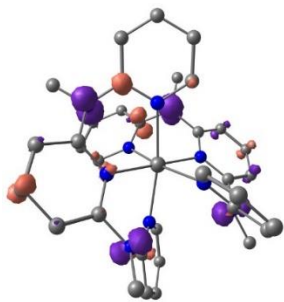
# 53 (314 nm)



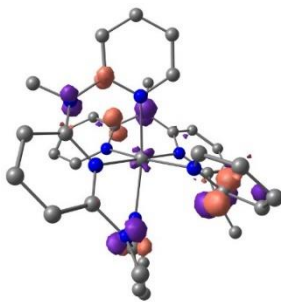
# 54 (313 nm)



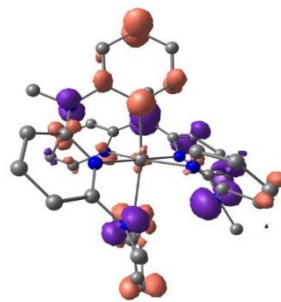
# 55 (310 nm)



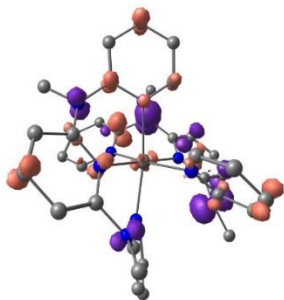
# 56 (306 nm)



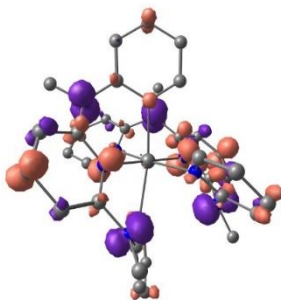
# 57 (306 nm)



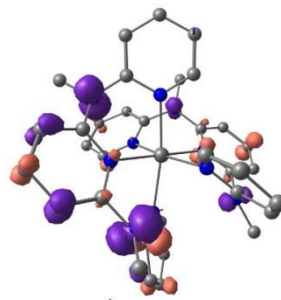
# 58 (305 nm)



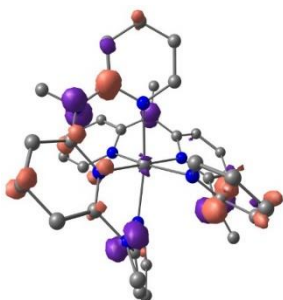
# 59 (305 nm)



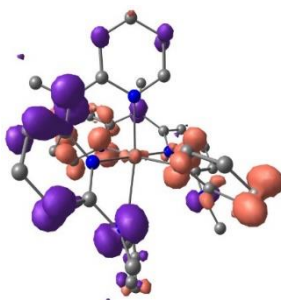
# 60 (305 nm)



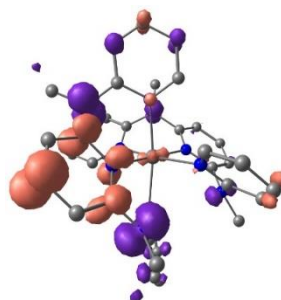
# 61 (305 nm)



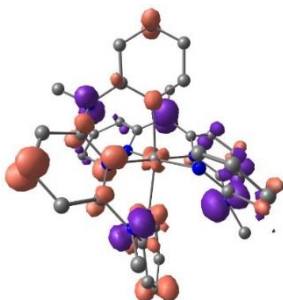
# 62 (303 nm)



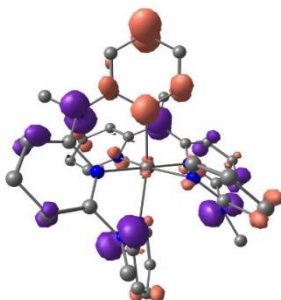
# 63 (302 nm)



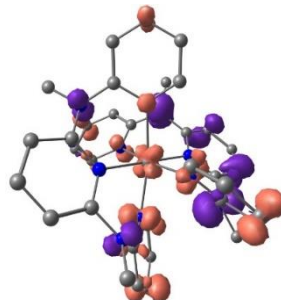
# 64 (302 nm)



# 65 (300 nm)



# 66 (299 nm)



# 67 (298 nm)

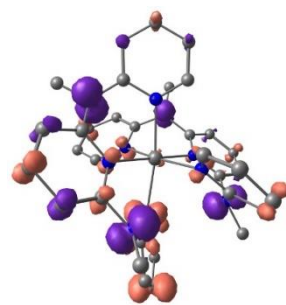
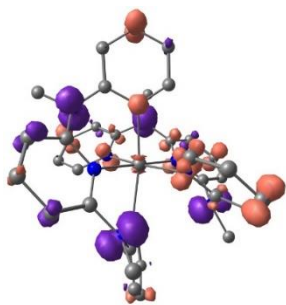
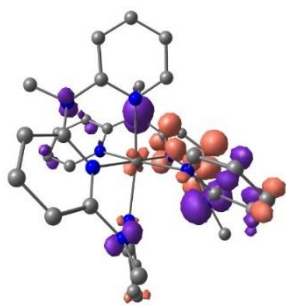


# 68 (298 nm)

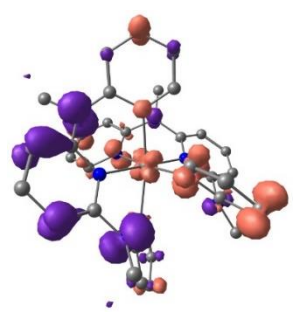


# 69 (298 nm)

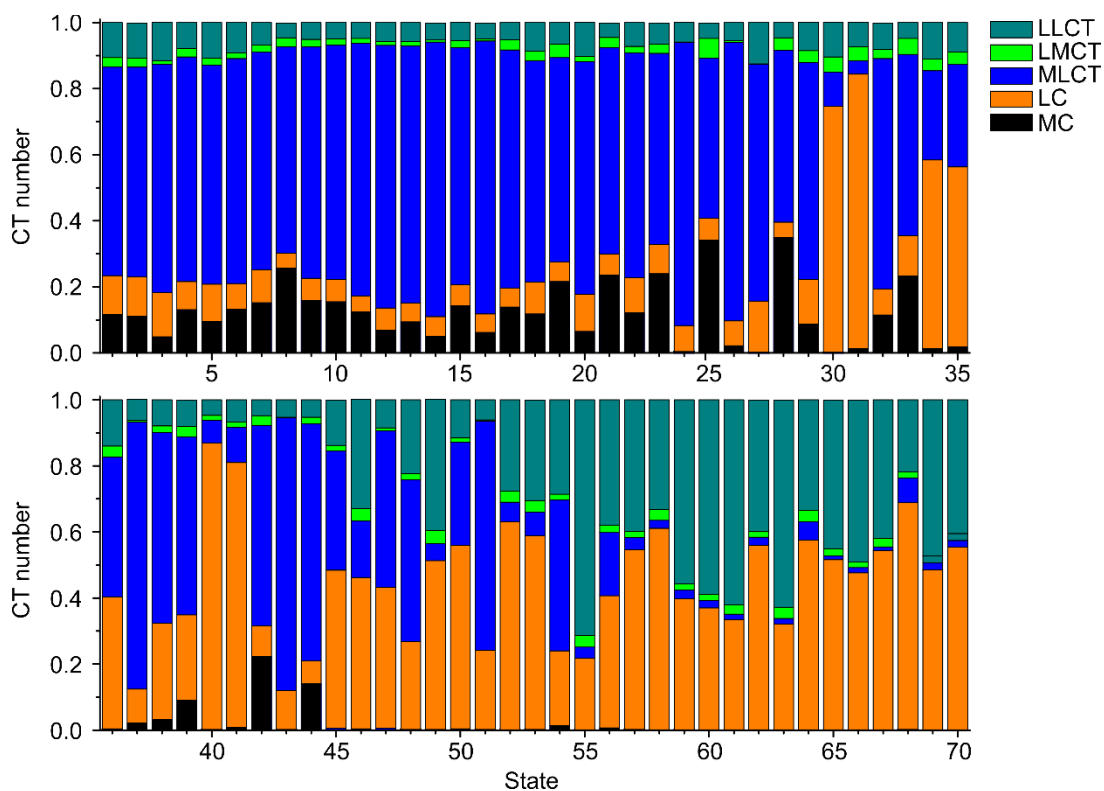




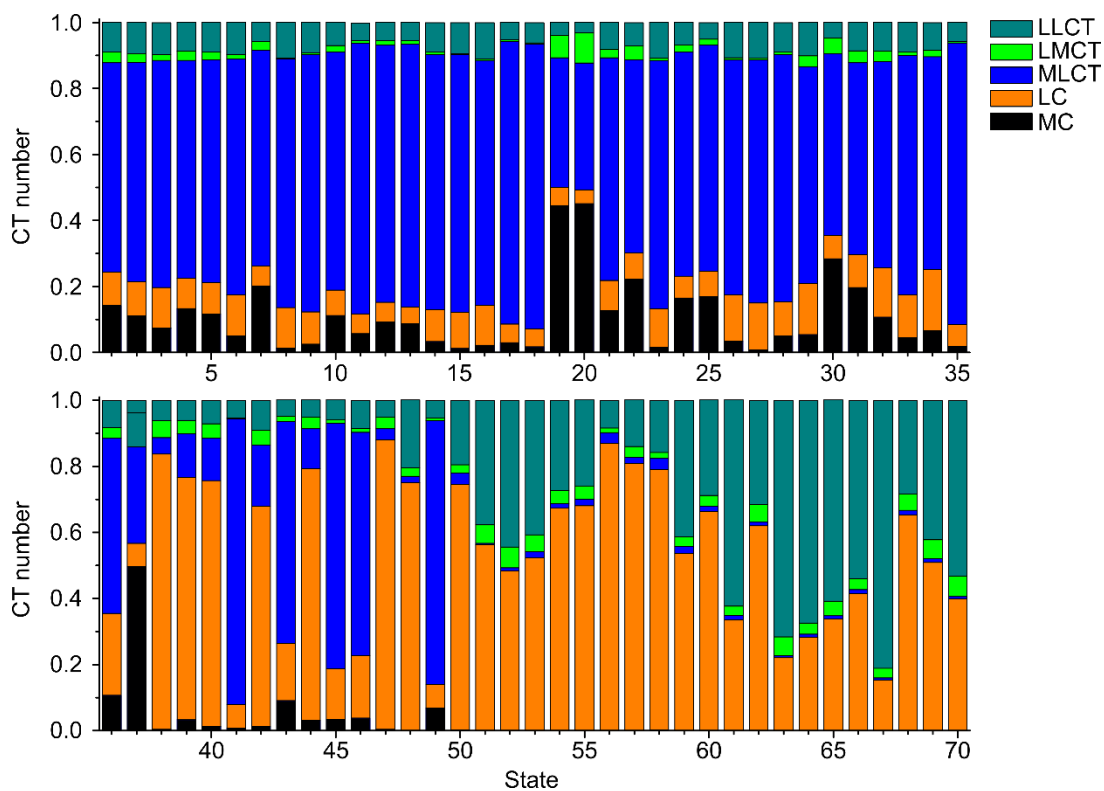
# 70 (298 nm)



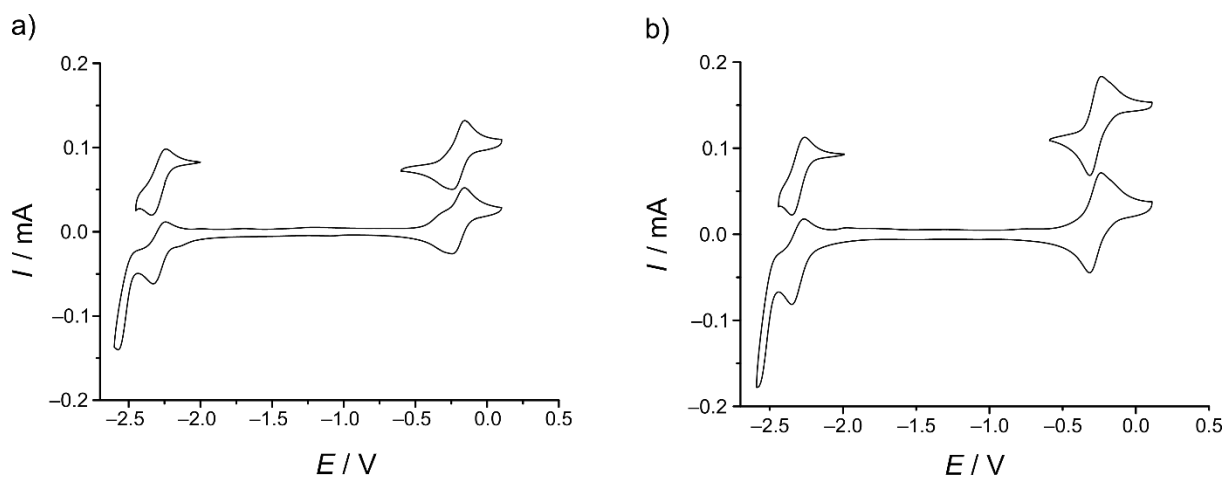
**Figure S11.** TD-DFT-UKS charge transfer (CT) numbers of the lowest-lying 70 quartet states of *cis-fac*-[V(ddpd)<sub>2</sub>]<sup>2+</sup> defined from 0 to 1.



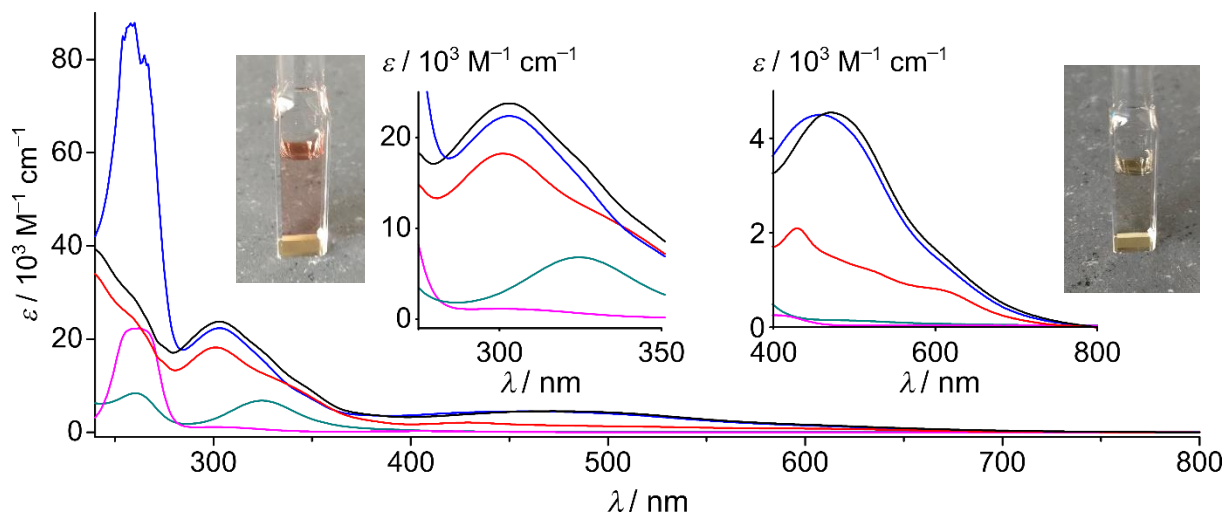
**Figure S12.** TD-DFT-UKS charge transfer (CT) numbers of the lowest-lying 70 quartet states of *mer*-[V(ddpd)<sub>2</sub>]<sup>2+</sup> defined from 0 to 1.



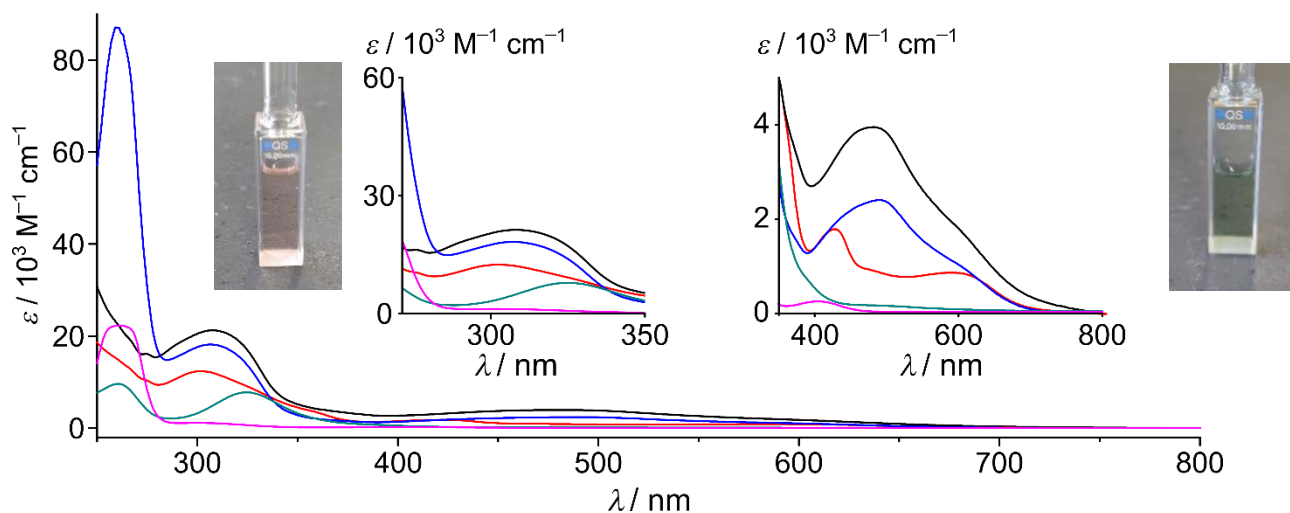
**Figure S13.** Cyclic voltammograms of a) *cis-fac*-[V(ddpd)<sub>2</sub>][BPh<sub>4</sub>]<sub>2</sub> and b) *mer*-[V(ddpd)<sub>2</sub>][BPh<sub>4</sub>]<sub>2</sub> with [nBu<sub>4</sub>N][PF<sub>6</sub>] as supporting electrolyte in CH<sub>3</sub>CN; *E* vs. ferrocene.



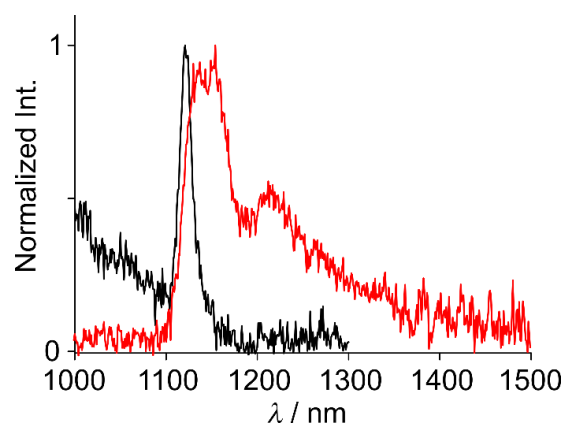
**Figure S14.** Absorption spectra of a solution of *cis-fac*-[V(ddpd)<sub>2</sub>][BPh<sub>4</sub>]<sub>2</sub> in acetonitrile ( $c = 5 \times 10^{-5}$  M) (black) after oxidation with 3 eq. of Ag[BF<sub>4</sub>] (red) and subsequent back-reduction with 3.1 eq. of CoCp<sub>2</sub> (blue). Absorption spectra of CoCp<sub>2</sub> (green) and [CoCp<sub>2</sub>][PF<sub>6</sub>] (pink) are given for comparison. Photographs depict the cuvettes before and after the oxidation.



**Figure S15.** Absorption spectra of a solution of *mer*-[V(ddpd)<sub>2</sub>][BPh<sub>4</sub>]<sub>2</sub> in acetonitrile ( $c = 5 \times 10^{-5}$  M) (black) after oxidation with 3 eq. of Ag[BF<sub>4</sub>] (red) and subsequent back-reduction with 3.1 eq. of CoCp<sub>2</sub> (blue). Absorption spectra of CoCp<sub>2</sub> (green) and [CoCp<sub>2</sub>][PF<sub>6</sub>] (pink) are given for comparison. Photographs depict the cuvettes before and after the oxidation.

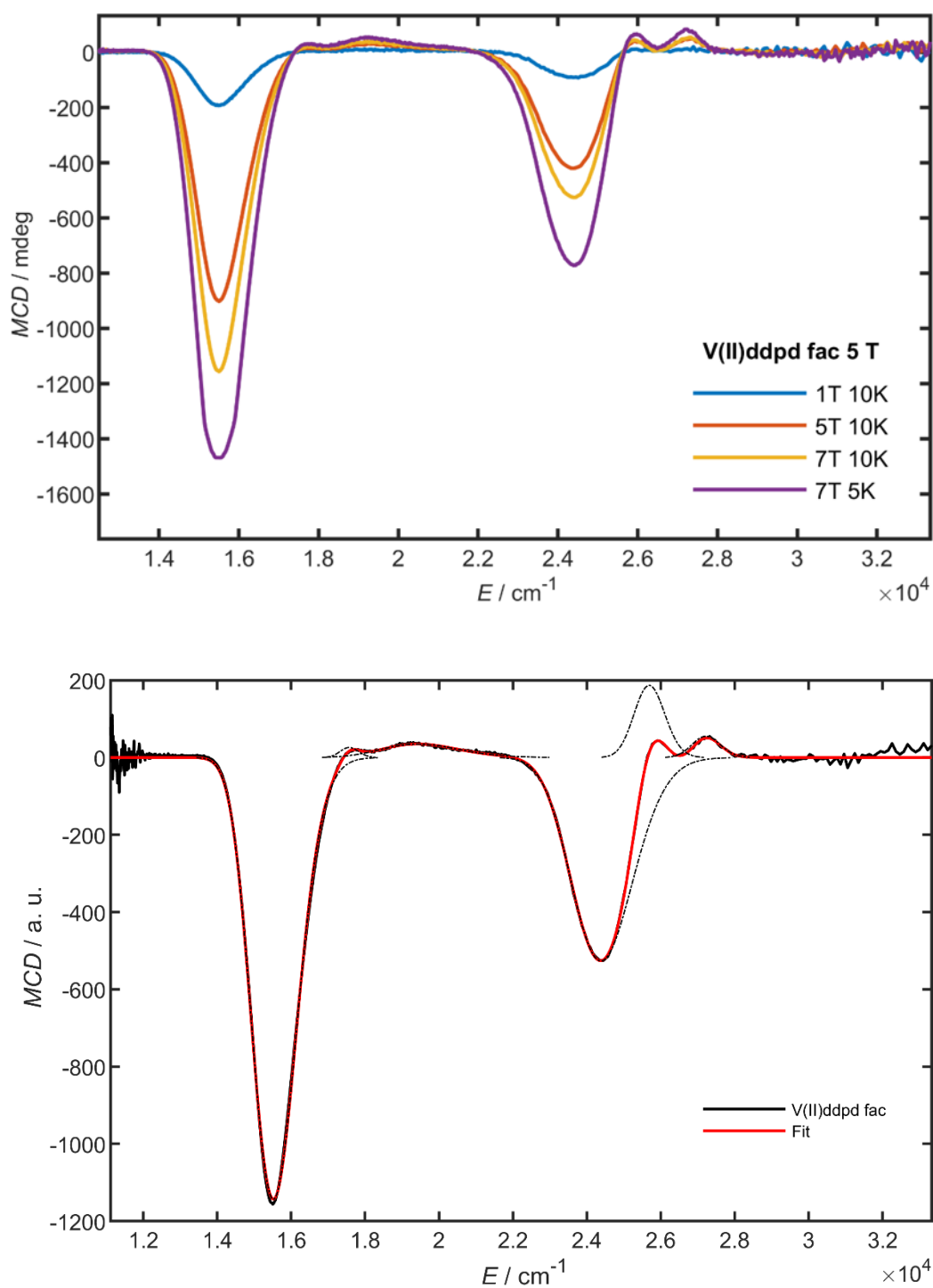


**Figure S16.** NIR emission spectra of *mer*-[V(ddpd)<sub>2</sub>][BPh<sub>4</sub>]<sub>2</sub> (black) and *cis-fac*-[V(ddpd)<sub>2</sub>][BPh<sub>4</sub>]<sub>2</sub> in butyronitrile glass at 78 K after oxidation with 3 eq. of Ag[BF<sub>4</sub>] to the respective vanadium(III) complexes.

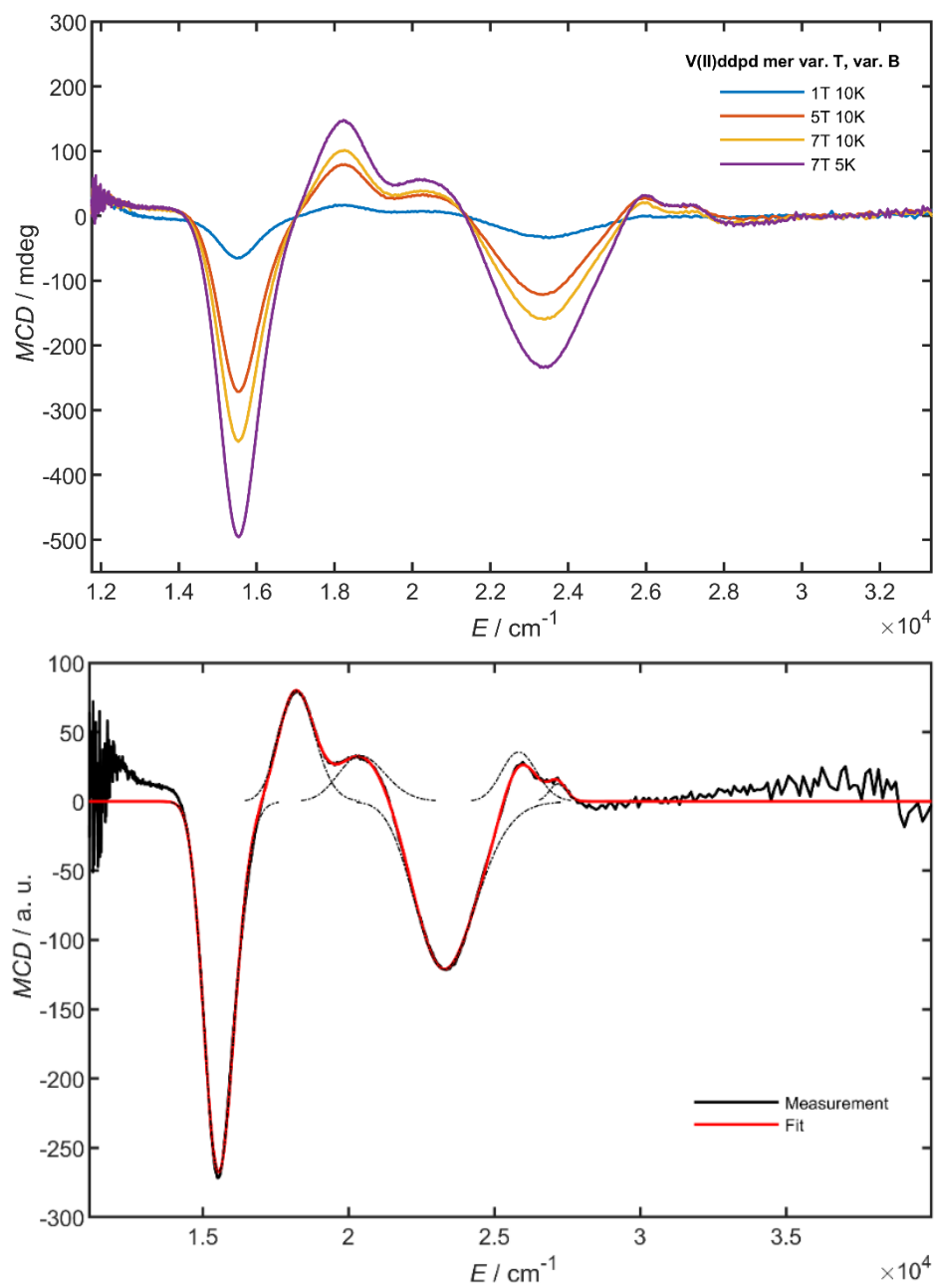




**Figure S17.** MCD spectra recorded for *cis-fac*-[V(ddpd)<sub>2</sub>][BPh<sub>4</sub>]<sub>2</sub> in 1 mM frozen solution at the indicated temperatures and magnetic fields (top). Bottom: Spectral components of the 7 T/10 K measurement obtained after deconvolution (black) and their sum (red).



**Figure S18.** MCD spectra recorded for *mer*-[V(ddpd)<sub>2</sub>][BPh<sub>4</sub>]<sub>2</sub> in 1mM frozen solution at the indicated temperatures and magnetic fields (top). Middle: Spectral components of the 7 T/5 K measurement obtained after deconvolution (black) and their sum (red). Bottom: Calculated MCD spectra for *mer*-[V(ddpd)<sub>2</sub>]<sup>2+</sup> using larger basis sets than def2-SVP.



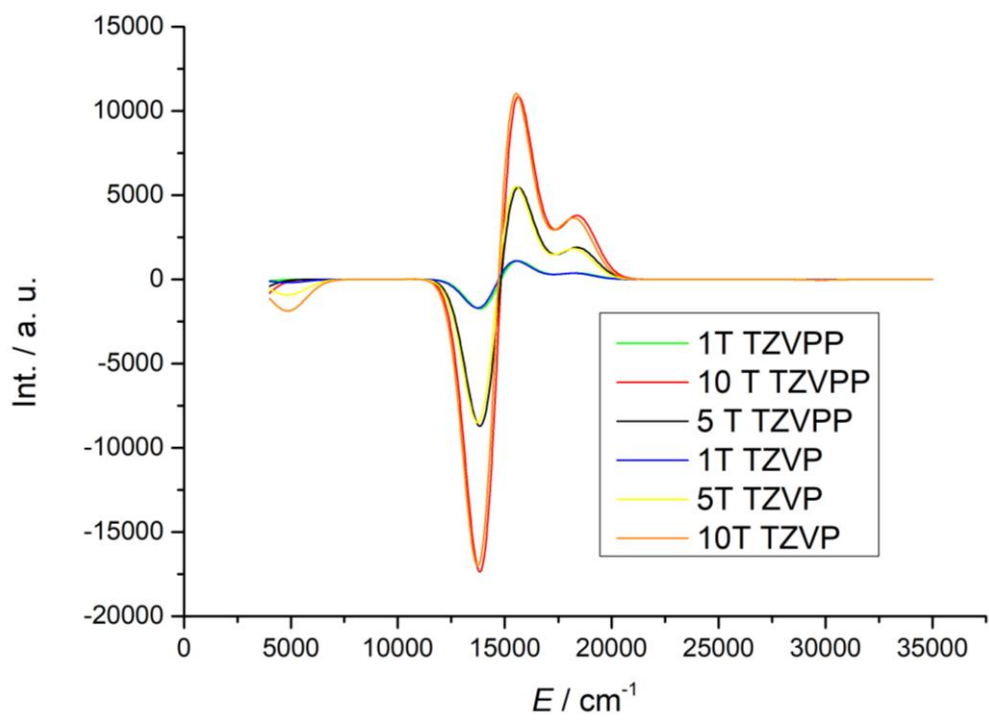


**Table S11.** Cartesian Coordinates of the DFT-UKS calculated lowest doublet state geometry of *cis-fac*-[V(ddpd)<sub>2</sub>]<sup>2+</sup>.

Atomic number	x	y	z
23	3.820683000	9.306950000	15.023187000
7	4.750891000	7.419021000	15.437260000
7	6.648605000	8.138243000	14.206751000
7	4.749678000	9.008549000	13.123297000
7	2.750154000	9.673272000	12.074898000
7	2.139892000	8.446432000	14.012237000
7	5.518456000	10.398363000	15.742930000
7	5.232674000	11.908665000	13.934704000
7	3.084882000	11.282143000	14.658261000
7	1.018334000	10.684908000	15.609728000
7	2.703317000	9.544262000	16.836491000
6	4.153433000	6.475015000	16.194590000
1	3.149029000	6.688523000	16.519759000
6	4.767046000	5.305128000	16.584356000
1	4.235556000	4.600411000	17.206149000
6	6.071706000	5.074755000	16.161236000
1	6.594237000	4.169270000	16.436889000
6	6.690433000	6.014935000	15.359154000
1	7.688215000	5.842965000	14.989060000
6	6.006055000	7.180092000	15.003332000
6	8.104520000	8.241078000	14.330045000
1	8.639162000	7.521570000	13.706997000
1	8.372814000	8.081392000	15.369866000
1	8.403182000	9.247491000	14.048785000
6	6.057965000	8.684357000	13.068366000
6	6.820738000	8.922948000	11.926432000
1	7.868140000	8.676602000	11.896244000
6	6.189630000	9.449239000	10.813572000
1	6.756453000	9.633265000	9.911319000
6	4.827132000	9.692535000	10.831253000
1	4.324735000	10.045628000	9.947485000
6	4.124144000	9.438665000	12.007193000
6	2.165111000	10.544660000	11.052569000
1	2.806898000	11.412309000	10.932380000
1	1.195066000	10.882183000	11.403890000
1	2.045870000	10.050046000	10.086388000
6	1.872247000	8.799596000	12.739995000
6	0.720470000	8.353045000	12.087218000
1	0.536113000	8.636742000	11.063925000
6	-0.167041000	7.527723000	12.752298000
1	-1.058429000	7.175457000	12.252172000
6	0.114042000	7.154695000	14.062147000
1	-0.549448000	6.519256000	14.629362000
6	1.269105000	7.630906000	14.641167000
1	1.495553000	7.393403000	15.667341000
6	6.235068000	9.991639000	16.810581000
1	5.879878000	9.107728000	17.313662000
6	7.391301000	10.608468000	17.234544000
1	7.926529000	10.218753000	18.087507000
6	7.840160000	11.720471000	16.530329000
1	8.738797000	12.242544000	16.828037000

6	7.110301000	12.160983000	15.441783000
1	7.424044000	13.035308000	14.895033000
6	5.948534000	11.481938000	15.067543000
6	6.003032000	12.560847000	12.872962000
1	5.460756000	12.453869000	11.938098000
1	6.955116000	12.048161000	12.777438000
1	6.181856000	13.620945000	13.063545000
6	3.859955000	12.150426000	13.974730000
6	3.311066000	13.231195000	13.287728000
1	3.933440000	13.911383000	12.732679000
6	1.942976000	13.428594000	13.359829000
1	1.492565000	14.262305000	12.838913000
6	1.155127000	12.597366000	14.135941000
1	0.100973000	12.785899000	14.242385000
6	1.768455000	11.537593000	14.803246000
6	-0.433446000	10.668666000	15.413642000
1	-0.637493000	10.641283000	14.346424000
1	-0.933408000	11.534627000	15.851861000
1	-0.829968000	9.762792000	15.861222000
6	1.502492000	10.159472000	16.817097000
6	0.712624000	10.249620000	17.965990000
1	-0.235693000	10.760981000	17.928436000
6	1.164789000	9.706015000	19.153547000
1	0.560233000	9.777717000	20.046982000
6	2.409628000	9.086755000	19.179579000
1	2.810140000	8.646807000	20.080608000
6	3.136220000	9.038187000	18.010471000
1	4.095553000	8.548169000	17.993893000

**Table S12.** Cartesian Coordinates of the DFT-UKS calculated lowest doublet state geometry of *mer*-[V(ddpd)<sub>2</sub>]<sup>2+</sup>.

Atomic number	x	y	z
23	-0.437484	4.882287	1.502872
7	0.022931	4.404842	3.509542
7	0.598281	2.226374	2.814841
7	1.19658	3.644682	1.008239
7	1.750465	5.115875	-0.775931
7	-0.597527	5.190984	-0.596835
7	-1.852263	3.317272	1.384583
7	-2.999456	4.268395	3.21187
7	-2.080129	6.102229	2.017521
7	-1.113092	7.891141	0.787559
7	0.705053	6.674097	1.661188
6	-0.172477	5.306839	4.494232
1	-0.391923	6.313274	4.170702
6	-0.142761	4.979465	5.830719
1	-0.330451	5.736712	6.577236
6	0.121991	3.656989	6.178064
1	0.151264	3.351963	7.214968
6	0.376619	2.733283	5.180823
1	0.624734	1.715801	5.434026
6	0.338093	3.139502	3.843231
6	0.411899	0.805679	3.120335
1	-0.521019	0.693358	3.666431
1	1.225022	0.380865	3.712417
1	0.331148	0.261659	2.184016
6	1.445147	2.532884	1.73561
6	2.502695	1.682521	1.430424
1	2.698121	0.814962	2.038648
6	3.317672	1.991781	0.355332
1	4.145487	1.345094	0.099283
6	3.070559	3.131261	-0.389761
1	3.681539	3.372107	-1.243981
6	1.997151	3.943697	-0.038389
6	2.919634	5.784661	-1.354829
1	2.676631	6.833305	-1.503605
1	3.234538	5.351584	-2.306208
1	3.737661	5.718885	-0.644316
6	0.504707	5.410069	-1.334021
6	0.411171	5.94381	-2.625823
1	1.298985	6.125378	-3.208286
6	-0.835392	6.202208	-3.162194
1	-0.916017	6.607137	-4.161571
6	-1.976318	5.9109	2.418057
1	-2.968842	6.082126	-2.806951
6	-1.807914	5.403429	-1.149975
1	-2.655513	5.178713	-0.519619
6	-1.694286	2.317105	0.49254
1	-0.934023	2.474881	-0.257698

6	-2.412501	1.144153	0.543029
1	-2.227495	0.365269	-0.181592
6	-3.36089	0.997124	1.552512
1	-3.94657	0.092002	1.634516
6	-3.569871	2.035632	2.441562
1	-4.327878	1.95337	3.202904
6	-2.807282	3.202281	2.326132
6	-3.608533	3.960185	4.508248
1	-3.144655	3.058235	4.899115
1	-4.688821	3.811347	4.45342
1	-3.39533	4.779192	5.188562
6	-3.07836	5.603432	2.77985
6	-4.165466	6.384313	3.159313
1	-4.963701	5.961629	3.746909
6	-4.219879	7.701686	2.738569
1	-5.054612	8.327493	3.022487
6	-3.203552	8.215141	1.952147
1	-3.218618	9.245048	1.635658
6	-2.141091	7.387148	1.604934
6	-1.496298	8.906854	-0.197567
1	-0.769152	8.892801	-1.005115
1	-1.547738	9.914324	0.220384
1	-2.466911	8.639669	-0.603765
6	0.235204	7.823157	1.146071
6	1.079741	8.923365	0.951293
1	0.696213	9.838866	0.532581
6	1.987645	6.617033	2.070699
6	2.403879	8.83536	1.335112
6	2.870967	7.661988	1.922779
1	2.300138	5.677653	2.502237
1	3.894815	7.557505	2.249085
1	3.060824	9.682985	1.196447

**Figure S19.** Temperature dependence of the magnetic susceptibility in  $\chi_M T$  vs.  $T$  for *cis-fac*-[V(ddpd)<sub>2</sub>][BPh<sub>4</sub>]<sub>2</sub>. The red line corresponds to the fit obtained with  $S = 3/2$ ;  $g_{1,2,3} = 1.99, 1.99, 2.0$ ;  $D = 0.40(2) \text{ cm}^{-1}$  and  $E = 0.3D$ .

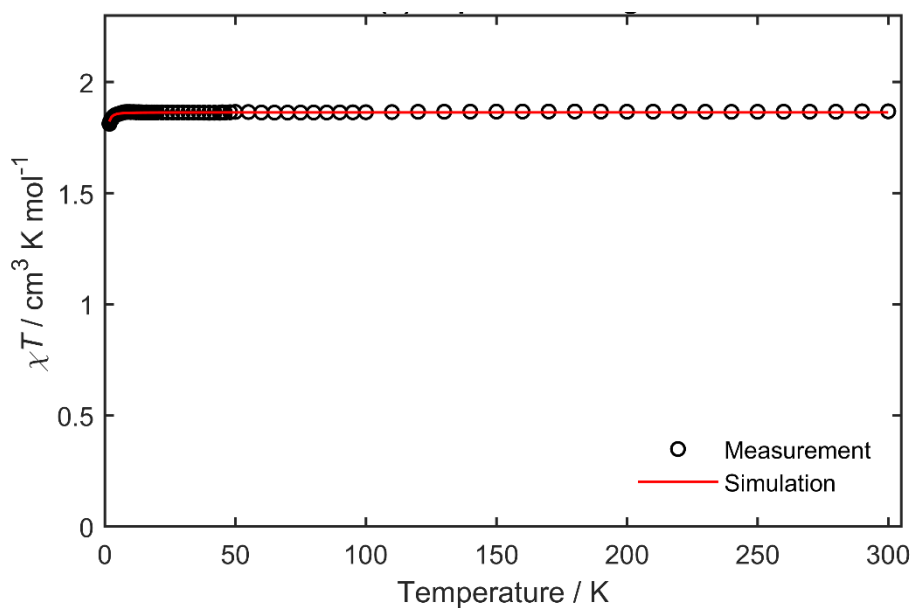


**Figure S20.** Field dependence of the magnetization of *cis-fac*-[V(ddpd)<sub>2</sub>][BPh<sub>4</sub>]<sub>2</sub> at different temperatures. Best fit with  $S = 3/2$ ;  $g_{1,2,3} = 1.99, 1.99, 2.0$ ;  $D = 0.40(2) \text{ cm}^{-1}$  and  $E = 0.3D$ .

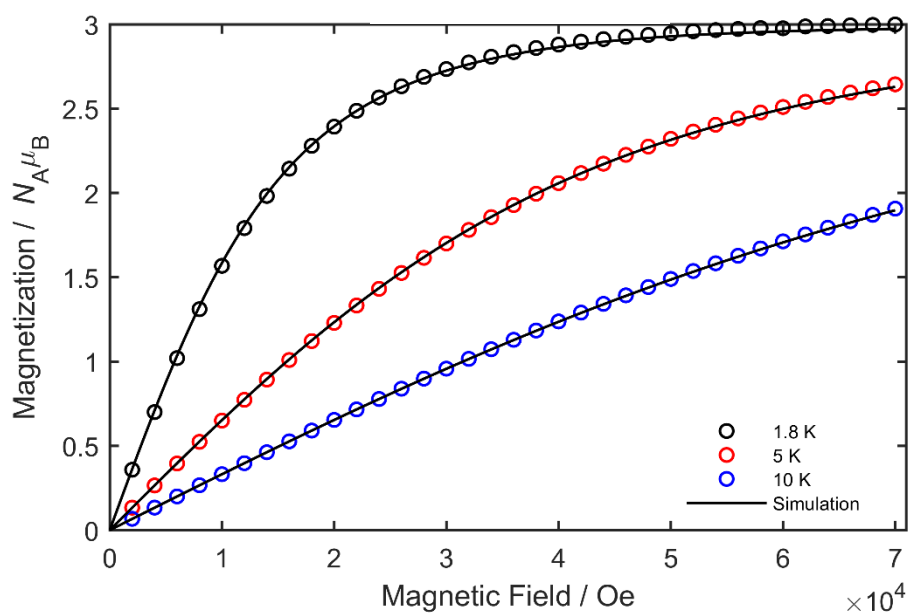




**Figure S21.** Temperature dependence of the magnetic susceptibility in  $\chi_M T$  vs.  $T$  for *mer*-[V(ddpd)<sub>2</sub>][BPh<sub>4</sub>]<sub>2</sub>. The red line corresponds to the fit obtained with  $S = 3/2$ ;  $g = 1.99(1)$ ;  $D = 0.2(1)$  cm<sup>-1</sup> and  $E = 0$  cm<sup>-1</sup>.

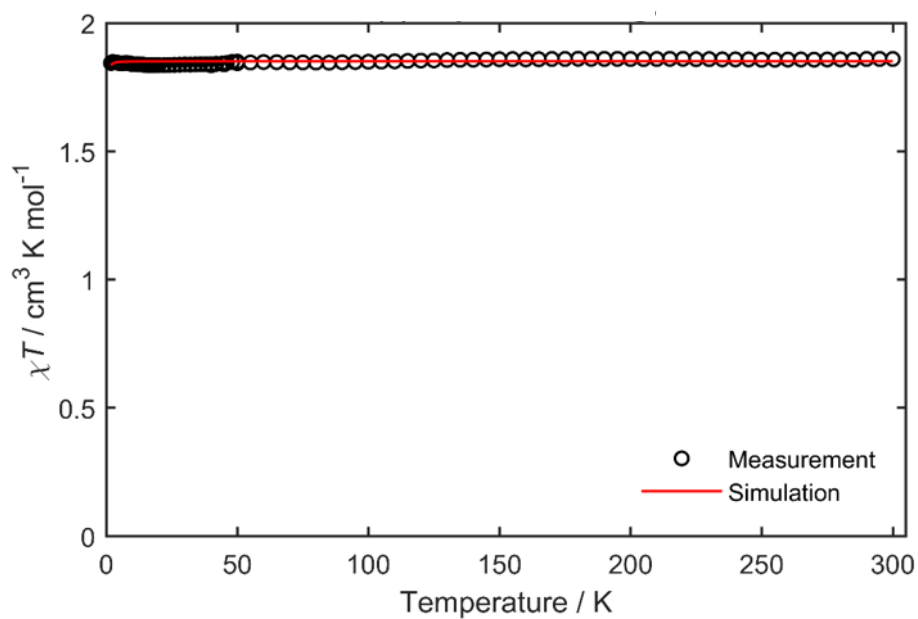


**Figure S22.** Field dependence of the magnetization of *mer*-[V(ddpd)<sub>2</sub>][BPh<sub>4</sub>]<sub>2</sub> at different temperatures. Best fit with  $S = 3/2$ ;  $g = 1.99(1)$ ;  $D = 0.2(1)$  cm<sup>-1</sup> and  $E = 0$  cm<sup>-1</sup>.

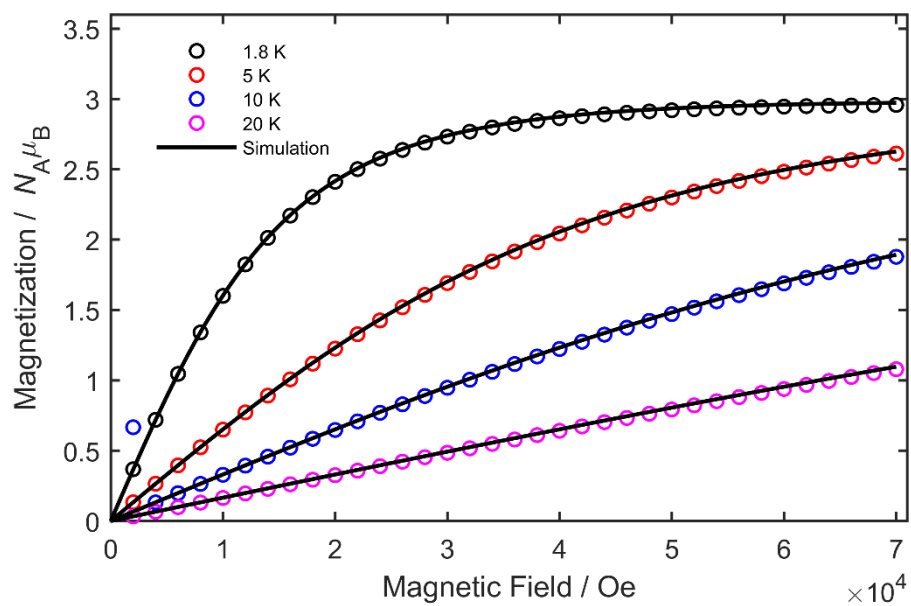


**Figure S23.** HFEPR spectra of *cis-fac*-[V(ddpd)<sub>2</sub>][BPh<sub>4</sub>]<sub>2</sub> at 5 K and different frequencies as indicated (top) together with simulations (bottom) based on the spin Hamiltonian parameters of  $S = 3/2$ ;  $g_{1,2,3} = 1.99, 1.99, 2.0$ ;  $D = 0.47(2) \text{ cm}^{-1}$  and  $E = 0.19 D$ . The vertical axis corresponds to the microwave frequency.

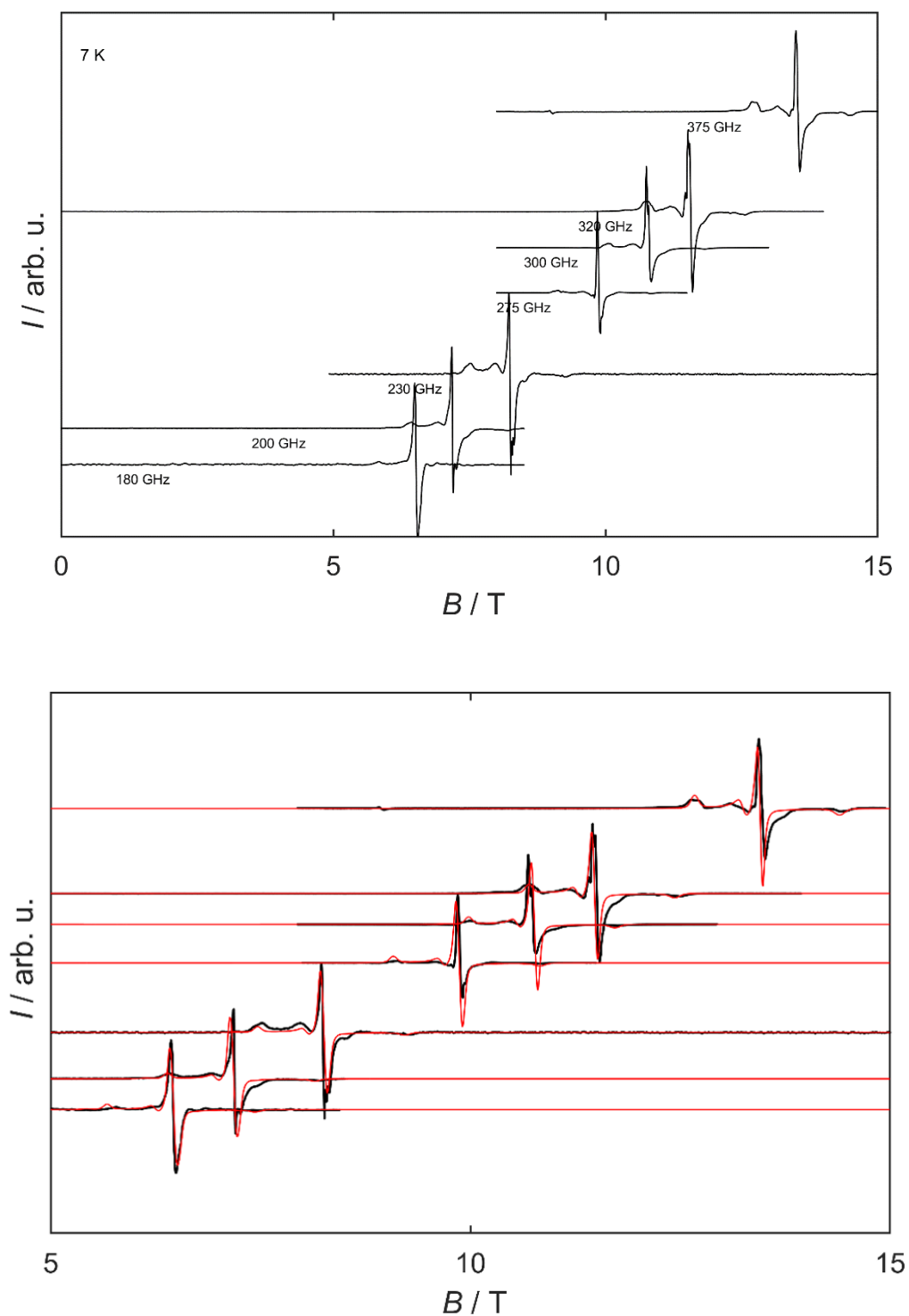


**Figure S24.** Measured and simulated HFEPR spectra of *cis-fac*-[V(ddpd)<sub>2</sub>][BPh<sub>4</sub>]<sub>2</sub> at 375 GHz and different temperatures as indicated. The simulations are based on the spin Hamiltonian parameters of  $S = 3/2$ ;  $g_{1,2,3} = 1.99, 1.99, 2.0$ ;  $D = 0.47(2) \text{ cm}^{-1}$  and  $E = 0.19 D$ .

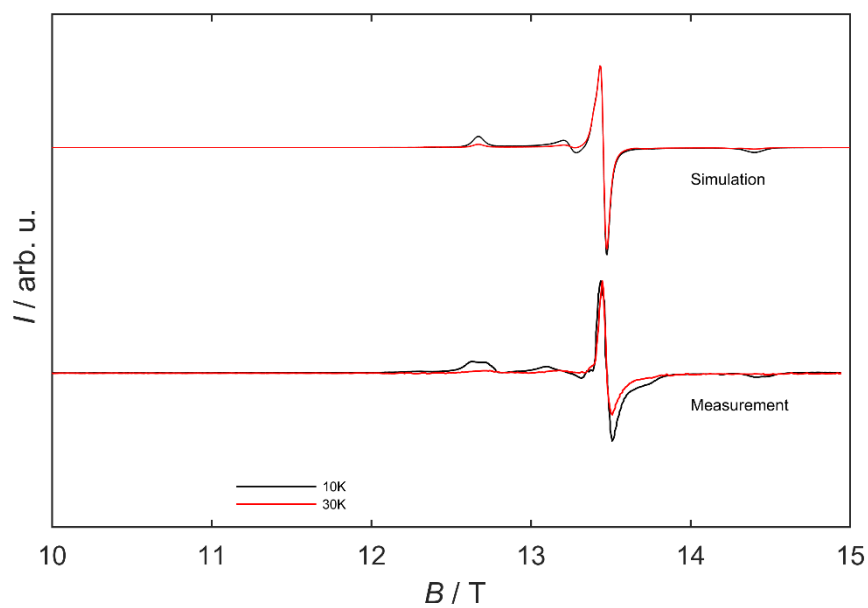


**Figure S25.** HF EPR spectra of *mer*-[V(ddpd)<sub>2</sub>][BPh<sub>4</sub>]<sub>2</sub> at 5 K and different frequencies as indicated (top) together with simulations (bottom) based on the spin Hamiltonian parameters of  $S = 3/2$ ;  $g_{1,2,3} = 1.985(5)$ ,  $1.993(5)$ ,  $1.996(4)$ ;  $D = 0.2(1) \text{ cm}^{-1}$  and  $E = 0.08 D$ . The vertical axis corresponds to the microwave frequency.

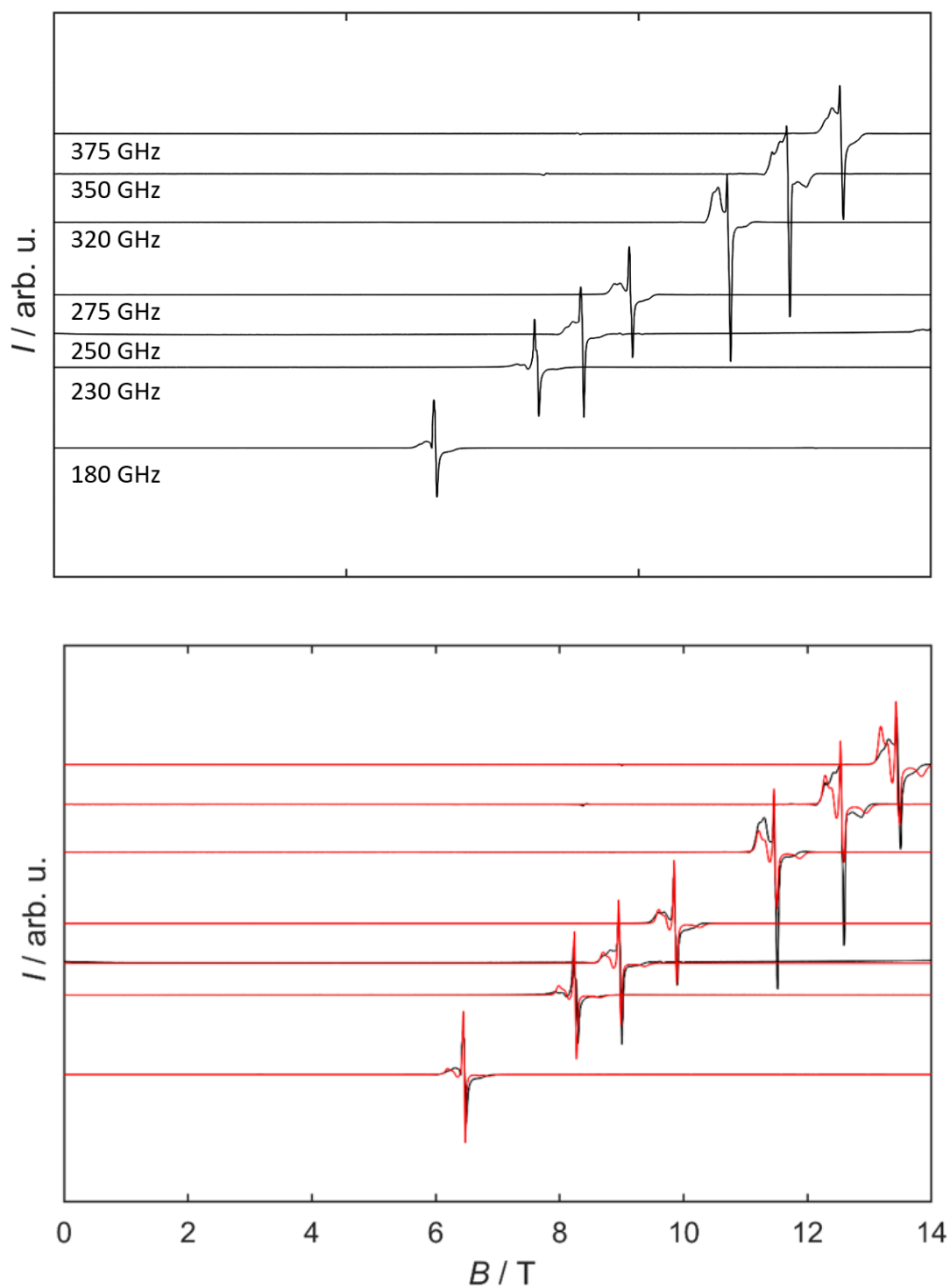


**Figure S26.** Measured and simulated HFEPR spectra of *mer*-[V(ddpd)<sub>2</sub>][BPh<sub>4</sub>]<sub>2</sub> at 275 GHz and different temperatures as indicated. Top: Simulations based on a positive value for  $D$  with the spin Hamiltonian parameters of  $S = 3/2$ ;  $g_{1,2,3} = 1.985(5), 1.993(5), 1.996(4)$ ;  $D = 0.2(1) \text{ cm}^{-1}$  and  $E = 0.08 D$ . Bottom: Measurements and best simulation based on a ZFS parameter with a negative sign ( $g_{1,2,3} = 1.94(2), 1.966(4), 1.966(4)$ ;  $D = -0.08(1) \text{ cm}^{-1}$  and  $E = 0.29 D$ ).

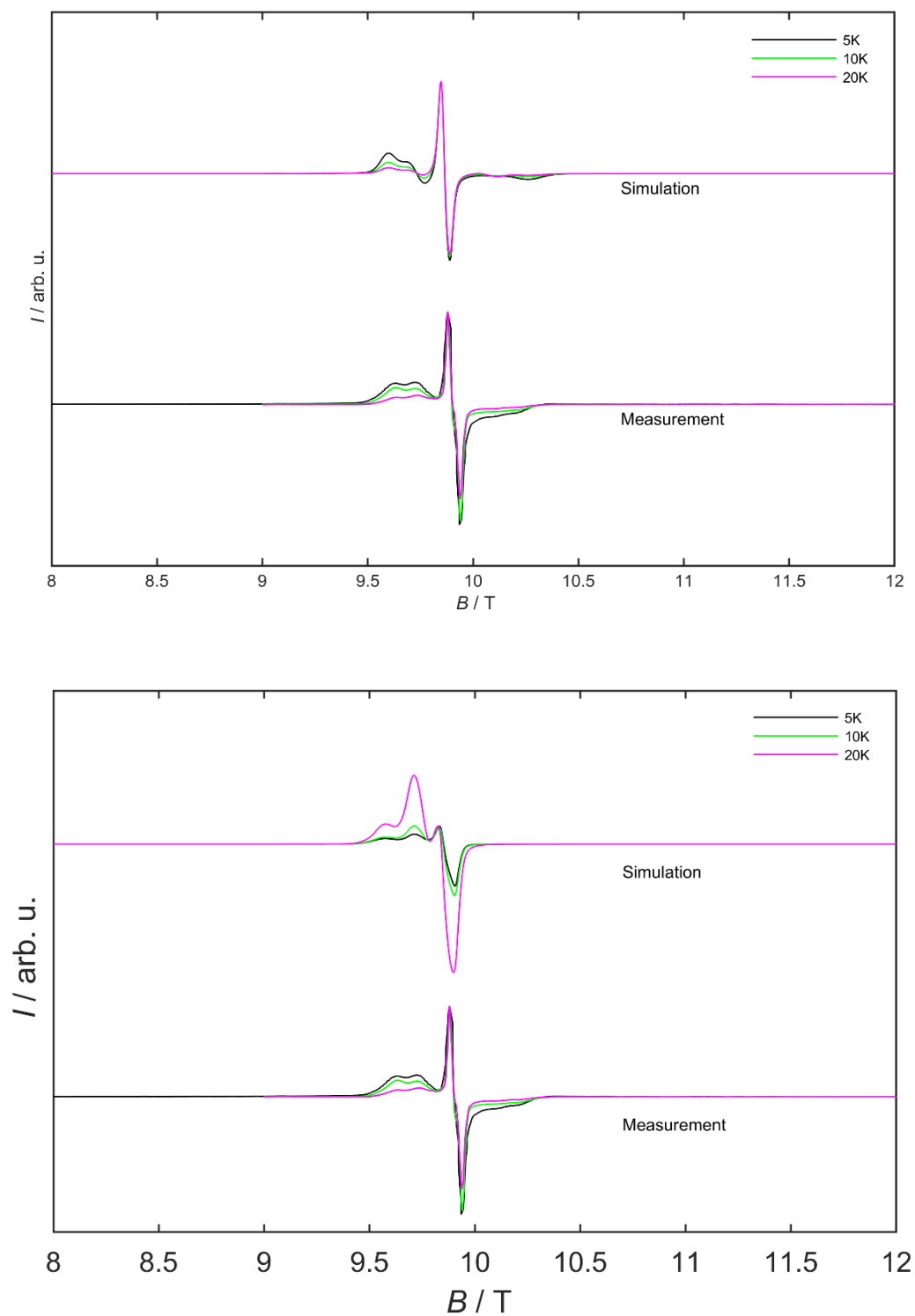


**Figure S27.** Measured and simulated X-Band EPR spectra of *cis-fac*-[V(ddpd)<sub>2</sub>][BPh<sub>4</sub>]<sub>2</sub> (top) and *mer*-[V(ddpd)<sub>2</sub>][BPh<sub>4</sub>]<sub>2</sub> (bottom) at 7 K in a 3 mM butyronitrile/propionitrile (1:1) solution. Simulations are based on the following parameters: *cis-fac*-[V(ddpd)<sub>2</sub>][BPh<sub>4</sub>]<sub>2</sub>:  $S = 3/2$ ;  $g = 1.94(1)$ ;  $D = 0.30(2) \text{ cm}^{-1}$  and  $E = 0.3 D$ ;  $A = 200(20) \text{ MHz}$  and for *mer*-[V(ddpd)<sub>2</sub>][BPh<sub>4</sub>]<sub>2</sub>:  $S = 3/2$ ;  $g = 1.989(5)$ ;  $D = 0.12(2) \text{ cm}^{-1}$  and  $E = 0.08 D$ ;  $A = 200(20) \text{ MHz}$ .

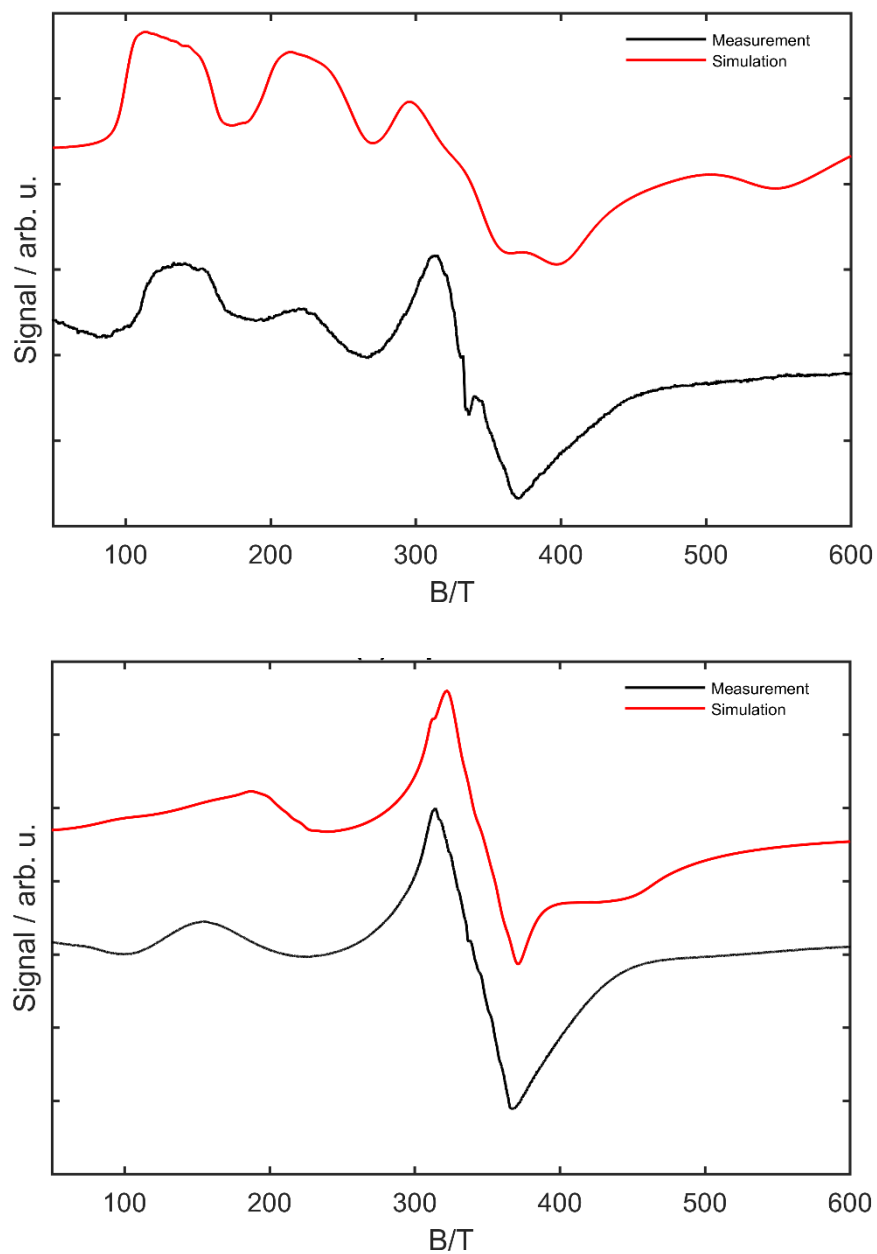


**Figure S28.** Measured inversion recovery curves of *cis-fac*-[V(ddpd)<sub>2</sub>][BPh<sub>4</sub>]<sub>2</sub> in a 3 mM solution (butyronitrile/propionitrile (1:1)) at the indicated fields and temperatures. The fits are based on an exponential of the form  $I(\tau) = -A \exp\left(-\frac{\tau}{T_1}\right) + y$ .

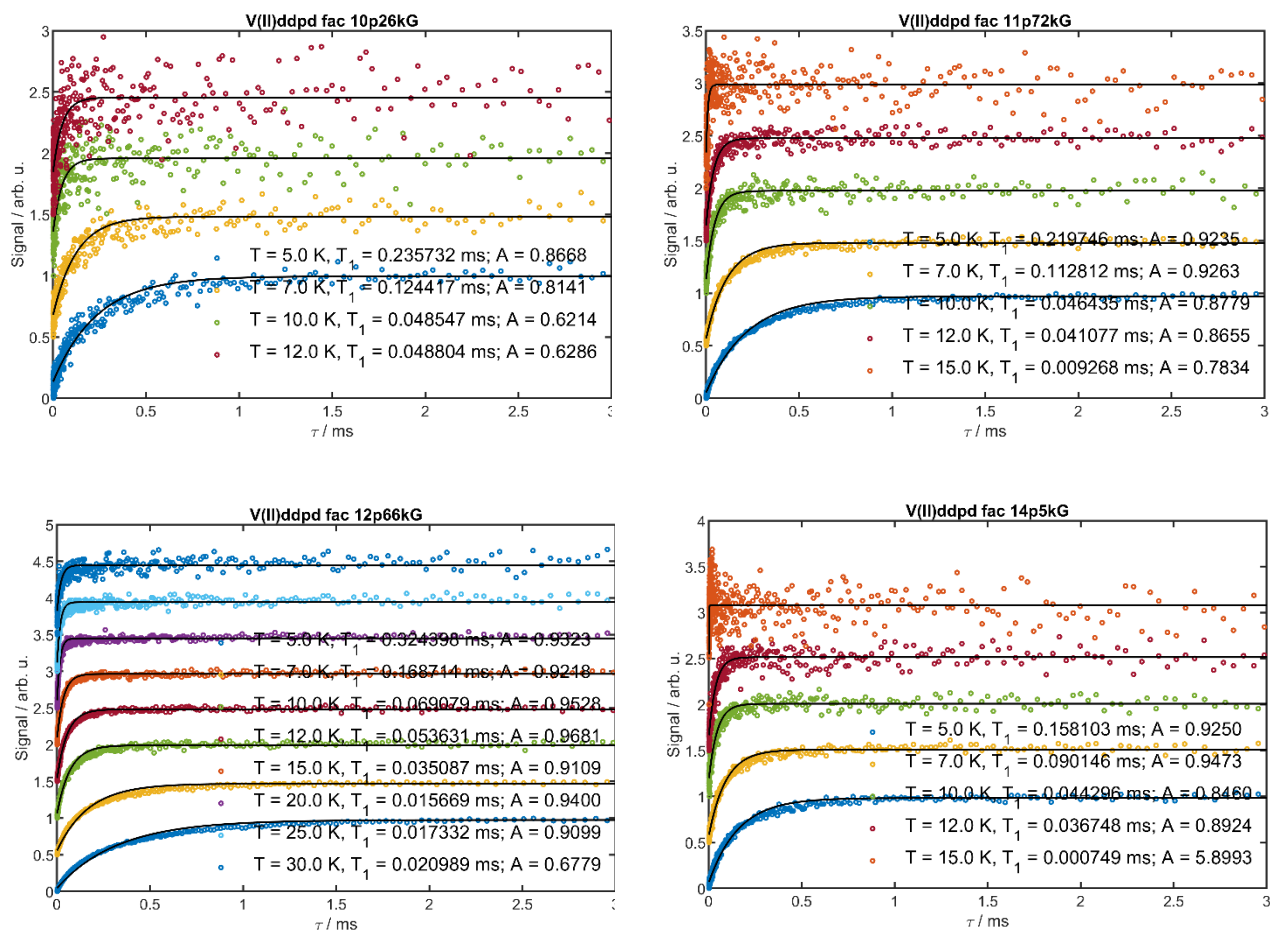


**Figure S29.** Measured Hahn-Echo decay curves of *cis-fac*-[V(ddpd)<sub>2</sub>][BPh<sub>4</sub>]<sub>2</sub> in a 3 mM solution (butyronitrile/propionitrile (1:1)) at the indicated fields and temperatures. The fits are based on an exponential of the form  $I(\tau) = I(0)\exp(-\tau/T_M)^k$ .

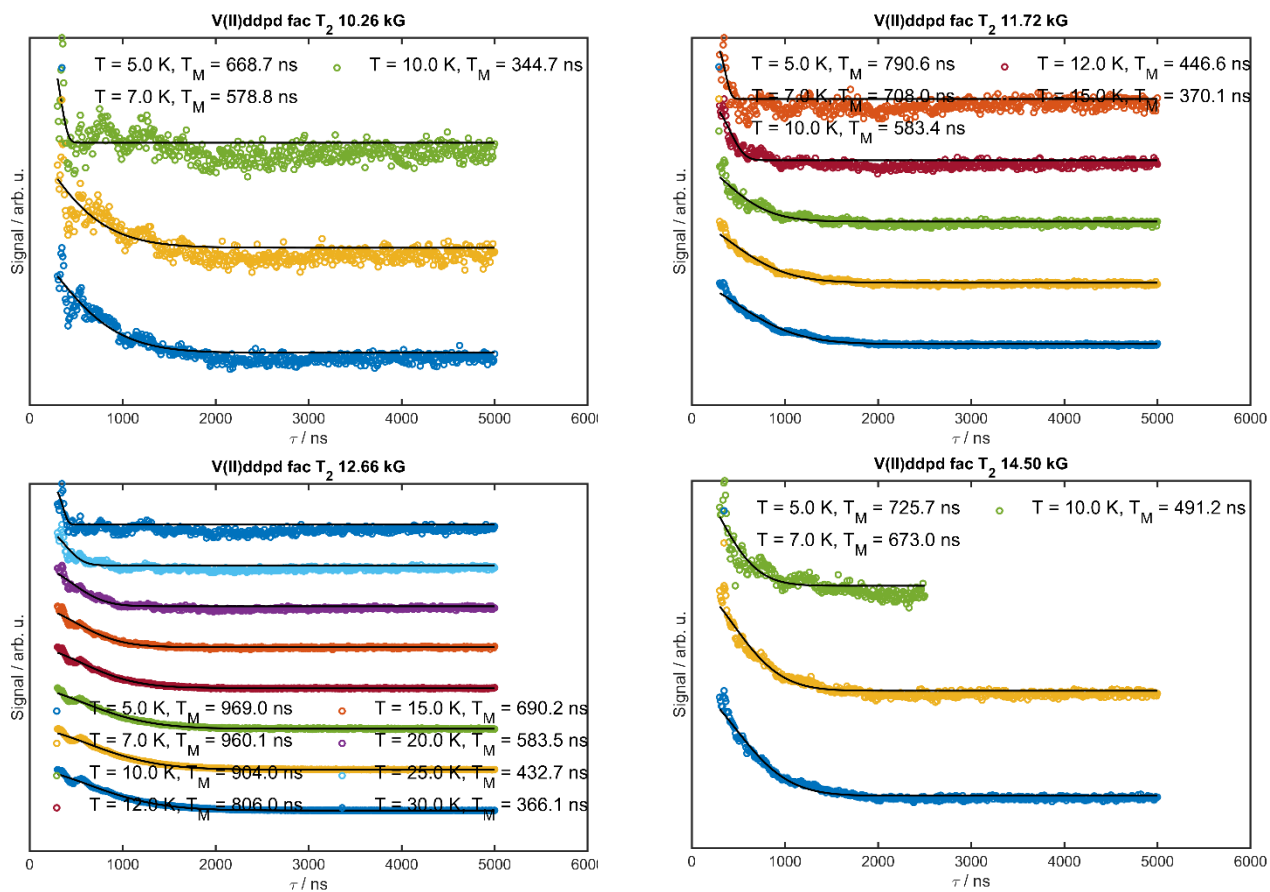




**Figure S30.** Measured inversion recovery curves of *mer*-[V(ddpd)<sub>2</sub>][BPh<sub>4</sub>]<sub>2</sub> in a 3 mM solution (butyronitrile/propionitrile (1:1)) at the indicated temperatures at 1100 mT (left) and at 1275 mT (right). The fits are based on an exponential of the form  $I(\tau) = -A \exp\left(-\frac{\tau}{T_1}\right) + y$ .

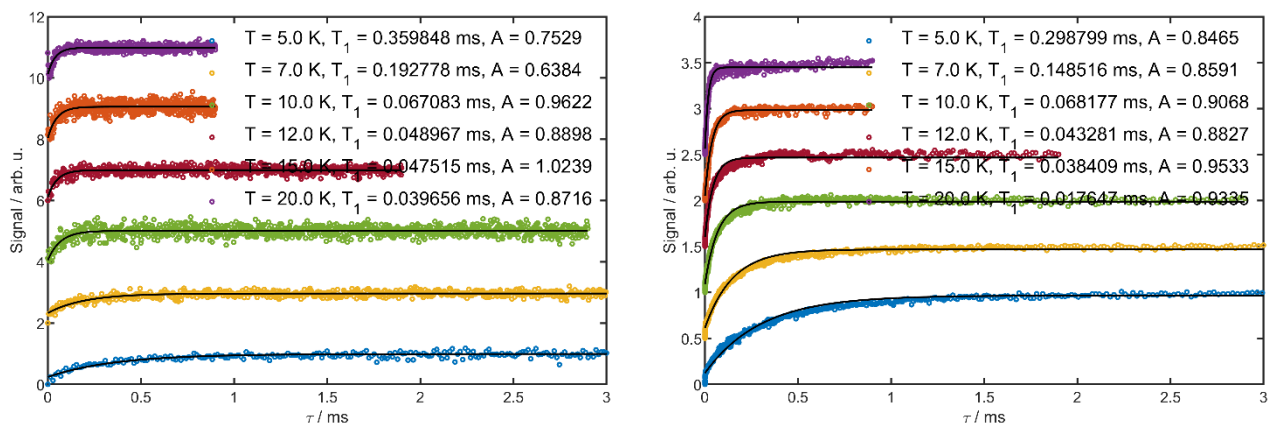


**Figure S31.** Measured Hahn-Echo decay curves of *mer*-[V(ddpd)<sub>2</sub>][BPh<sub>4</sub>]<sub>2</sub> in a 3 mM solution (butyronitrile/propionitrile (1:1)) at the indicated temperatures at 1100 mT (left) and 1275 mT (right). The fits are based on an exponential of the form  $I(\tau) = I(0)\exp(-\tau/T_M)^k$ .

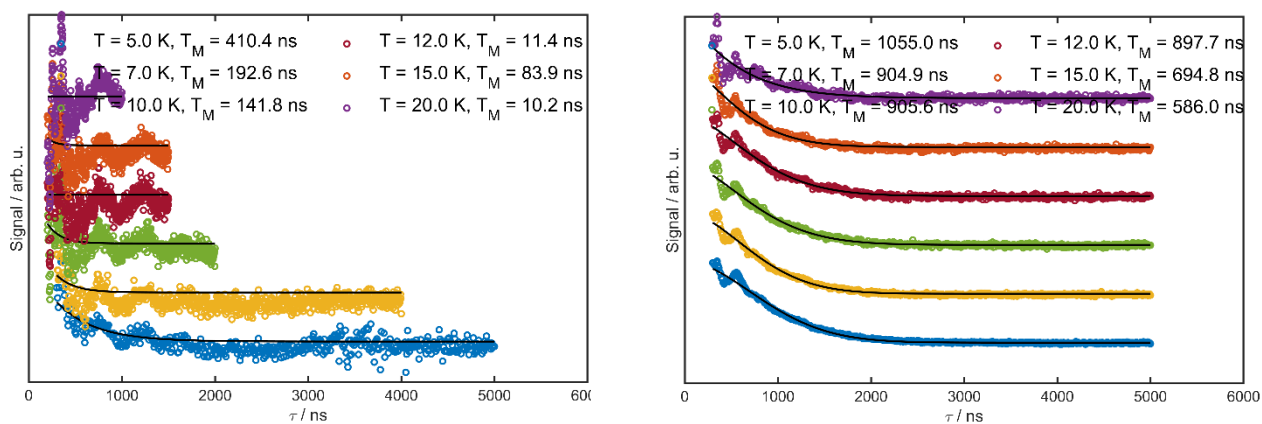


**Figure S32.** Fourier transform of the subtraction of the experiment and the exponential decay of the Hahn-Echo decay curves of *cis-fac*-[V(ddpd)<sub>2</sub>][BPh<sub>4</sub>]<sub>2</sub> (experiments see Figure S29).

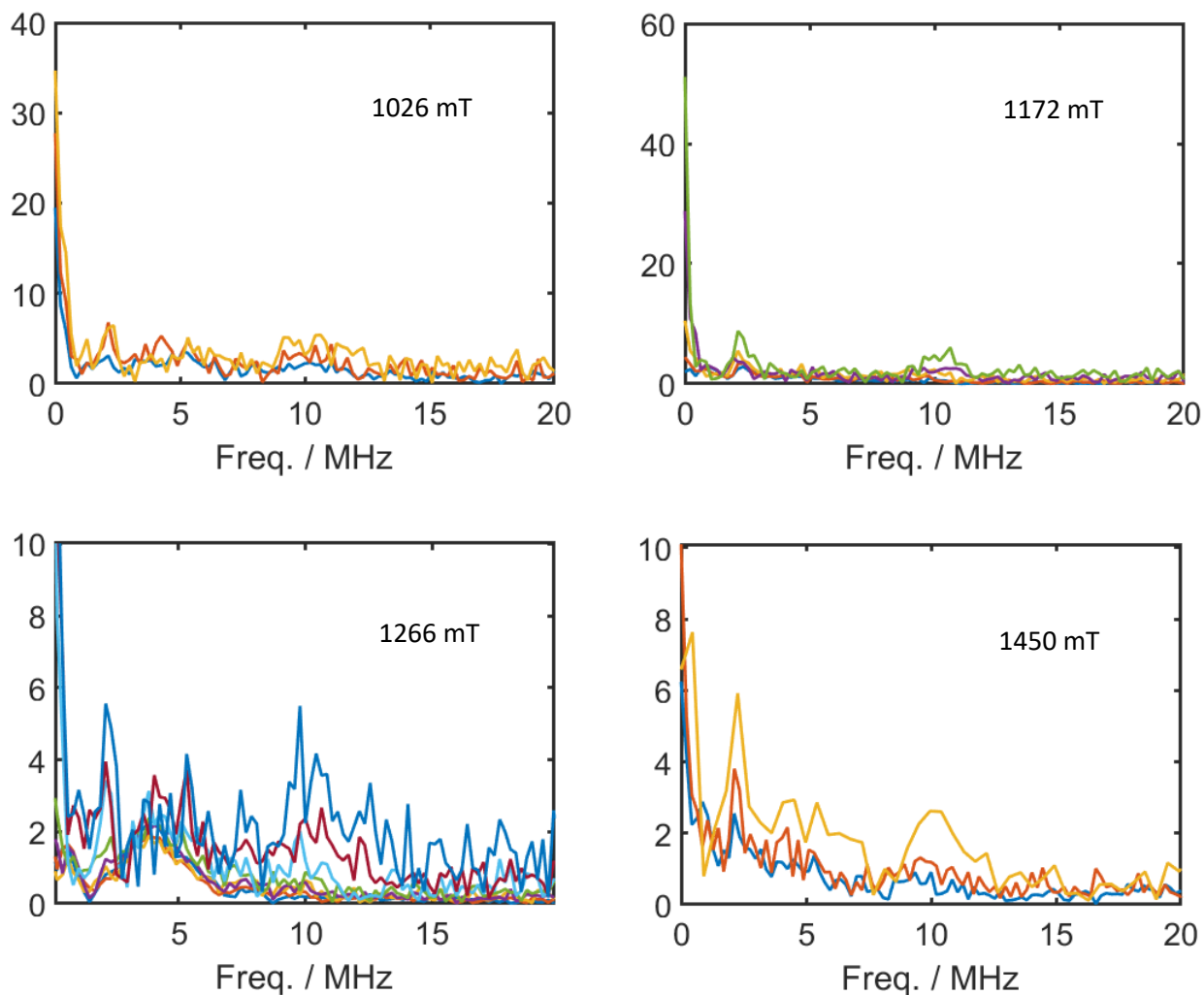


**Figure S33.** Fourier transform of the subtraction of the experiment and the exponential decay of the Hahn-Echo decay curves of *mer*-[V(ddpd)<sub>2</sub>][BPh<sub>4</sub>]<sub>2</sub> (experiments see Figure S31).

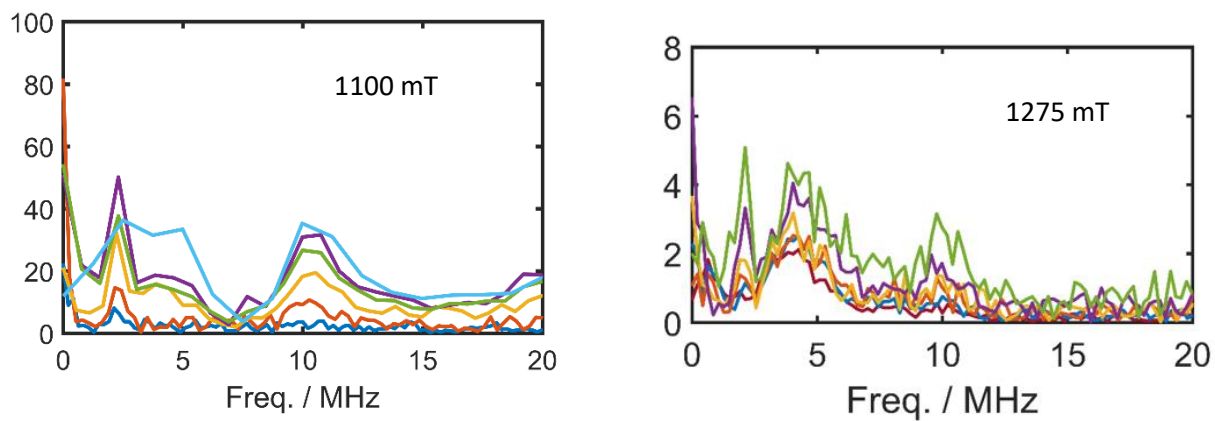
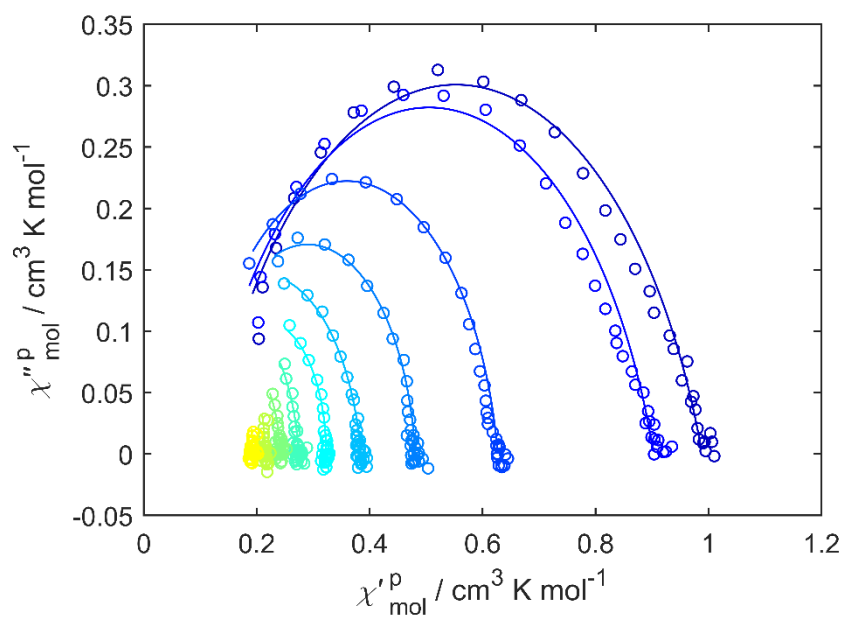


**Figure S34.** Cole-Cole plot of the AC susceptometry measurements on a pressed pellet of *mer*-[V(ddpd)<sub>2</sub>][BPh<sub>4</sub>]<sub>2</sub>. Measured values are shown as open circles, while fits to the standard modified Debye function are shown as solid lines.



## Derivation of the $\Lambda$ Tensor

The lambda tensor is given as<sup>[34]</sup>

$$\Lambda_{ab} = \sum_{k \neq 0} \frac{\langle 0 | \hat{L}_a | k \rangle \langle k | \hat{L}_b | 0 \rangle}{E_k - E_0} \quad (1)$$

where  $a, b \in \{x, y, z\}$ . Here  $|0\rangle$  is the electronic ground state,  $|k\rangle$  are the excited states, and  $E_{k/0}$  their respective energies.

The ZFS parameters  $D$  and  $E$  can be obtained from the lambda tensor via

$$D = \frac{1}{2} \lambda^2 (2 \Lambda_{zz} - \Lambda_{xx} - \Lambda_{yy}); E = \frac{1}{2} \lambda^2 (\Lambda_{xx} - \Lambda_{yy}) \quad (2)$$

A matrix element is non-vanishing only when the direct product of the symmetries of the three terms of the integrand spans the totally symmetric irrep. This symmetry requirement allows the determination of the relevant excited states from the symmetries spanned by the ground state and the orbital angular momentum. The relevant symmetry point group for the present complex *cis-fac*-[V(ddpd)<sub>2</sub>]<sup>2+</sup> is  $C_2$ . The excited states transform either as  $E$ ,  $T_1$  or  $T_2$ , while the orbital angular momentum operator transforms as  $T_1$ . The ground state transforms as  $A_2$ . Hence, non-vanishing matrix elements are only obtained for the  $T_2$  excited state. Additionally, only the diagonal elements of the lambda tensor are non-zero.

## Evaluation of the matrix elements<sup>[35]</sup>

Making use of the Wigner-Eckhart theorem and considering the effects of symmetry lowering (from  $O$  to  $C_2$ ) according Butler's chain of groups, each matrix element can be written as products of 2jm symbols, 3jm symbols and a reduced matrix element (RME) as:

$$\begin{aligned} \langle \Gamma_{GS} | \Gamma_{\hat{L}} | \Gamma_{ES} \rangle^{O \supset D_4 \supset D_2 \supset C_2} &= \begin{pmatrix} \Gamma_{GS}(O) \\ GS \end{pmatrix}^0 \cdot \begin{pmatrix} \Gamma_{GS}(O) & \Gamma_{\hat{L}}(O) & \Gamma_{ES}(O) \\ GS & k & ES \end{pmatrix}^0 \cdot \begin{pmatrix} \Gamma_{GS}(O) \\ \Gamma_{GS}(D_4) \end{pmatrix}_{D_4}^0 \cdot \\ &\begin{pmatrix} \Gamma_{GS}(O) & \Gamma_{\hat{L}}(O) & \Gamma_{ES}(O) \\ \Gamma_{GS}(D_4) & \Gamma_{\hat{L}}(D_4) & \Gamma_{ES}(D_4) \end{pmatrix}_{D_4}^0 \cdot \begin{pmatrix} \Gamma_{GS}(D_4) \\ \Gamma_{GS}(D_2) \end{pmatrix}_{D_2}^{D_4} \cdot \begin{pmatrix} \Gamma_{GS}(D_4) & \Gamma_{\hat{L}}(D_4) & \Gamma_{ES}(D_4) \\ \Gamma_{GS}(D_2) & \Gamma_{\hat{L}}(D_2) & \Gamma_{ES}(D_2) \end{pmatrix}_{D_2}^{D_4} \cdot \begin{pmatrix} \Gamma_{GS}(D_2) \\ \Gamma_{GS}(C_2) \end{pmatrix}_{C_2}^{D_2} \cdot \\ &\begin{pmatrix} \Gamma_{GS}(D_2) & \Gamma_{\hat{L}}(D_2) & \Gamma_{ES}(D_2) \\ \Gamma_{GS}(C_2) & \Gamma_{\hat{L}}(C_2) & \Gamma_{ES}(C_2) \end{pmatrix}_{C_2}^{D_2} \cdot \langle \Gamma_{GS} || \Gamma_{\hat{L}} || \Gamma_{ES} \rangle^O \end{aligned} \quad (3)$$

Here, the first 2jm and the first 3jm symbol are due to the decomposition of the integral due to the Wigner-Eckhart theorem. The following 2jm and 3jm symbols take into account the symmetry lowering.  $GS$  and  $ES$  ( $\zeta$ ,  $\xi$ , or  $\eta$  for  $T_2$ ) are the components of the ground state and excited state irreps, respectively. Since the ground state is non degenerate,  $GS$  is in all cases  $a_2$ .  $k$  is the component of the irrep of the orbital angular momentum operator ( $x$ ,  $y$ , or  $z$  for  $T_1$ ).<sup>[37]</sup>

Only a few combinations of components will deliver non-zero results, and Table C12.1 in Piepho and Schatz can be used to find non-zero contributions.<sup>[36]</sup> All 2jm- and 3jm-symbols are tabulated in Butler.<sup>[35]</sup> Finally, the reduced matrix element is evaluated under the assumption that the transition from ground to excited state can be assigned to a transition of one electron from an orbital to another orbital. In our case, the transition from ground to excited state is always assumed to correspond to excitation of one electron ( $l=2$ ) from an  $e$ - to a  $t_2$ -orbital in  $O$  symmetry. The symmetries of the states are then replaced by those of the orbitals and that of the total orbital angular momentum operator to that of the one-electron orbital angular momentum operator. The effect of symmetry reduction from the pure rotational symmetry  $SO_3$  of the angular momentum to the  $O$  point group is considered as:

$$\begin{aligned} \langle \Gamma_{GS} \| \Gamma_{\hat{l}} \| \Gamma_{ES} \rangle^0 &= \langle e \| \Gamma_{\hat{l}} \| t_2 \rangle^0 = \langle t_2 \| \Gamma_{\hat{l}} \| e \rangle^0 = \begin{pmatrix} 2 \\ e \end{pmatrix}_0^{SO_3} \cdot \begin{pmatrix} 2 & 1 & 2 \\ e & t_1 & t_2 \end{pmatrix}_0^{SO_3} \sqrt{l(l+1)(2l+1)} = 1 \cdot \left( -\frac{\sqrt{2}}{\sqrt{5}} \right) \cdot \sqrt{30} \\ &= -2\sqrt{3} \end{aligned}$$

### Derivation of the relevant integrals

With the above, the only non-zero integrals are:

$$\begin{aligned} &\langle A_2 | T_{1x} | T_{2\xi} \rangle^{O \supset D_4 \supset D_2 \supset C_2} \\ &\langle A_2 | T_{1y} | T_{2\eta} \rangle^{O \supset D_4 \supset D_2 \supset C_2} \\ &\langle A_2 | T_{1z} | T_{2\zeta} \rangle^{O \supset D_4 \supset D_2 \supset C_2} \\ &\langle T_{2\xi} | T_{1x} | A_2 \rangle^{O \supset D_4 \supset D_2 \supset C_2} \\ &\langle T_{2\eta} | T_{1y} | A_2 \rangle^{O \supset D_4 \supset D_2 \supset C_2} \\ &\langle T_{2\zeta} | T_{1z} | A_2 \rangle^{O \supset D_4 \supset D_2 \supset C_2} \end{aligned}$$

These integrals can be solved by using the Wigner-Eckhart theorem as stated above. For the first integral this is:

$$\langle A_2 | T_{1x} | T_{2\xi} \rangle^{O \supset D_4 \supset D_2 \supset C_2} = \begin{pmatrix} A_2 \\ a_2 \end{pmatrix}^0 \cdot \begin{pmatrix} A_2 & T_{1x} & T_{2\xi} \\ a_2 & x & \xi \end{pmatrix}^0 \cdot \begin{pmatrix} A_2 \\ B_1 \end{pmatrix}_{D_4}^0 \cdot \begin{pmatrix} A_2 & T_{1x} & T_{2\xi} \\ B_1 & E & E \end{pmatrix}_{D_4}^0 \cdot \begin{pmatrix} B_1 \\ A_1 \end{pmatrix}_{D_2}^{D_4} \cdot \begin{pmatrix} B_1 & E & E \\ A_1 & B_1 & B_1 \end{pmatrix}_{D_2}^{D_4} \cdot \begin{pmatrix} A_1 \\ A_1 \end{pmatrix}_{C_2}^{D_2} \cdot \begin{pmatrix} A_1 & B_1 & B_1 \\ A_1 & B_1 & B_1 \end{pmatrix}_{C_2}^{D_2} \cdot RME$$

The 2jm and 3jm signals are tabulated in Butler. For this, one has to move to the corresponding Butler notation. For the above integral this is:

$$\langle A_2 | T_{1x} | T_{2\xi} \rangle^{O \supset D_4 \supset D_2 \supset C_2} = \begin{pmatrix} A_2 \\ a_2 \end{pmatrix}^0 \begin{pmatrix} A_2 & T_{1x} & T_{2\xi} \\ a_2 & x & \xi \end{pmatrix}^0 \cdot \begin{pmatrix} 0 \\ 2 \end{pmatrix}_{D_4}^0 \cdot \begin{pmatrix} 0 & 1 & \bar{1} \\ 2 & 1 & 1 \end{pmatrix}_{D_4}^0 \cdot \begin{pmatrix} 2 \\ 0 \end{pmatrix}_{D_2}^{D_4} \cdot \begin{pmatrix} 2 & 1 & 1 \\ 0 & \bar{1} & \bar{1} \end{pmatrix}_{D_2}^{D_4} \cdot \begin{pmatrix} 0 \\ 0 \end{pmatrix}_{C_2}^{D_2} \cdot \begin{pmatrix} 0 & \bar{1} & \bar{1} \\ 0 & 1 & 1 \end{pmatrix}_{C_2}^{D_2} \cdot RME$$

With the 2jm and 3jm symbols evaluated:

$$\begin{aligned} \langle A_2 | T_{1x} | T_{2\xi} \rangle^{O \supset D_4 \supset D_2 \supset C_2} &= 1 \cdot \frac{1}{\sqrt{3}} \cdot 1 \cdot -\frac{\sqrt{2}}{\sqrt{3}} \cdot 1 \cdot -\frac{1}{\sqrt{2}} \cdot 1 \cdot -1 \cdot RME = 1 \cdot \frac{1}{\sqrt{3}} \cdot 1 \cdot -\frac{\sqrt{2}}{\sqrt{3}} \cdot 1 \cdot -\frac{1}{\sqrt{2}} \cdot 1 \cdot -1 \cdot -2\sqrt{3} \\ &= \frac{1}{\sqrt{3}} \cdot -\frac{\sqrt{2}}{\sqrt{3}} \cdot -\frac{1}{\sqrt{2}} \cdot 2\sqrt{3} = \frac{2\sqrt{3}}{3} \end{aligned}$$

For the other matrix elements, the procedure is equivalent and will lead to the elements of the lambda tensor:

$$\Lambda_{zz} = \frac{4}{3E_1}, \Lambda_{yy} = \frac{4}{3E_2} \text{ and } \Lambda_{xx} = \frac{4}{3E_3}. \text{ With that the ZFS parameters are the following:}$$

$$D = \frac{1}{2} \lambda^2 \left( 2 \frac{4}{3E_1} - \frac{4}{3E_3} - \frac{4}{3E_2} \right) \text{ and } E = \frac{1}{2} \lambda^2 \left( \frac{4}{3E_3} - \frac{4}{3E_2} \right)$$

## References

- [1] S. J. Anderson, F. J. Wells, G. Wilkinson, B. Hussain, M. B. Hursthouse, *Polyhedron* **1988**, *7*, 2615–2626.
- [2] a) A. Breivogel, C. Förster, K. Heinze, *Inorg. Chem.* **2010**, *49*, 7052–7056. b) C. Wang, W. R. Kitzmann, F. Weigert, C. Förster, X. Wang, K. Heinze, U. Resch-Genger, *ChemPhotoChem* **2022**, *6*, e202100296.
- [3] P. Neugebauer, D. Bloos, R. Marx, P. Lutz, M. Kern, D. Aguila, J. Vaverka, O. Laguta, C. Dietrich, R. Clerac, J. van Slageren, *Phys. Chem. Chem. Phys.* **2018**, *20*, 15528–15534.
- [4] S. Stoll, A. Schweiger, *J. Magn. Reson.* **2006**, *178*, 42–55.
- [5] Y. Rechkemmer, PhD Thesis, University of Stuttgart, **2016**.
- [6] I. Tkach, A. Baldansuren, E. Kalabukhova, S. Lukin, A. Sitnikov, A. Tsvir, M. Ischenko, Y. Rosentzweig, E. Roduner, *Appl. Magn. Reson.* **2008**, *35*, 95–112.
- [7] D. Dengler, PhD Thesis, University of Stuttgart, **2016**.
- [8] STOE & Cie. X-Red, Darmstadt, Germany, **2002**.
- [9] R. H. Blessing, *Acta Crystallogr., Sect. A* **1995**, *51*, 33–38.
- [10] A. L. Spek, *Acta Crystallogr., Sect. D* **2009**, *65*, 148–155.
- [11] G. M. Sheldrick. SHELXL-2014/7, Göttingen, Germany, **2014**.
- [12] G. M. Sheldrick, *Acta Crystallogr., Sect. A* **2015**, *71*, 3–8.
- [13] F. Neese, *WIREs Comput. Mol. Sci.* **2012**, *2*, 73–78.
- [14] A. D. Becke, *J. Chem. Phys.* **1993**, *98*, 5648–5652.
- [15] F. Weigend, R. Ahlrichs, *Phys. Chem. Chem. Phys.* **2005**, *7*, 3297–3305.
- [16] F. Weigend, *Phys. Chem. Chem. Phys.* **2006**, *8*, 1057–1065.
- [17] D. A. Pantazis, X.-Y. Chen, C. R. Landis, F. Neese, *J. Chem. Theory Comput.* **2008**, *4*, 908–919.
- [18] E. van Lenthe, E. J. Baerends, J. G. Snijders, *J. Chem. Phys.* **1993**, *99*, 4597–4610.
- [19] S. Grimme, J. Antony, S. Ehrlich, H. Krieg, *J. Chem. Phys.* **2010**, *132*, 154104.
- [20] S. Grimme, S. Ehrlich, L. Goerigk, *J. Comput. Chem.* **2011**, *32*, 1456–1465.
- [21] V. Barone, M. Cossi, *J. Phys. Chem. A* **1998**, *102*, 1995–2001.
- [22] F. Plasser, TheoDORE: at <http://theodore-qc.sourceforge.net>.
- [23] F. Plasser, *J. Chem. Phys.* **2020**, *152*, 84108.
- [24] B. O. Roos, P. R. Taylor, P. E. Siegbahn, *Chem. Phys.* **1980**, *48*, 157–173.
- [25] P. E. M. Siegbahn, J. Almlöf, A. Heiberg, B. O. Roos, *J. Chem. Phys.* **1981**, *74*, 2384–2396.
- [26] C. Angeli, R. Cimiraglia, S. Evangelisti, T. Leininger, J.-P. Malrieu, *J. Chem. Phys.* **2001**, *114*, 10252–10264.
- [27] C. Angeli, R. Cimiraglia, *Theoret. Chim. Acta* **2002**, *107*, 313–317.

- [28] F. Neese, *J. Chem. Phys.* **2005**, *122*, 034107.
- [29] B. A. Hess, C. M. Marian, In *Computational Molecular Spectroscopy*, P. B. Jensen, Ed. Wiley: New York, **2000**, pp. 169.
- [30] B. Cahier, R. Maurice, H. Bolvin, T. Mallah, N. Guihéry, *Magnetochemistry* **2016**, *2*, 31.
- [31] B. O. Roos, P. A. Malmqvist, *Phys. Chem. Chem. Phys.* **2004**, *6*, 2919–2927.
- [32] P. Durand, J.-P. Malrieu, In *Advances in Chemical Physics: Ab Initio Methods in Quantum Chemistry*, K. P. Lawley, Ed., John Wiley & Sons Ltd.: Hoboken, NJ, **1987**, Vol. 67, Part 1, pp. 321–412.
- [33] P. Alemany, D. Casanova, S. Alvarez, C. Dryzun, D. Avnir, *Continuous Symmetry Measures: A New Tool in Quantum Chemistry* in *Reviews in Computational Chemistry* (Eds.: A. L. Parrill, K. B. Lipkowitz), Vol. 30, John Wiley & Sons, Hoboken, NJ, USA, **2017**, pp. 289–352.
- [34] R. Boça, *Coord. Chem. Rev.* **2004**, *248*, 757–815.
- [35] P. H. Butler, *Point Group Symmetry Applications: Methods and Tables*, Plenum Press, New York, **1981**.
- [36] S. B. Piepho and P. N. Schatz, *Group Theory in Spectroscopy with Applications to Magnetic Circular Dichroism*, John Wiley & Sons, New York, **1983**.
- [37] J. Bradley, A. Thomson, E. McInnes, R. Winpenny, G. Timco, *Dalton Trans.* **2008**, 3311–3319.